

A STUDY OF LEVEL CROSSING EFFECTS IN TCNQ SALTS

Francisco Xavier Cabañas

B.Sc. The University of British Columbia., 1979

M.Sc The University of British Columbia., 1982

A THESIS SUBMITTED IN PARTIAL FULFILLMENT OF  
THE REQUIREMENTS FOR THE DEGREE OF  
DOCTOR OF PHILOSOPHY

in

THE FACULTY OF GRADUATE STUDIES  
DEPARTMENT OF PHYSICS

We accept this thesis as conforming  
to the required standard

THE UNIVERSITY OF BRITISH COLUMBIA

February 1988

© Francisco Xavier Cabañas , 1988

59

In presenting this thesis in partial fulfilment of the requirements for an advanced degree at the University of British Columbia, I agree that the Library shall make it freely available for reference and study. I further agree that permission for extensive copying of this thesis for scholarly purposes may be granted by the head of my department or by his or her representatives. It is understood that copying or publication of this thesis for financial gain shall not be allowed without my written permission.

Department of physics  
The University of British Columbia  
1956 Main Mall  
Vancouver, Canada

Date:

29<sup>th</sup> February 1988

## Abstract

ESR results for  $\text{DEM}(\text{TCNQ})_2$  and for  $\text{MEM}(\text{TCNQ})_2$  are presented as examples of TCNQ salts with and without level crossing effects. In the case of  $\text{DEM}(\text{TCNQ})_2$  we are performing ESR on a system with two types of spins. The latter are due to the two kinds of stacks of the acceptor TCNQ molecules in  $\text{DEM}(\text{TCNQ})_2$ . The level crossing occurs when the  $g$  value of these two kinds of electrons are the same. This is compared to the case of  $\text{MEM}(\text{TCNQ})_2$  where there is only one kind of TCNQ stack and consequently no level crossing effect. It is found that  $g$  values and susceptibilities of the ESR spectra for  $\text{DEM}(\text{TCNQ})_2$  can be fitted very well to an interaction between the stacks of the form  $J \sum_{i,j} \mathbf{S}_i \mathbf{S}_j$  with  $J > 0$ . This gives an antiferromagnetic coupling between every spin on one type of stack with every spin on the other type of stack. This type of interaction is also in qualitative agreement with the published results for  $\text{HMM}(\text{TCNQ})_2$ . The experimental results in  $\text{DEM}(\text{TCNQ})_2$  and  $\text{MEM}(\text{TCNQ})_2$  also show that there are small but significant differences in the  $g$  tensors when the temperature or the crystalline environment are changed, and consequently the  $g$  tensor in these compounds does not depend only on the orientation of TCNQ molecule in the magnetic field as previously assumed. These differences in  $g$  are typically less than  $2 \times 10^{-4}$ .

## Contents

<b>Abstract</b>	<b>ii</b>
<b>List of Tables</b>	<b>vi</b>
<b>List of Figures</b>	<b>vii</b>
<b>Acknowledgements</b>	<b>x</b>
<b>1 Introduction</b>	<b>1</b>
1.1 Quasi-one-dimensional TCNQ salts . . . . .	1
1.2 Magnetic Properties . . . . .	3
1.3 Scope of this Thesis . . . . .	8
<b>2 The ESR Experiment</b>	<b>11</b>
2.1 The ESR Apparatus . . . . .	11
2.2 Experimental Method . . . . .	13
2.3 Determination of the $g$ Tensor . . . . .	16
2.4 Correlation of the $g$ Tensor to the Crystal Structure . . . . .	17
<b>3 MEM(TCNQ)<sub>2</sub> Results</b>	<b>20</b>
3.1 The $g$ value Measurements . . . . .	20
3.2 The Halfwidth Measurements . . . . .	28

3.3	Discussion of the Results . . . . .	35
<b>4</b>	<b>Theory for Salts with Crossing Energy Levels</b>	<b>36</b>
4.1	Introduction . . . . .	36
4.2	Complete Correlation between the <i>A</i> and <i>B</i> Spins . . . . .	38
4.3	No Correlation between the <i>A</i> and <i>B</i> Spins . . . . .	41
4.4	Fit of the Theory for the case of no Correlation to the Experimental Data . . . . .	48
<b>5</b>	<b>DEM(TCNQ)<sub>2</sub> Results</b>	<b>51</b>
5.1	The <i>g</i> Value Measurements . . . . .	51
5.2	Relationship of the <i>g</i> Tensors to the Crystal Structure . . . . .	60
5.3	The Susceptibility Measurements . . . . .	62
5.4	The Halfwidth Measurements . . . . .	70
5.5	Discussion of the Results . . . . .	78
<b>6</b>	<b>Power Saturation Measurements of DEM(TCNQ)<sub>2</sub></b>	<b>80</b>
6.1	The ESR Experiment . . . . .	80
6.2	Saturation and Overmodulation of the Coupled Spin System . . . . .	81
6.3	Experimental Results . . . . .	83
6.4	Conclusions from the Power Data . . . . .	83
<b>7</b>	<b>Conclusion and Comparison with Other Results</b>	<b>88</b>
7.1	Preliminary Results on HMM(TCNQ) <sub>2</sub> . . . . .	88
7.2	The Dependence of the <i>g</i> Tensor on the Environment of the TCNQ Molecules and on the Temperature . . . . .	92
7.3	Conclusions and Further Experiments . . . . .	94



## List of Tables

I	$g$ Tensor of MEM(TCNQ) <sub>2</sub> at 298 K . . . . .	20
II	$g$ Tensor of MEM(TCNQ) <sub>2</sub> at 77 K . . . . .	27
III	$g$ Tensor of the <i>A</i> Stack of DEM(TCNQ) <sub>2</sub> at 298 K . . . . .	52
IV	$g$ Tensor of the <i>B</i> Stack of DEM(TCNQ) <sub>2</sub> at 298 K . . . . .	52
V	$g$ Tensor of the <i>A</i> Stack of DEM(TCNQ) <sub>2</sub> at 77 K . . . . .	52
VI	$g$ Tensor of the <i>B</i> Stack of DEM(TCNQ) <sub>2</sub> at 77 K . . . . .	59
VII	The Relative Orientation of the $g$ Tensors and the TCNQ molecules in DEM(TCNQ) <sub>2</sub> . . . . .	61
VIII	Inter Stack Exchange Constant and Ratio of Susceptibilities for DEM- (TCNQ) <sub>2</sub> . . . . .	69
IX	$g$ Tensor of Various TCNQ Compounds . . . . .	93

## List of Figures

1	The TCNQ Molecule . . . . .	2
2	The Morpholinium Molecule . . . . .	3
3	Susceptibility of MEM(TCNQ) <sub>2</sub> . . . . .	5
4	ESR Spectra of DEM(TCNQ) <sub>2</sub> . . . . .	7
5	The ESR Spectrometer . . . . .	12
6	Typical spectra of DEM(TCNQ) <sub>2</sub> . . . . .	14
7	<i>g</i> Value of MEM(TCNQ) <sub>2</sub> for a Rotation about <b>a</b> at 298 K . . . . .	21
8	<i>g</i> Value of MEM(TCNQ) <sub>2</sub> for a Rotation about <b>b</b> at 298 K . . . . .	22
9	<i>g</i> Value of MEM(TCNQ) <sub>2</sub> for a Rotation about <b>c</b> at 298 K . . . . .	23
10	<i>g</i> Value of MEM(TCNQ) <sub>2</sub> for a Rotation about <b>a</b> at 77 K . . . . .	24
11	<i>g</i> Value of MEM(TCNQ) <sub>2</sub> for a Rotation about <b>b</b> at 77 K . . . . .	25
12	<i>g</i> Value of MEM(TCNQ) <sub>2</sub> for a Rotation about <b>c</b> at 77 K . . . . .	26
13	Peak to Peak Halfwidth of MEM(TCNQ) <sub>2</sub> for a Rotation about <b>a</b> at 298 K . . . . .	29
14	Peak to Peak Halfwidth of MEM(TCNQ) <sub>2</sub> for a Rotation about <b>b</b> at 298 K . . . . .	30
15	Peak to Peak Halfwidth of MEM(TCNQ) <sub>2</sub> for a Rotation about <b>c</b> at 298 K . . . . .	31

16	Peak to Peak Halfwidth of MEM(TCNQ) <sub>2</sub> for a Rotation about <b>a</b> at 77 K . . . . .	32
17	Peak to Peak Halfwidth of MEM(TCNQ) <sub>2</sub> for a Rotation about <b>b</b> at 77 K . . . . .	33
18	Peak to Peak Halfwidth of MEM(TCNQ) <sub>2</sub> for a Rotation about <b>c</b> at 77 K . . . . .	34
19	<i>g</i> Value of DEM(TCNQ) <sub>2</sub> for a Rotation about <b>a</b> at 298 K . . . . .	53
20	<i>g</i> Value of DEM(TCNQ) <sub>2</sub> for a Rotation about <b>b</b> at 298 K . . . . .	54
21	<i>g</i> Value of DEM(TCNQ) <sub>2</sub> for a Rotation about <b>c</b> at 298 K . . . . .	55
22	<i>g</i> Value of DEM(TCNQ) <sub>2</sub> for a Rotation about <b>a</b> at 77 K . . . . .	56
23	<i>g</i> Value of DEM(TCNQ) <sub>2</sub> for a Rotation about <b>b</b> at 77 K . . . . .	57
24	<i>g</i> Value of DEM(TCNQ) <sub>2</sub> for a Rotation about <b>c</b> at 77 K . . . . .	58
25	Normalized Susceptibility of DEM(TCNQ) <sub>2</sub> for a Rotation about <b>a</b> at 298 K . . . . .	63
26	Normalized Susceptibility of DEM(TCNQ) <sub>2</sub> for a Rotation about <b>b</b> at 298 K . . . . .	64
27	Normalized Susceptibility of DEM(TCNQ) <sub>2</sub> for a Rotation about <b>c</b> at 298 K . . . . .	65
28	Normalized Susceptibility of DEM(TCNQ) <sub>2</sub> for a Rotation about <b>a</b> at 77 K . . . . .	66
29	Normalized Susceptibility of DEM(TCNQ) <sub>2</sub> for a Rotation about <b>b</b> at 77 K . . . . .	67
30	Normalized Susceptibility of DEM(TCNQ) <sub>2</sub> for a Rotation about <b>c</b> at 77 K . . . . .	68
31	Linewidths of DEM(TCNQ) <sub>2</sub> for a Rotation about <b>a</b> at 298 K . . . . .	71

32	Linewidths of DEM(TCNQ) <sub>2</sub> for a Rotation about <b>b</b> at 298 K . . . .	72
33	Linewidths of DEM(TCNQ) <sub>2</sub> for a Rotation about <b>c</b> at 298 K . . . .	73
34	Linewidths of DEM(TCNQ) <sub>2</sub> for a Rotation about <b>a</b> at 77 K . . . .	74
35	Linewidths of DEM(TCNQ) <sub>2</sub> for a Rotation about <b>b</b> at 77 K . . . .	75
36	Linewidths of DEM(TCNQ) <sub>2</sub> for a Rotation about <b>c</b> at 77 K . . . .	76
37	Susceptibility as a Function of Power for DEM(TCNQ) <sub>2</sub> . . . . .	84
38	Peak to Peak Halfwidth as a Function of Power for DEM(TCNQ) <sub>2</sub> .	85
39	<i>g</i> value of HMM(TCNQ) <sub>2</sub> assuming no Interaction between the Stacks	90
40	<i>g</i> value of HMM(TCNQ) <sub>2</sub> assuming an Interaction between the Stacks	91

## **Acknowledgements**

I wish to acknowledge the supervision, assistance and suggestions of my supervisor Dr. C. F. Schwerdtfeger during the performance of the experiments and the preparation of the thesis. I would also like to thank Dr. M. Bloom for his suggestions and very stimulating discussions. Also I would like to thank Dr B. Bergersen, Dr. J. F. Carolan and Dr. R. R. Johnson for thier suggestions and comments. The samples for this research were provided by Dr. B. van Bodegom of the University of Groningen.

A Post Graduate Scholarship from the Natural Sciences and Engineering Research Council of Canada together with a University of British Columbia Graduate Fellowship are gratefully acknowleged. Further financial support for this thesis was provided by the Natural Sciences and Engineering Research Council of Canada through grants to Dr. Schwerdtfeger.

*To the memory of  
Pablo and Maria J. Cabañas  
my parents*

## Chapter 1

### Introduction

#### 1.1 Quasi-one-dimensional TCNQ salts

The quasi-one-dimensional 7, 7, 8, 8 - tetracyano - p - quinodimethane (TCNQ) salts have received considerable attention for some time. An introduction to these materials is given in the review article by Shchegolev [1]. An example of more recent work is the systematic project undertaken at the University of Groningen [2,3,4,5]. The initial expectation of high temperature superconductivity in these materials has not materialized; however the TCNQ salts have provided a system where the physics of low dimensional solids can be experimentally studied and compared to the simpler one-dimensional theories.

The quasi-one-dimensional behavior arises from the stacking of the organic electron acceptor TCNQ molecules. The planar TCNQ molecules stack above one another with the molecular planes parallel to each other. In general the stacking direction is not perpendicular to the plane of the TCNQ molecules, namely there is an incomplete overlap between adjacent TCNQ molecules. The wide variety of possible donor molecules has led to a large number of different stacking arrangements for the TCNQ molecules. A further factor is that the stacks can consist of a regular, dimerized or tetramerized lattice of TCNQ molecules. This can have a

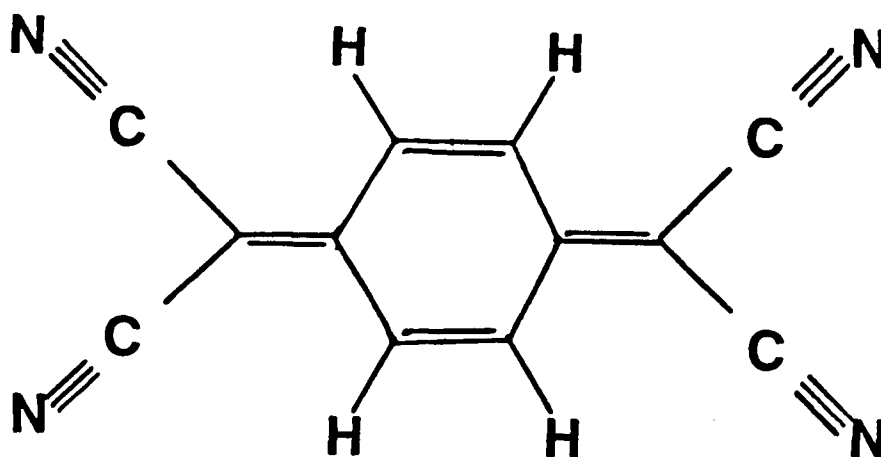


Figure 1: The TCNQ molecule

significant impact on the electric and magnetic properties of the one-dimensional system [3]. An empirical classification scheme based on the electrical conductivity has been presented by Torrance [6], a further classification is provided by Visser [5, p. 16].

In this thesis we will be concerned primarily with the morpholinium compounds, in particular N - methyl - N - ethyl - morpholinium - tetracyanoquinodimethane,  $\text{MEM}(\text{TCNQ})_2$ , and N - ethyl - N - ethyl - morpholinium - tetracyanoquinodimethane,  $\text{DEM}(\text{TCNQ})_2$ . The crystal structure of these materials is given by van Bodegom [2], and also by Morssink and von Bodegom [8] for  $\text{DEM}(\text{TCNQ})_2$  and Bosch and van Bodegom [9] for  $\text{MEM}(\text{TCNQ})_2$ . The structure of  $\text{DEM}(\text{TCNQ})_2$  is triclinic, space group  $P\bar{1}$ . There are two inequivalent TCNQ stacks with the DEM molecules in between the stacks.  $\text{MEM}(\text{TCNQ})_2$  is triclinic, space group  $P1$  with

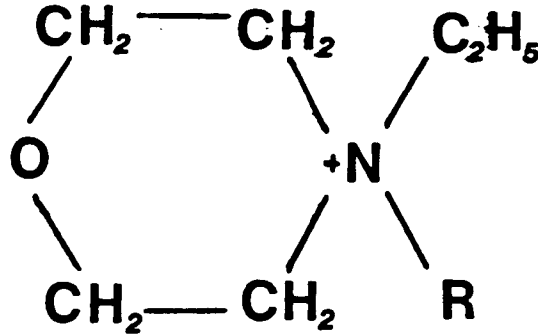


Figure 2: The morpholinium molecule,  $R=CH_3$ : MEM,  $R=C_2H_5$ : DEM

only one type of TCNQ stack. We can study DEM(TCNQ)<sub>2</sub> as an example of a compound with crossing energy levels and can compare the results to the case of MEM(TCNQ)<sub>2</sub> where there are no level crossing effects.

## 1.2 Magnetic Properties

The magnetic properties of the TCNQ salts have been explained in terms of one-dimensional models. The Hubbard [7] Hamiltonian

$$\mathcal{H} = \sum_{i,\sigma} t_{i,i+1} (c_{i+1,\sigma}^\dagger c_{i,\sigma} + c_{i,\sigma}^\dagger c_{i+1,\sigma}) + \frac{1}{2} \sum_{i \neq j} V_{i-j} n_i n_j + \frac{U}{2} \sum_{i,\sigma} n_{i,\sigma} n_{i,-\sigma} \quad (1.1)$$

where  $c_{i,\sigma}$  is the destruction operator for an electron of spin  $\sigma$  at the site  $i$ ,  $n_{i,\sigma} = c_{i,\sigma}^\dagger c_{i,\sigma}$  is the occupation operator of the state  $i,\sigma$ ,  $n_i = \sum_{\sigma} n_{i,\sigma}$  gives the total number of electrons at the site  $i$ ,  $t_{i,i+1}$  is the transfer integral between the sites  $i$

and  $i + 1$ <sup>1</sup>,  $U$  is the interaction, between electrons at the same site, and  $V_n = V_{-n}$  is the interaction of electrons  $n$  nearest neighbour sites apart, has been used as a starting point for models of the conduction electrons on the TCNQ stacks. In this Hamiltonian the ratio  $U/t$  is a critical parameter [3]. This ratio determines to what degree the electrons are localized on the individual sites on the stacks. In the TCNQ salts we have  $U/t \rightarrow \infty$ . The Hubbard model predicts two transitions. The  $4k_F$  transition corresponds to the electronic-Peierls distortion. This transition occurs at high temperature and produces an opening of a gap at the Fermi level. Above this transition we have a regular chain with one half an electron per unit cell, while below the transition the stack is dimerized with one electron per unit cell. As the temperature is increased past the  $4k_F$  transition we expect a significant increase in the conductivity. This is in fact observed in  $\text{MEM}(\text{TCNQ})_2$  at 335 K [10]. Below the  $2k_F$  or spin-Peierls transition the stacks are tetramerized with two electrons per unit cell, with the spins paired leading to a marked decrease in the magnetic susceptibility.

Oostra [4, p. 22] has shown that, for a dimerized stack, equation 1.1 leads to an effective exchange interaction between the spins on adjacent TCNQ dimers of the form

$$\mathcal{H}_{spin} = 2J \sum_i \mathbf{S}_i \mathbf{S}_{i+1} \quad (1.2)$$

where  $J = t_2^2/U$ ,  $t_2$  being the smaller of the two transfer integrals for a dimerized stack, and for a tetramerized stack he [4, p. 26] gives an equation in terms of two exchange constants  $J_1$  and  $J_2$  of the form

$$\mathcal{H}_{spin} = \sum_i (J_1 \mathbf{S}_{2i} \mathbf{S}_{2i+1} + J_2 \mathbf{S}_{2i+1} \mathbf{S}_{2i+2}) \quad (1.3)$$

---

<sup>1</sup>The transfer integral has been allowed to vary along the stack to allow for dimerized or tetramerized stacks, this is an extension of the Hamiltonian in Hubbard's paper, where a constant transfer integral is assumed. See also: [4, p. 11].

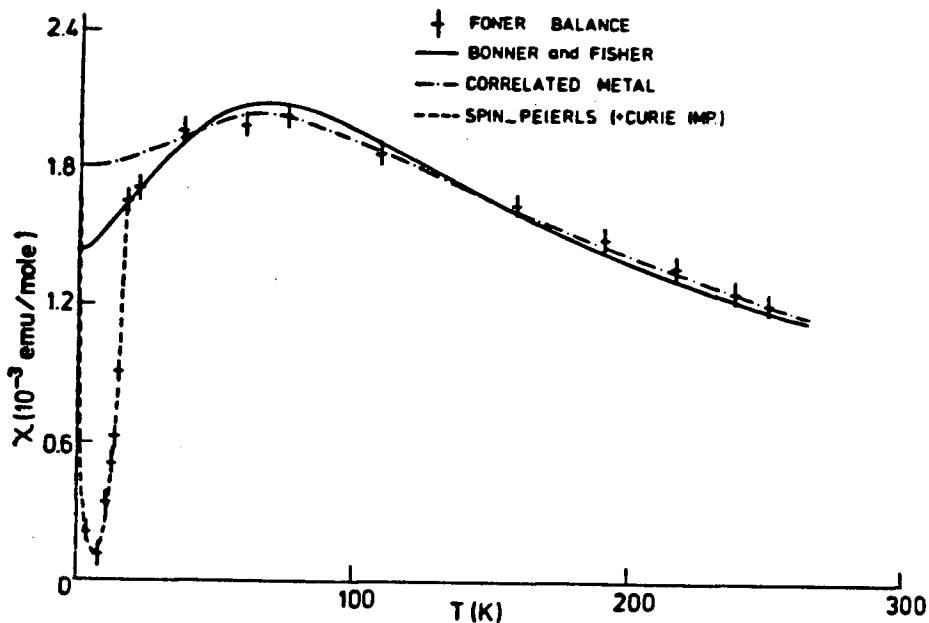


Figure 3: Spin susceptibility of  $\text{MEM}(\text{TCNQ})_2$ : Experimental points as obtained on a Foner balance and theoretical fits with the correlated metal model ( $U \sim 0.4$  eV,  $4t \sim 0.1$  eV) and the Bonner and Fisher Model ( $J = 53$  K,  $g = 2.003$ ). Also indicated is the theoretical curve below the spin-Peierls transition. This figure is from ref. [12].

Bonner and Fisher [11] have calculated numerically the susceptibility as a function of temperature for the spin Hamiltonian given by equation 1.2 for a finite number of spins,  $N$ , with  $2 \leq N \leq 11$ , and the results for  $N \rightarrow \infty$  have been fitted to the electron spin resonance (ESR) and static susceptibilities [12,13]. The results for  $\text{MEM}(\text{TCNQ})_2$  [12] follow the Bonner-Fisher curve above the spin-Peierls transition at 19 K, with an exchange interaction  $J$  of 53 K see figure 3. Two phase transitions have been reported in  $\text{MEM}(\text{TCNQ})_2$  at 20 K and at 335 K [10], which correspond to the  $2k_F$  (the spin-Peierls transition) and  $4k_F$  (the electronic-Peierls transition) transitions respectively.

For  $\text{DEM}(\text{TCNQ})_2$ , Schwerdtfeger *et al.*[13] report values of 45 K and 75 K for  $J$ , corresponding to the inequivalent A and B stacks<sup>2</sup> in  $\text{DEM}(\text{TCNQ})_2$ , and the spin-Peierls phase transition at 23 K in the B stack, with no corresponding phase transition in the A stack. Further phase transitions have been reported in  $\text{DEM}(\text{TCNQ})_2$  at 400 K and 447 K [14] and 483 K [8].

Schwerdtfeger *et al.* also report an unexplained anisotropy in the angular dependence of the relative susceptibility associated with the two ESR lines observed in  $\text{DEM}(\text{TCNQ})_2$ . Similar results have also been reported in  $\text{HMM}(\text{TCNQ})_2$  [15]<sup>3</sup>. Oostra gives a discussion of this phenomenon [4, p. 102], comparing the results for  $\text{DEM}(\text{TCNQ})_2$  and for  $\text{HMM}(\text{TCNQ})_2$ . In  $\text{HMM}(\text{TCNQ})_2$ , unlike  $\text{DEM}(\text{TCNQ})_2$  where the stacks are not related by symmetry, the effect occurs between two stacks that are related by a symmetry operation. The phenomenon always has the high field line vanishing and the low field line growing as the energy level crossing is approached. At the level crossing point there is only one line. The  $g$  values were reported to be close to where the  $g$  values usually reported for a single TCNQ line. Typical ESR spectra for  $\text{DEM}(\text{TCNQ})_2$  at X-band are shown in fig. 4. This leads to the conclusion that the effect is due only to the fact that the energy levels are crossing [4, p. 107, and also 16]. No explanation for the effect was given.

The  $g$  value for the TCNQ salts has typically been found vary from  $g = 2.0023$  to  $g = 2.0036$  depending on the orientation of the crystal. Tomkiewicz *et al.* [16] and Walsh *et al.* [17] have proposed that the  $g$  values only depend on the orientation of the TCNQ molecules with respect to the magnetic field, and not depend on the temperature or on the crystalline environment of the TCNQ molecules. The experimental results from different TCNQ compounds [4, p. 104] indicate that the

<sup>2</sup>The stacks of  $\text{DEM}(\text{TCNQ})_2$  are labelled following reference [13].

<sup>3</sup> $\text{HMM}(\text{TCNQ})_2$  has  $\text{R}=\text{H}$  and a methyl group,  $\text{CH}_3$ , instead of the ethyl group,  $\text{C}_2\text{H}_5$  in fig. 2

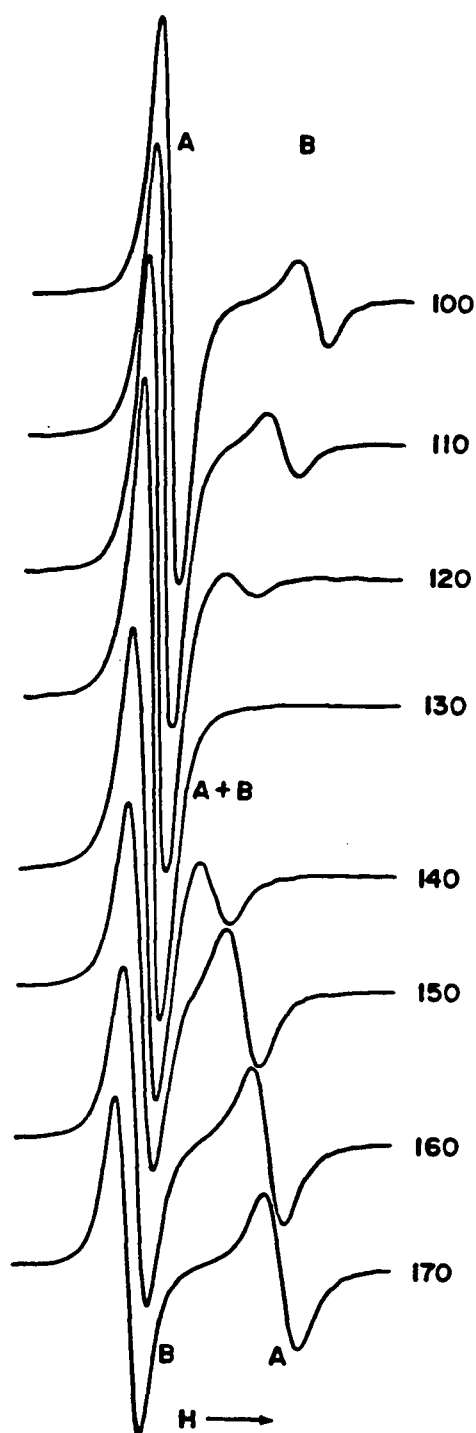


Figure 4: Typical ESR spectra at X-band for  $\text{DEM}(\text{TCNQ})_2$  from ref. [13]. The curves are plotted with the same magnetic field scale, but have been shifted horizontally to emphasize the anisotropy of the susceptibility. The angles correspond to fig. 5 in ref. [13].

orientation of TCNQ molecule itself determines the  $g$  value to a first approximation. It is not clear however that the crystalline environment, or the temperature of the TCNQ molecules can be neglected entirely, particularly when higher accuracy in  $g$  than the  $\pm 0.0004$  allowed for in Tomkiewicz's analysis of TTF-TCNQ [16] is implied. The assertion that the  $g$  values depend only on the orientation of the TCNQ molecules has, for example, been disputed by Conwell [18], who has proposed a systematic trend with temperature in the  $g$  value of  $\text{Qn}(\text{TCNQ})_2$  between 300 K and 1.4 K based upon the data of Clark *et al.* [19]. The data of Clark *et al.* show a difference in the  $g$  value of 0.00011 between their results at 300 K and 1.4 K. This difference, as Conwell points out, is barely outside their quoted experimental error of 0.00005 in each  $g$  value measurements; however Clark *et al.* do not indicate if any part of their error is systematic to all their measurements. If there is a systematic component to this error then this difference in  $g$  value with temperature may be very significant.

### 1.3 Scope of this Thesis

This thesis presents a detailed study of the ESR spectra of  $\text{MEM}(\text{TCNQ})_2$  and  $\text{DEM}(\text{TCNQ})_2$  at 298 K and 77 K. These two materials provide examples of a single stack compound, and a compound with two inequivalent stacks. A further characteristic is that the susceptibility in  $\text{MEM}(\text{TCNQ})_2$  behaves in a manner qualitatively similar to the B stack in  $\text{DEM}(\text{TCNQ})_2$ . An explanation for the anomalous variation with angle of the susceptibility of the individual lines in the TCNQ samples with crossing energy levels is proposed, using  $\text{DEM}(\text{TCNQ})_2$  and  $\text{MEM}(\text{TCNQ})_2$  as models of compounds with and without crossing levels.

A further question we investigated was the variability of the  $g$  value of the TCNQ

compounds with temperature and sample. The two compounds to be studied provide three different TCNQ stacks, that can be studied under the same experimental conditions eliminating most systematic errors when comparisons are made. Another characteristic of these two compounds is that there are no phase transitions between 77 K and 295 K thereby eliminating problems caused by small structural changes [14,8] when comparing the results at 77 K and 295 K.

In chapter 2 we describe the apparatus and the experimental procedure used for the ESR measurements, together with the calculation of the  $g$  tensor from the  $g$  value data for a TCNQ salt. We also consider the assumptions made in relating the  $g$  tensor to the crystal structure.

Chapter 3 contains the ESR results for  $\text{MEM}(\text{TCNQ})_2$ . We find that there is a small but significant change in the  $g$  tensor between 298 K and 77 K, without any change in the direction cosines with respect to a fixed axis. This is indicative of the expected change in the  $g$  value with temperature when there are no phase transitions and no interactions due to more than one kind of stack.

In chapter 4 the theory for an interaction of the form  $\sum_{i,j} J_{i,j} \mathbf{S}_i \mathbf{S}_j$  is developed. It is found that for a constant  $J$  the theory agrees well with the experimental results. Another prediction of the theory is that the halfwidth of the stronger line will vanish at the crossover. This was not found experimentally; however the measurement of the halfwidth of a line with vanishing halfwidth is not reliable because of saturation and overmodulation effects.

Chapter 5 contains the ESR results for  $\text{DEM}(\text{TCNQ})_2$ . Apart from the agreement with the theory we find that, after correcting for the interaction between the different stacks, the  $g$  tensors for the different stacks are not the same. There is also a small but significant change in the measured  $g$  values between 298 K and 77 K, similar to that observed in  $\text{MEM}(\text{TCNQ})_2$ . The bulk of the difference between the

measured results at 298 K and 77 K is however due to the interaction between the different stacks, and can be accounted for by the theory. We also find that  $J$  has the same temperature dependence as the total susceptibility.

Measurements with respect to power are presented in chapter 6. We show that in the region close to the overlap the line is saturated and overmodulated. The source of the overmodulation is the modulation of the microwave frequency by the Automatic Frequency Control (AFC). This indicates that the single line at the crossover point may be extremely narrow, and could even have a vanishing halfwidth in agreement with the theory.

In chapter 7 we discuss the results, and compare our measurements with other published results. We find that the variation of the susceptibility with angle for the level crossing TCNQ compounds can be explained by a relatively simple theory in terms of an interaction between the different stacks of the form  $J \sum_{i,j} \mathbf{S}_i \mathbf{S}_j$ . We also find that in general there are small but measurable differences in the  $g$  tensors of TCNQ molecules in different environments, and for the same compound at different temperatures.

## Chapter 2

### The ESR Experiment

#### 2.1 The ESR Apparatus

The ESR experiments were performed at Q-band using a cylindrical cavity operating in the  $TE_{012}$  mode at a frequency of approximately 36 GHz. The microwave source was an OKI 35V10 klystron, whose reflector voltage was controlled by an automatic frequency control circuit operating at 33 kHz. This phase locked the frequency to the cavity resonance. The reflected power was then detected with a HP R422A diode. The absorption signal was first passed through a preamplifier, and then detected with an Ithaco Dynatrac 391 lock-in amplifier, phase locked to the magnetic field modulation frequency of 2 kHz. The spectrum obtained is then the derivative of the absorption signal.

To measure the Q-band frequency an X-band frequency of approximately 8.6 GHz was generated using a Varian V153 klystron. The reflector voltage of the klystron was controlled by an automatic frequency control circuit operating at 10 kHz, which phase locked the X-band frequency to a tunable cavity. This cavity was tuned such that the fourth harmonic of the X-band frequency was about 5-10 MHz away from the Q-band resonance. The X-band frequency was then counted with a HP 5245L frequency counter with a HP 5255A frequency converter. The beat frequency formed

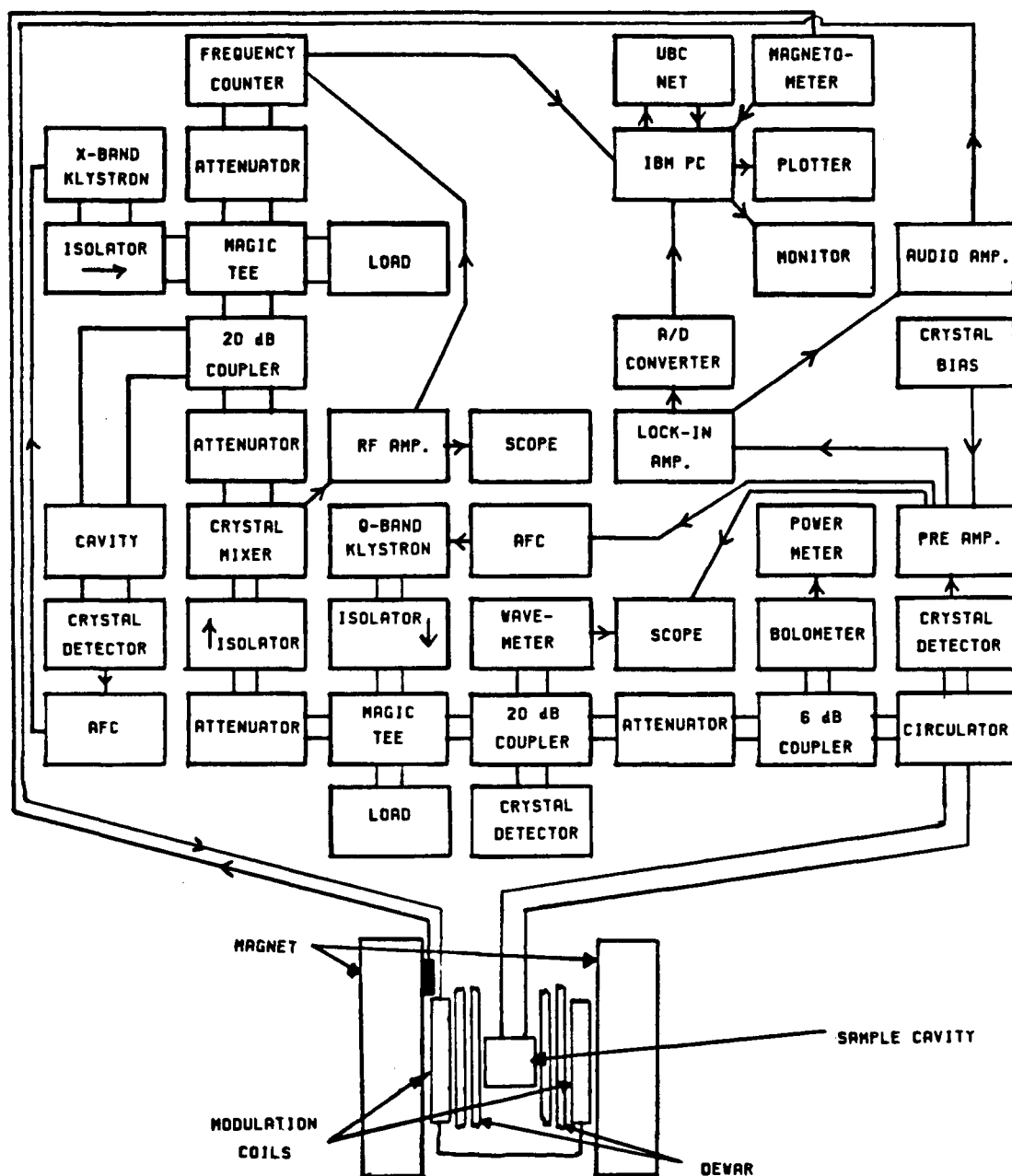


Figure 5: The ESR spectrometer

when the fourth harmonic of the X-band frequency was mixed with the Q-band frequency was also counted with the HP counter. This allowed the measurement of the Q-band cavity frequency to about 30 kHz.

The magnetic field was generated using a Varian V-3601 12 in. electromagnet operating at approximately 12.3 kilogauss. The magnet was powered using a Varian V-2800 Fieldial Mark 1 power supply, and was stabilized using a Hall probe feedback circuit. The magnetic field was swept over the ESR resonances, with a typical sweep of 8 gauss. The magnetic field was calibrated using a sample of LiF:Li, with  $g = 2.002317(2)$ [20], that was mounted next to the samples to be measured. The sweep was calibrated using a SENTEC type 1000 NMR magnetometer. Typical spectra of  $\text{DEM}(\text{TCNQ})_2$  are shown in fig. 6.

## 2.2 Experimental Method

A problem that has been reported with ESR measurements in the TCNQ salts at Q-band is the choice of the sample size[4, p. 108]. In particular it was reported that the AFC could not follow the sample resonance because of the strong and narrow lines that are found in these materials. We found that in order to avoid this problem the sample volume had to be no larger than approximately  $0.0001\text{mm}^3$ . For samples this small it is difficult to obtain any reliable absolute orientation of the crystal in the magnetic field. In order to obtain relative measurements the sample to be measured and the calibration sample were mounted with silicon grease on a cube of lucite that was 1mm on each side. All the measurements were then made with respect to the cube. The coordinates of the crystal axes can, in certain circumstances, be related to the coordinates of the cube by making use of the orientation of the TCNQ stacks with respect to the coordinates of the cube. This relationship can be determined

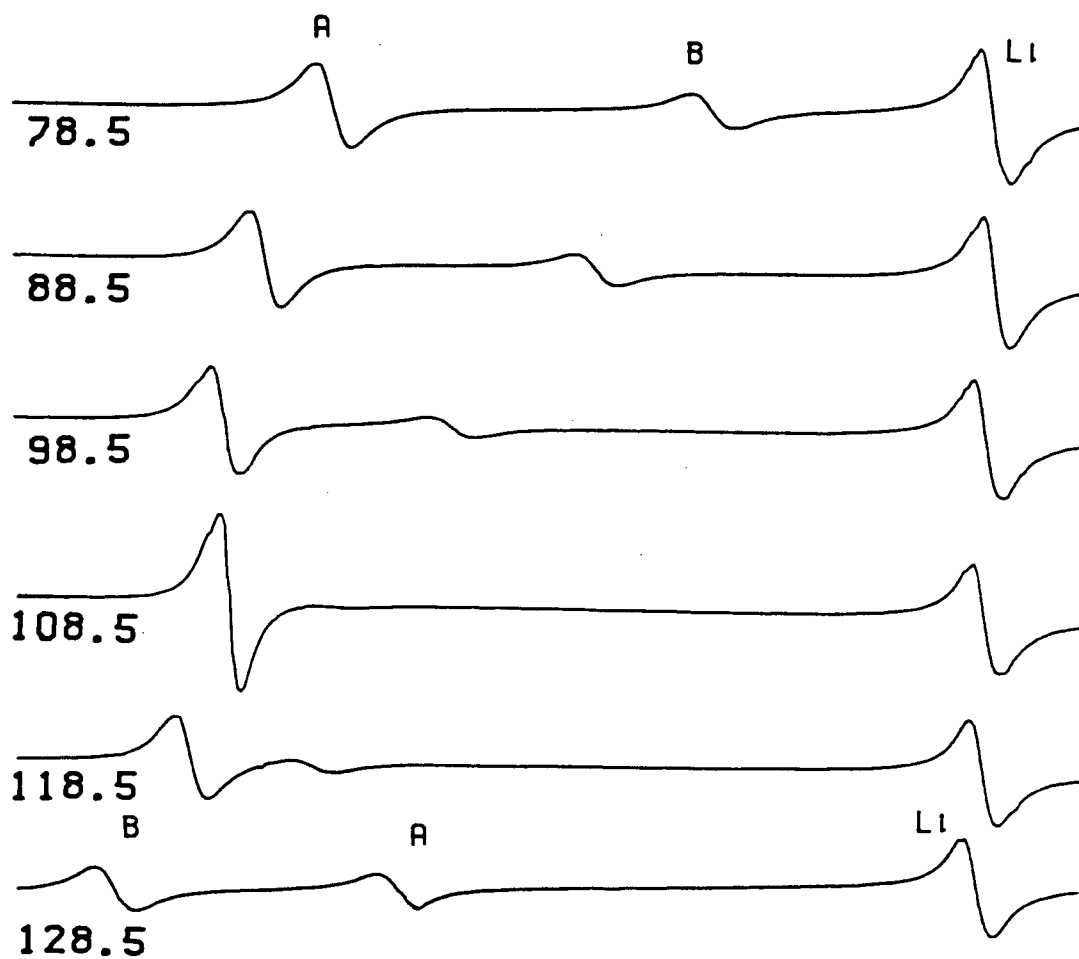


Figure 6: Typical spectra of  $\text{DEM}(\text{TCNQ})_2$  at 298 K. The letters A, B, and Li refer to the lines that are dominated by the A and B stacks of  $\text{DEM}(\text{TCNQ})_2$  and to the line due to the LiF:Li calibration

from the  $g$  value measurements.

The cube was then mounted on the end of a long rod, and then inserted into the microwave cavity through a hole at the top on the cavity axis. The rod could be then rotated from the top of the dewar system. This method allowed the angle of rotation to be determined to an accuracy of 0.1 deg. The sample was then rotated with respect to the magnetic field through an angle of 180 deg, along three orthogonal axes. The ESR spectra were obtained in one degree increments for DEM-(TCNQ)<sub>2</sub>, and every five degrees for MEM(TCNQ)<sub>2</sub>. The data were digitized and collected by an IBM-PC microcomputer. The computer was also used to record the frequency of the X-band reference before and after the run, and the beat frequency during the run. Since the X-band reference does not change during the run the measurement of the beat frequency during the run actually provides a measure of the dispersion of the ESR signal. The average value of the beat frequency was used in the calculation of the resonance frequency of the ESR cavity. Apart from error estimation no further use of the dispersion data was made, since it was in general much more noisy than the absorption data.

For the TCNQ salts a Lorentzian lineshape was assumed since a Lorentzian lineshape has been reported at X-band, consequently the spectra were then fit to a Lorentzian derivative for each line observed in the TCNQ sample. No assumptions as to the position of the lines or the relative strengths of the lines were made. The LiF:Li line was fitted to a Dysonian lineshape, since a slightly asymmetric line would be expected for the Li metal domains in the LiF. The  $g$  values, relative susceptibilities and halfwidth of the spectra were obtained from the parameters of the Lorentzian lines that gave the best fit to the spectra. The experimental method does not provide accurate values of the absolute susceptibility as a function of angle, since the microwave power at the sample and the Li calibration crystal

change as the sample is rotated in the cavity. This occurs because the size of the cube on which the samples are mounted is significant enough to change the position of the samples in the cavity mode when the cube is rotated. The method does provide however reliable results for relative measurements of the susceptibility as a function of power or of temperature at a fixed angle.

### 2.3 Determination of the $g$ Tensor

In general the  $g$  tensor of an arbitrary crystal has the form of a symmetric second-rank tensor. We propose to determine first the principal values, and the corresponding direction cosines with respect to the arbitrary coordinates of the cube. In determining the  $g$  tensor we follow the method of Waller and Rogers [21], using orthogonal rotation axes. The method requires in our case three rotations,  $\theta_a$ ,  $\theta_b$ , and  $\theta_c$ , about three orthogonal axes,  $\mathbf{a}$ ,  $\mathbf{b}$ , and  $\mathbf{c}$ , forming a right-handed coordinate system. The axes  $\mathbf{a}$ ,  $\mathbf{b}$ , and  $\mathbf{c}$  would form a cyclical relationship such that the position  $\theta_a = 90^\circ$  is equivalent to  $\theta_b = 0^\circ$ ,  $\theta_b = 90^\circ$  is equivalent to  $\theta_c = 0^\circ$ , and  $\theta_c = 90^\circ$  is equivalent to  $\theta_a = 0^\circ$ . The  $g$  value data are parameterized as follows:

$$g_i^2 = \alpha_i + \beta_i \cos 2\theta_i + \gamma_i \sin 2\theta_i \quad (2.1)$$

where  $i = a, b, \text{ or } c$ . The values of  $\alpha_i$ ,  $\beta_i$ , and  $\gamma_i$  are then used to calculate the  $W$  tensor, where  $\overline{\overline{\mathbf{W}}} = \overline{\overline{\mathbf{g}^2}}$ , using the equations:

$$\begin{aligned} W_{11} &= \alpha_a + \beta_a & W_{22} &= \alpha_b + \beta_b & W_{33} &= \alpha_c + \beta_c \\ W_{11} &= \alpha_a - \beta_a & W_{22} &= \alpha_b - \beta_b & W_{33} &= \alpha_c - \beta_c \\ W_{12} &= W_{21} = \gamma_a & W_{23} &= W_{32} = \gamma_b & W_{13} &= W_{31} = \gamma_c \end{aligned} \quad (2.2)$$

The diagonal elements,  $W_{ii}$ , are overdetermined by equations 2.2. Waller and Rogers provide an iterative method to calculate the error,  $\delta\theta_i$ , in the azimuthal angles,

or starting angle shift [21, p. 93], using this overdetermination of the  $W_{ii}$ . This correction is about 20 deg in our case, and cannot be neglected. The iterative solution involves first calculating the following error functions

$$\begin{aligned}\Delta_a &= (\alpha_c - \alpha_b - \beta_a)/\gamma_a \\ \Delta_b &= (\alpha_a - \alpha_c - \beta_b)/\gamma_b \\ \Delta_c &= (\alpha_b - \alpha_a - \beta_c)/\gamma_c\end{aligned}\tag{2.3}$$

A new set of parameters are then calculated using the equations

$$\begin{aligned}\alpha'_i &= \alpha_i \\ \beta'_i &= \beta_i \cos \Delta_i + \gamma_i \sin \Delta_i \\ \gamma'_i &= \gamma_i \cos \Delta_i - \beta_i \sin \Delta_i\end{aligned}\tag{2.4}$$

The new parameters are used again to obtain a new set of  $\Delta_i$  until the values of the error functions become negligible. The starting angle shifts,  $\delta\theta_i$ , are then obtained by continually summing  $\Delta_i/2$  throughout the iteration process. The  $W$  tensor is then calculated using the final values of  $\alpha_i$ ,  $\beta_i$  and  $\gamma_i$  from equations 2.2, and is then diagonalized to obtain the principal values and the corresponding direction cosines. The principal values of the  $g$  tensor are then the square-roots of the principal values of the  $W$  tensor. In our experiment we are making measurements at both 77 K and 298 K, using the same orientation of the crystal with respect to the cube and the same starting angles. This allowed a further overdetermination of the  $W$  tensor elements by using the same  $\delta\theta_i$  for both the 77 K and the 298 K measurements. These extra data were used to obtain an estimate of the error in the  $\delta\theta_i$ .

## 2.4 Correlation of the $g$ Tensor to the Crystal Structure

In order to consider the correlation of the direction cosines corresponding to the principal values of the  $g$  tensor with the crystal structure, we first assume that the

$g$  tensor is determined only by the TCNQ molecules. The TCNQ molecule itself is planar and has orthogonal symmetry. We can define three vectors  $\mathbf{M}$ ,  $\mathbf{L}$ , and  $\mathbf{N}$  on the TCNQ molecule as follows:  $\mathbf{M}$  is chosen in the plane of the TCNQ molecule and along the short axis of the molecule.  $\mathbf{L}$  is chosen in the plane of the molecule and along the long axis of the molecule. Finally  $\mathbf{N}$  is chosen normal to the plane of the molecule. The vectors  $\mathbf{M}$ ,  $\mathbf{L}$ , and  $\mathbf{N}$  are then orthogonal because of the orthogonal symmetry of the TCNQ molecule. It would then follow by symmetry that the principal values of the  $g$  tensor would be the  $g$  values  $g_M$ ,  $g_L$ , and  $g_N$ , with the magnetic field parallel to  $\mathbf{M}$ ,  $\mathbf{L}$ , and  $\mathbf{N}$  respectively. The direction cosines can then be related to the crystal coordinates by identifying the measured principal values of the  $g$  tensor with the values  $g_M$ ,  $g_L$ , and  $g_N$ , found for other TCNQ compounds in the literature and by using the known crystal structure of the compounds under study[8,9]. A collection of such  $g$  values is provided, for example by Oostra[4, p. 104]. Typical values would be  $g_M = 2.00359$ ,  $g_L = 2.00276$ , and  $g_N = 2.00234$ <sup>1</sup>.

There is a significant limitation to this method in that the assumption is made that the  $g$  tensors of TCNQ compounds are not dependent upon the environment of the TCNQ molecules. The error introduced by this assumption can be estimated from the variation of the principal values of the  $g$  tensor from compound to compound. In particular the change in orientation that causes a change in the  $g$  tensor in one compound equal to the difference in the  $g$  tensor between compounds would be an estimate of this error. It should be stressed that this is an error in the interpretation of the principal values of the  $g$  tensor as  $g_M$ ,  $g_L$ , and  $g_N$  and not in the principal values or the direction cosines of the  $g$  tensor.

In the case of compounds with inequivalent TCNQ stacks, an independent check on the assumption that the  $g$  tensor is independent of the environment of the TCNQ

---

<sup>1</sup>These  $g$  values are the average for the  $g$  values quoted by Oostra[4, p. 104]

molecules can be made by comparing the relative orientation of the principal values of the  $g$  tensor with the relative orientation of the TCNQ molecules. If the  $g$  tensor is indeed independent of the environment of the TCNQ molecules, then the two relative orientations should agree. This comparison will be made in the section on the discussion of the DEM(TCNQ)<sub>2</sub> measurements.

## Chapter 3

### MEM(TCNQ)<sub>2</sub> Results

#### 3.1 The $g$ value Measurements

The ESR measurements were performed on MEM(TCNQ)<sub>2</sub> at both 77 K and 298 K by the method explained in chapter 2. The  $g$  values for rotations about **a**, **b**, and **c** are shown in figures 7 to 9 for the 298 K measurements and in figures 10 to 12 for the 77 K measurements. The  $g$  value data were parametrized using equation 2.1 and the resulting values for  $\alpha_i$ ,  $\beta_i$  and  $\gamma_i$  were used to calculate the  $g$  tensor principal values and corresponding direction cosines using the method of section 2.3. These results are shown in tables I and II for the 298 K and 77 K measurements respectively.

The experimental errors in the  $g$  tensors arise from various sources. We first consider the calibration errors. The first is the quoted experimental error in the

Principal Values	Direction Cosines		
	a	b	c
2.002318(7)	-0.412(4)	-0.682(3)	0.605(1)
2.002770(7)	-0.900(1)	0.409(2)	-0.152(9)
2.003332(8)	0.144(8)	0.607(4)	0.782(2)

Table I: Principal Values and Direction Cosines for the  $g$  Tensor of MEM(TCNQ)<sub>2</sub> at 298 K

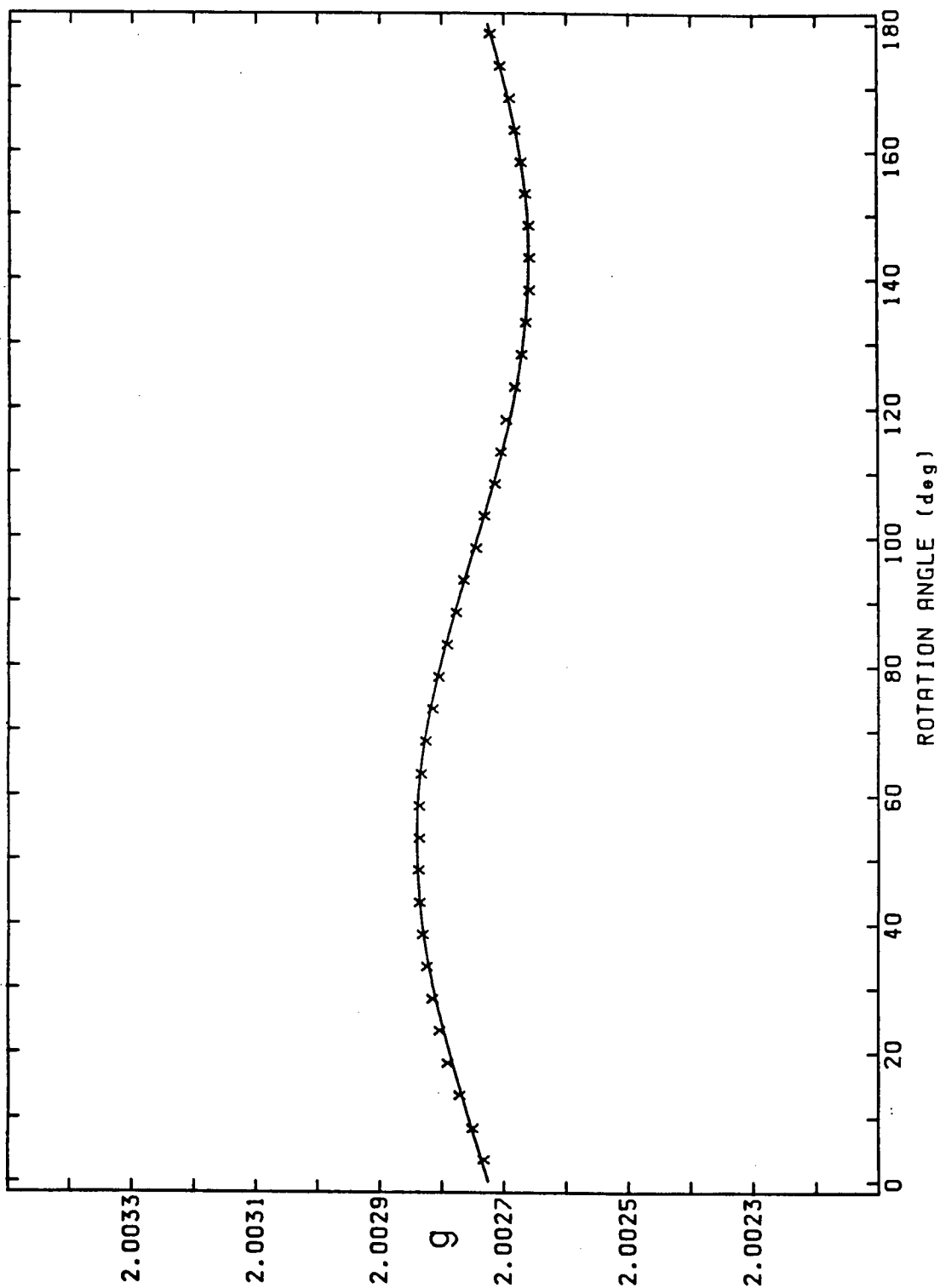


Figure 7:  $g$  Value of  $\text{MEM}(\text{TCNQ})_2$  for a rotation about  $a$  at 298 K. The solid line is a fit to equation 2.1

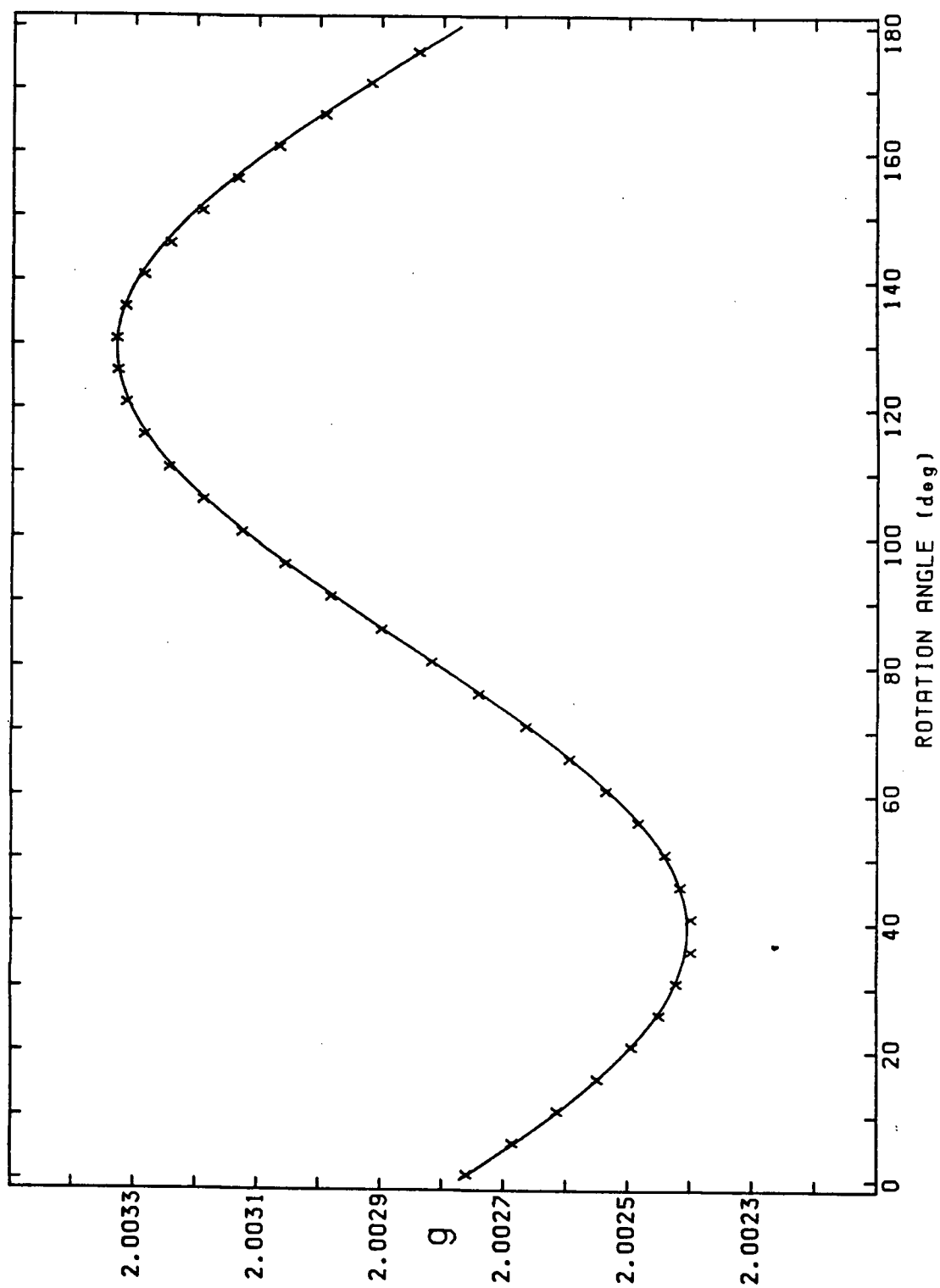


Figure 8:  $g$  Value of  $\text{MEM}(\text{TCNQ})_2$  for a rotation about  $b$  at 298 K. The solid line is a fit to equation 2.1

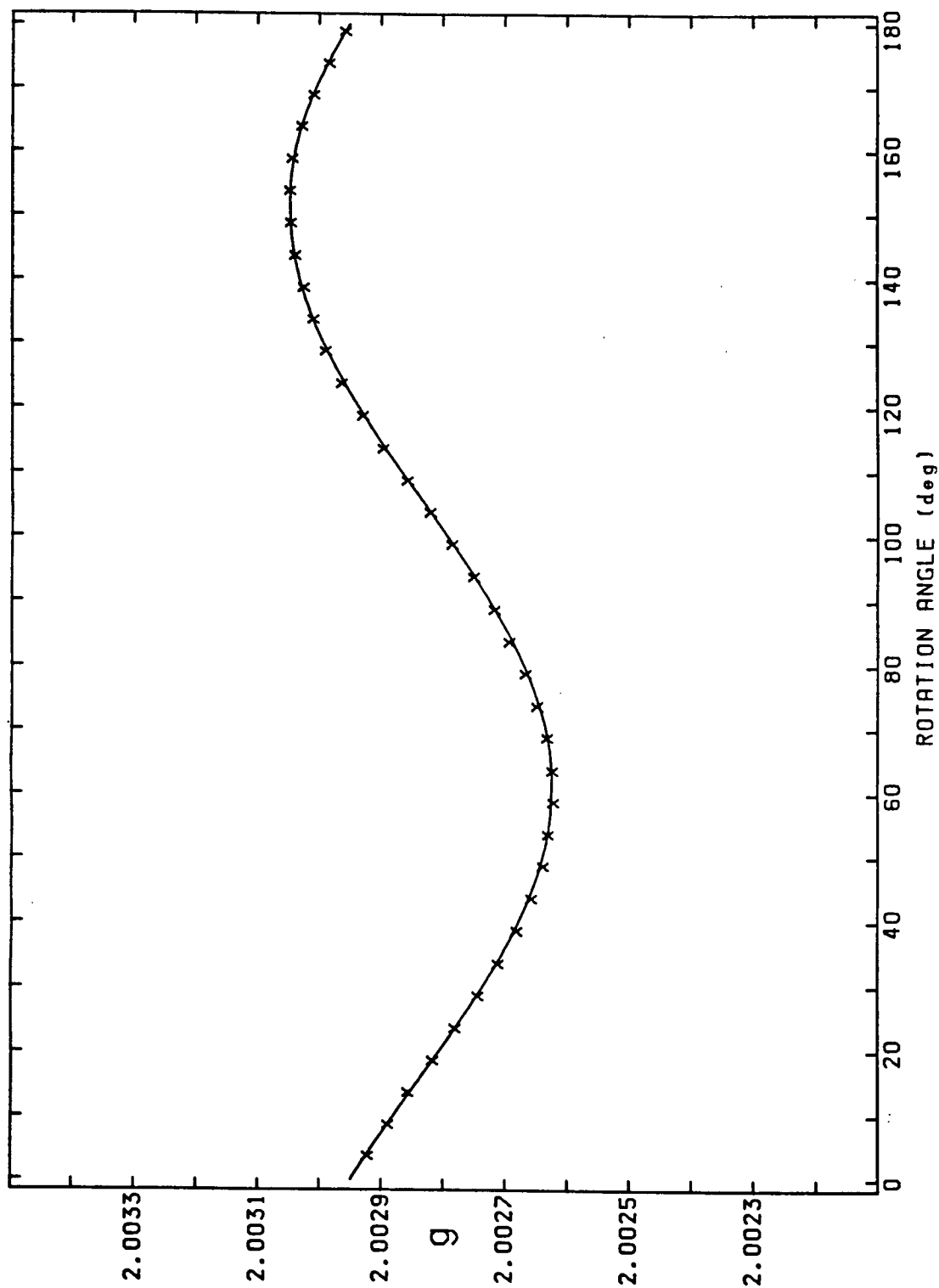


Figure 9:  $g$  Value of  $\text{MEM}(\text{TCNQ})_2$  for a rotation about  $c$  at 298 K. The solid line is a fit to equation 2.1

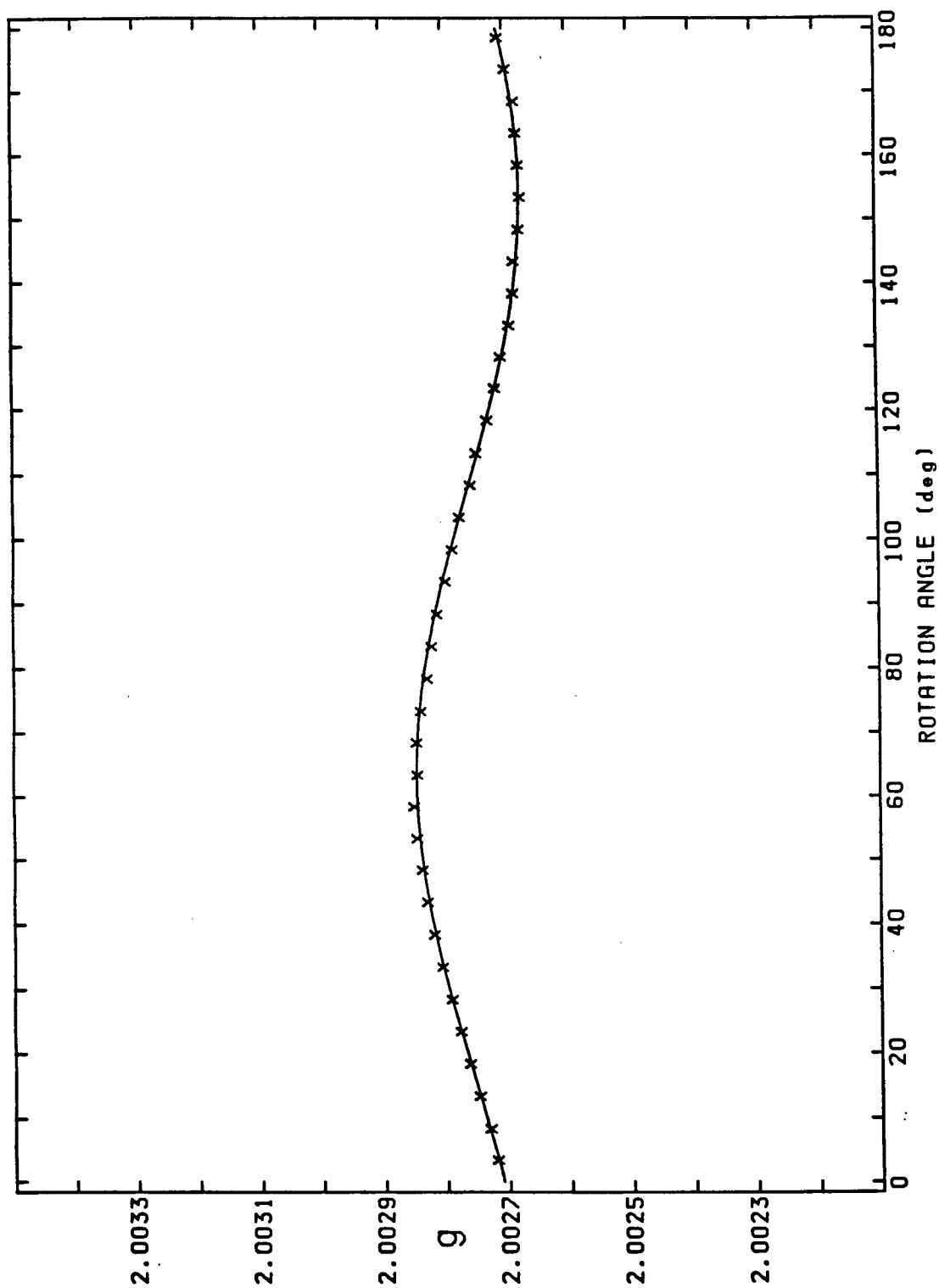


Figure 10:  $g$  Value of  $\text{MEM}(\text{TCNQ})_2$  for a rotation about  $a$  at 77 K. The solid line is a fit to equation 2.1

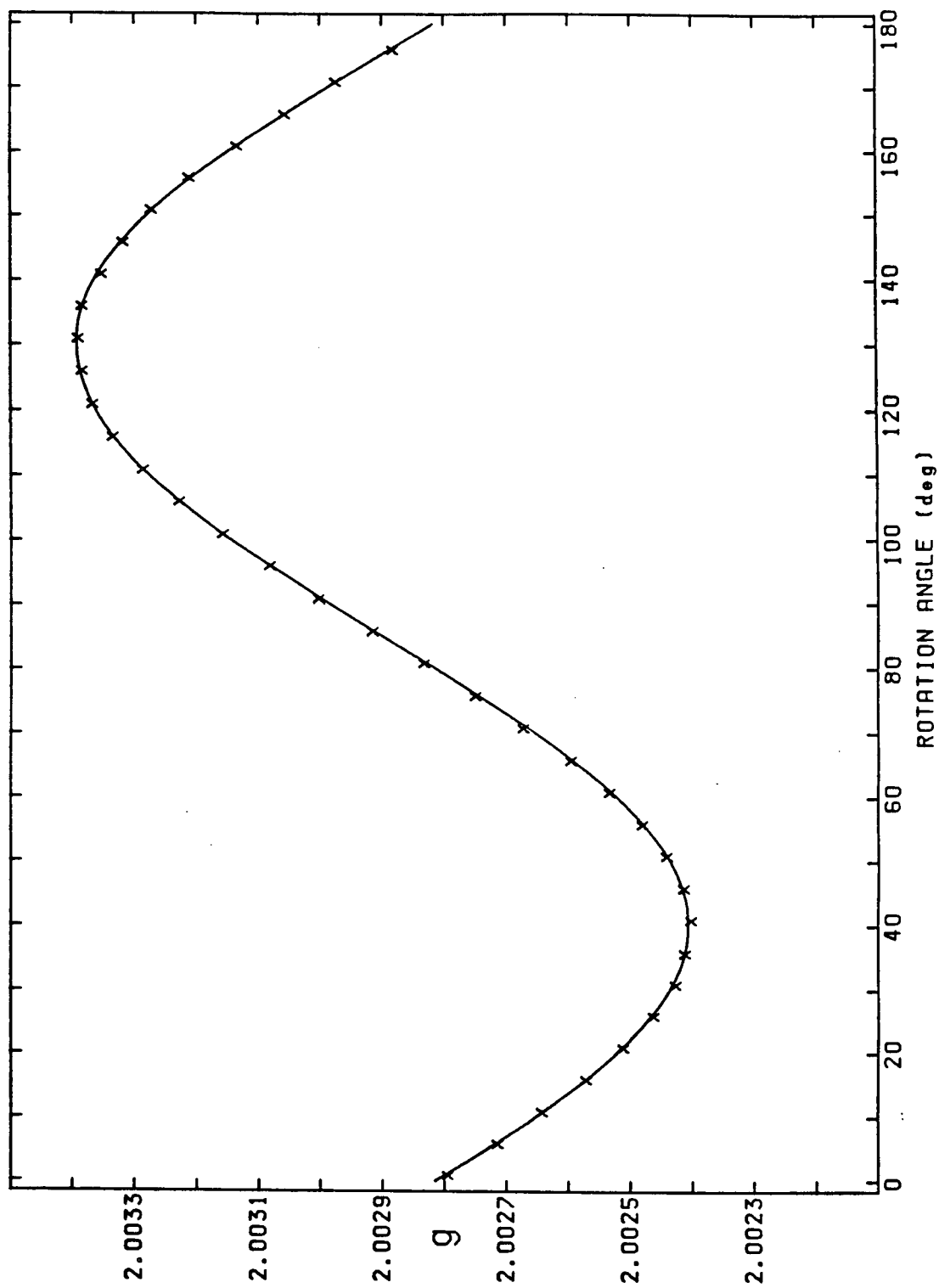


Figure 11:  $g$  Value of  $\text{MEM}(\text{TCNQ})_2$  for a rotation about  $b$  at 77 K. The solid line is a fit to equation 2.1

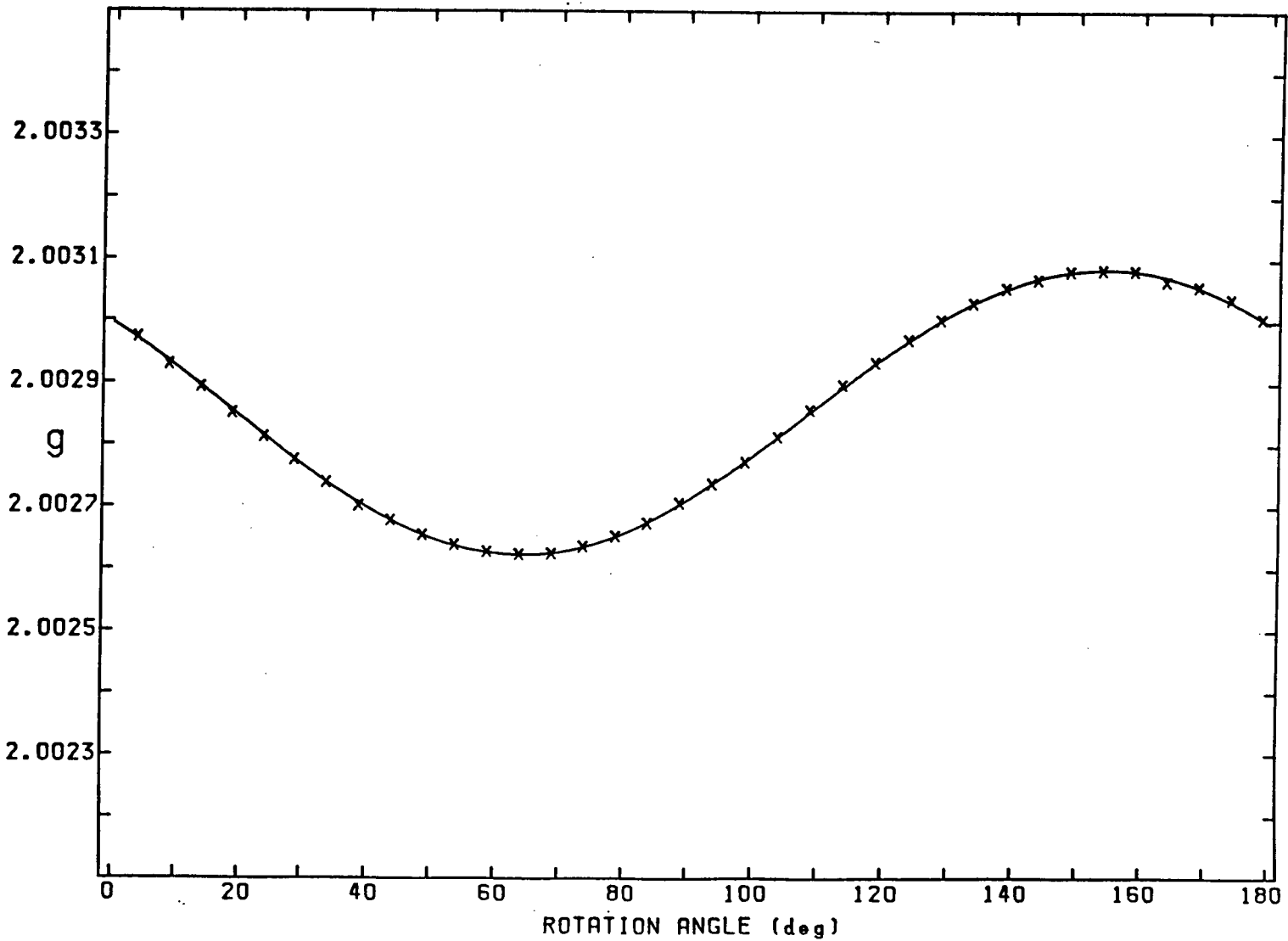


Figure 12:  $g$  Value of MEM(TCNQ)<sub>2</sub> for a rotation about  $c$  at 77 K. The solid line is a fit to equation 2.1

Principal Values	Direction Cosines		
	a	b	c
2.002333(7)	-0.420(3)	-0.673(3)	0.609(2)
2.002776(6)	-0.897(1)	0.411(1)	-0.164(6)
2.003413(8)	0.140(4)	0.615(4)	0.776(2)

Table II: Principal Values and Direction Cosines for the  $g$  Tensor of MEM(TCNQ)<sub>2</sub> at 77 K

calibration sample  $g$  value. This error is  $2 \times 10^{-6}$  and is systematic to all the measurements. A second source of calibration errors arises from the inhomogeneity of the magnetic field over the separation of the calibration and the MEM(TCNQ)<sub>2</sub> samples. This separation is about 0.2 mm. An estimate of the maximum magnetic field inhomogeneity was made by placing two Li calibration samples 0.5 cm apart in the cavity and then performing an ESR experiment. The measured difference in the  $g$  values of the two lines is a measure of this inhomogeneity. This difference was found to be less than  $4 \times 10^{-5}$ . For the actual separation between the calibration and MEM(TCNQ)<sub>2</sub> samples this inhomogeneity in the magnetic field leads to an error in the measured  $g$  values of MEM(TCNQ)<sub>2</sub> of less than  $2 \times 10^{-6}$ . The last calibration error arises from the calibration of the magnetic field sweep. This was estimated to result in an error in the  $g$  values between  $1 \times 10^{-7}$  and  $6 \times 10^{-7}$  depending upon the difference in  $g$  value between the MEM(TCNQ)<sub>2</sub> and the calibration samples. This estimate of the sweep error was obtained from repeated calibration of the magnetic field sweep with the SENTEC NMR magnetometer.

The most significant source of errors comes from the alignment of the cube so that the axis of rotation is perpendicular to one of the planes of the cube. This is in fact an error in the orthogonality of the rotation axes. In order to calculate this error we kept the  $\delta\theta$ , the same for both the 77 K and 298 K results. The inconsistency in the  $g$  values produced from the deviation from orthogonality of the

rotation axes will lead to different results for the  $\delta\theta_i$  for each of the results at 77 K and 298 K. An estimate of the error in the principal values and the corresponding direction cosines was made by solving for the principal values and direction cosines of the  $g$  tensor at each temperature using the results for  $\delta\theta_i$  of both temperatures, and also the average results for  $\delta\theta_i$ . The difference in the resulting principal values and direction cosines, at each temperature, provided an estimate of the error. The values quoted in tables I and II were calculated using the average values for  $\delta\theta_i$ . The error in  $g$  from this source was found to be between  $5 \times 10^{-6}$  and  $7 \times 10^{-6}$ . In the direction cosines this error is the actual quoted error in tables I and II. These error estimates in the  $g$  values from this source were compared to the differences in the measured  $g$  values for MEM(TCNQ)<sub>2</sub>, at either 77 K or 298 K, between the equivalent positions mentioned in section 2.3 and were found to agree.

The random errors in  $\alpha_i$ ,  $\beta_i$ , and  $\gamma_i$  that arise from the fit of equation 2.1 to the data are much smaller than the above errors and consequently were neglected.

### 3.2 The Halfwidth Measurements

The halfwidth of the spectra mentioned in the previous section are presented in figures 13 to 18. The experimental errors in the halfwidth are dominated by the error in fitting the spectra to a Lorentzian line. These errors are statistical in nature and are manifested in the scatter of the data points. The only systematic error one can consider is the magnetic field sweep calibration error. This error is 0.05% of the magnetic field sweep, and consequently is negligible when compared to the statistical error of the fit.

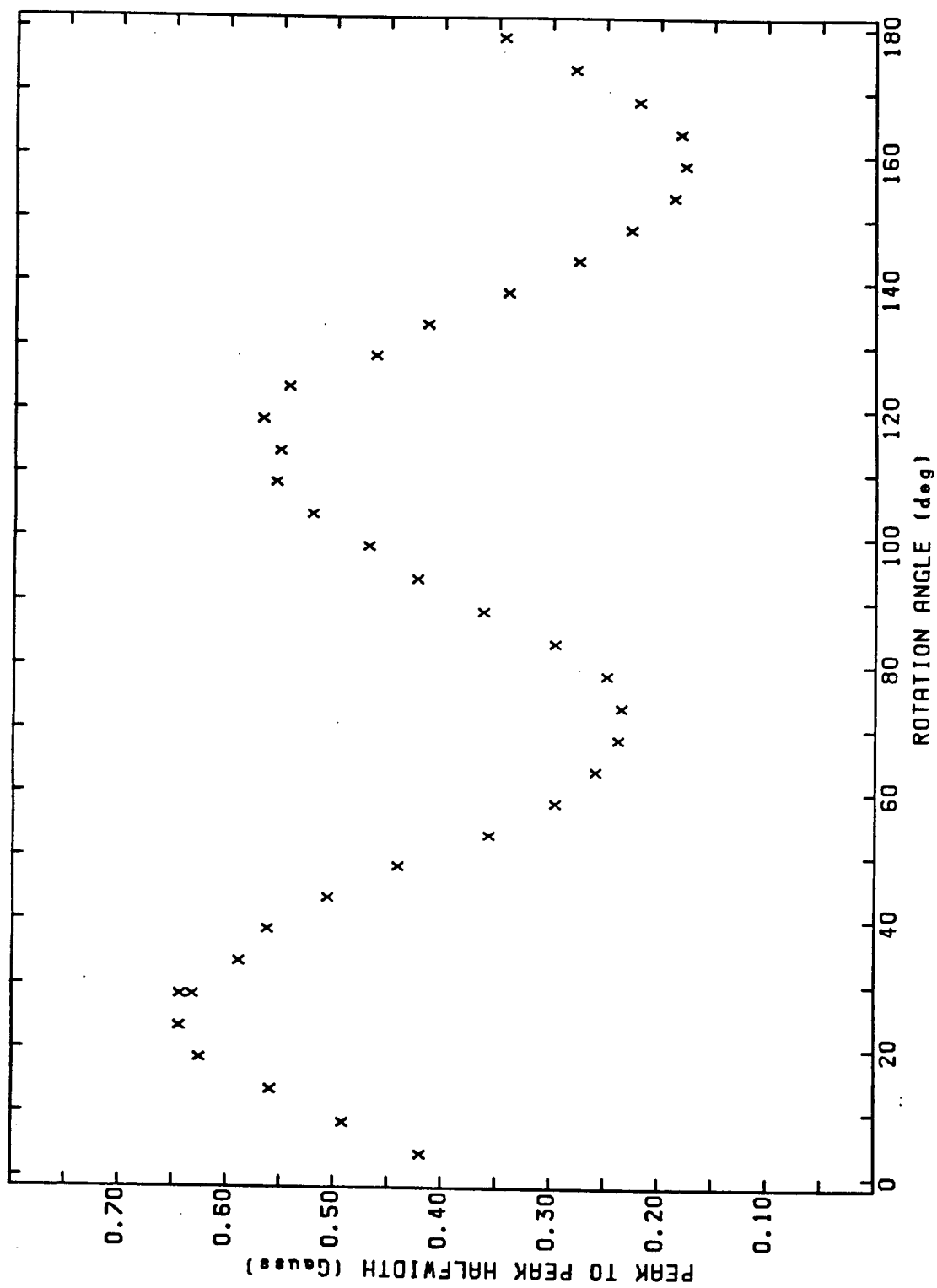


Figure 13: Peak to peak halfwidth of MEM(TCNQ)<sub>2</sub> for a rotation about a at 298 K

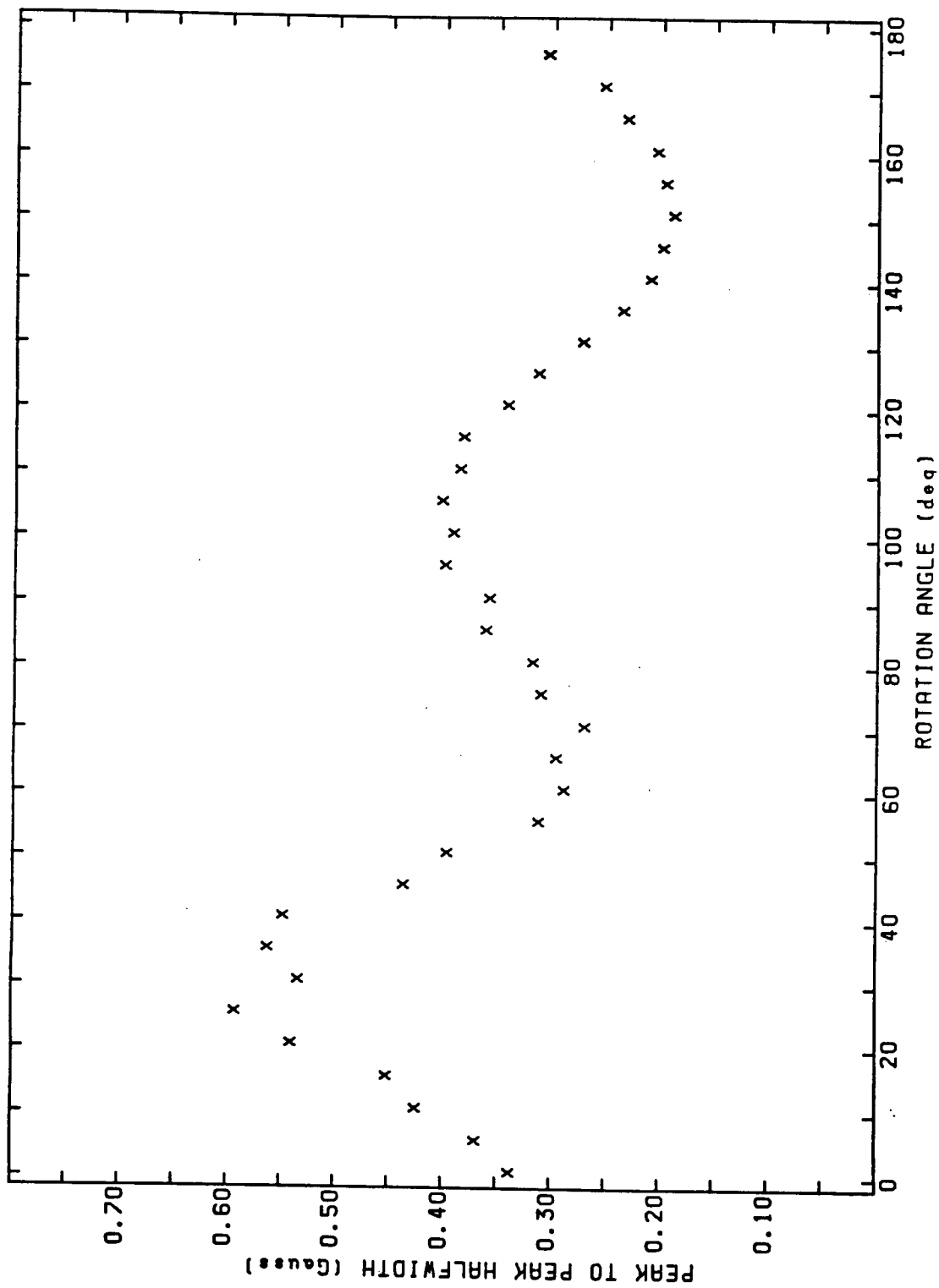
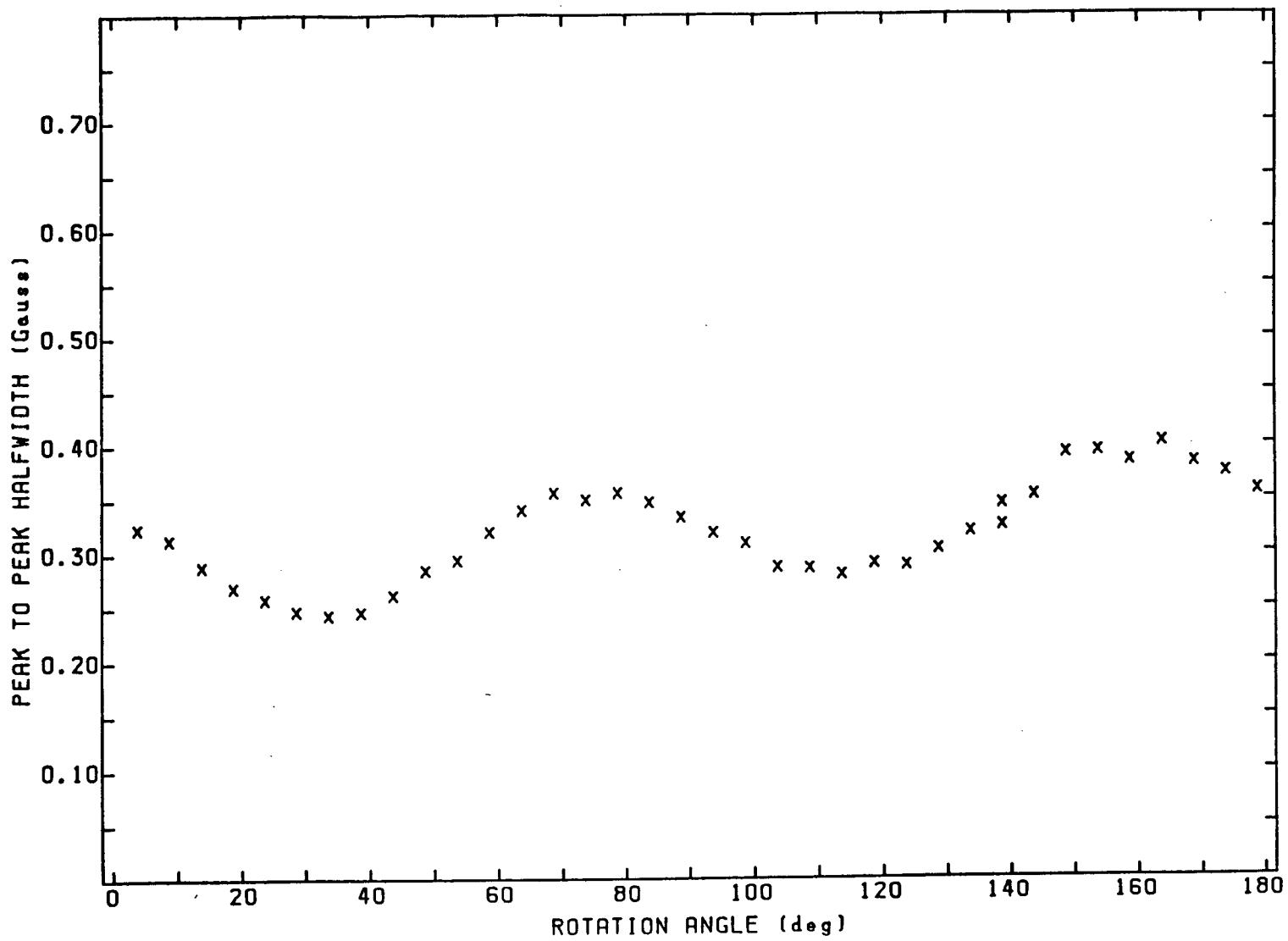


Figure 14: Peak to peak halfwidth of MEM(TCNQ)<sub>2</sub> for a rotation about b at 298 K

Figure 15: Peak to peak halfwidth of MEM(TCNQ)<sub>2</sub> for a rotation about c at 298 K



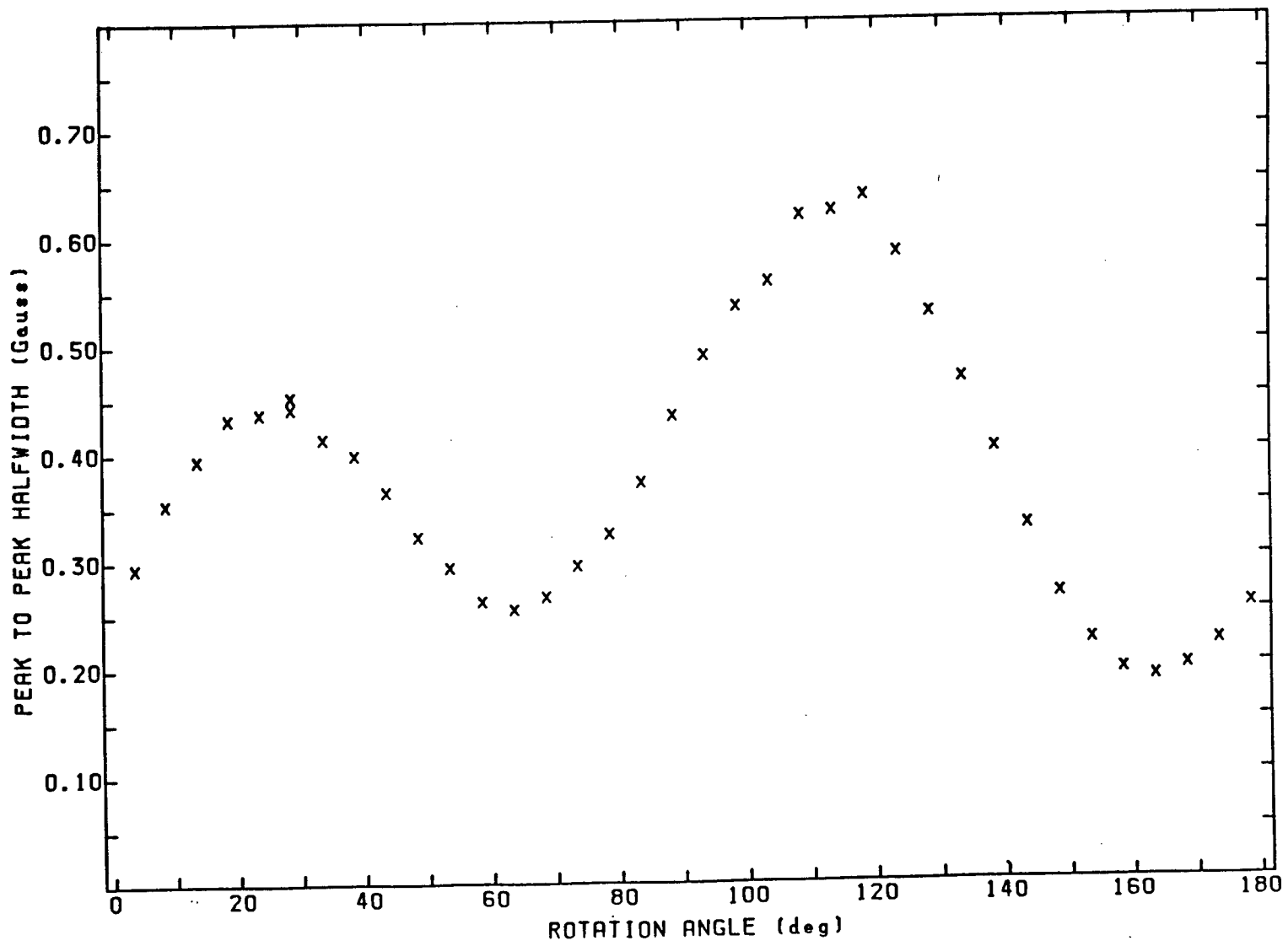


Figure 16: Peak to peak halfwidth of MEM(TCNQ)<sub>2</sub> for a rotation about a at 77 K

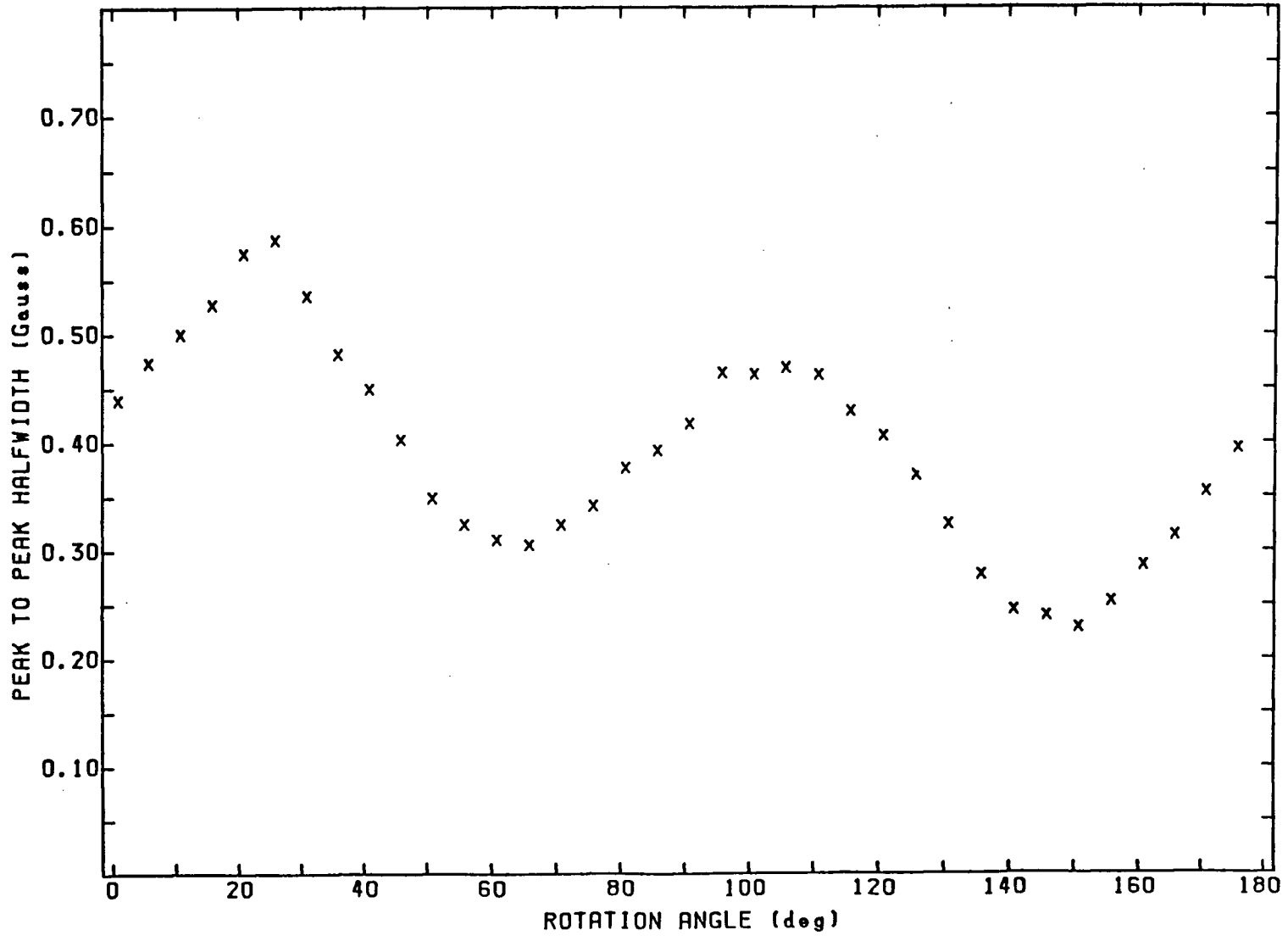
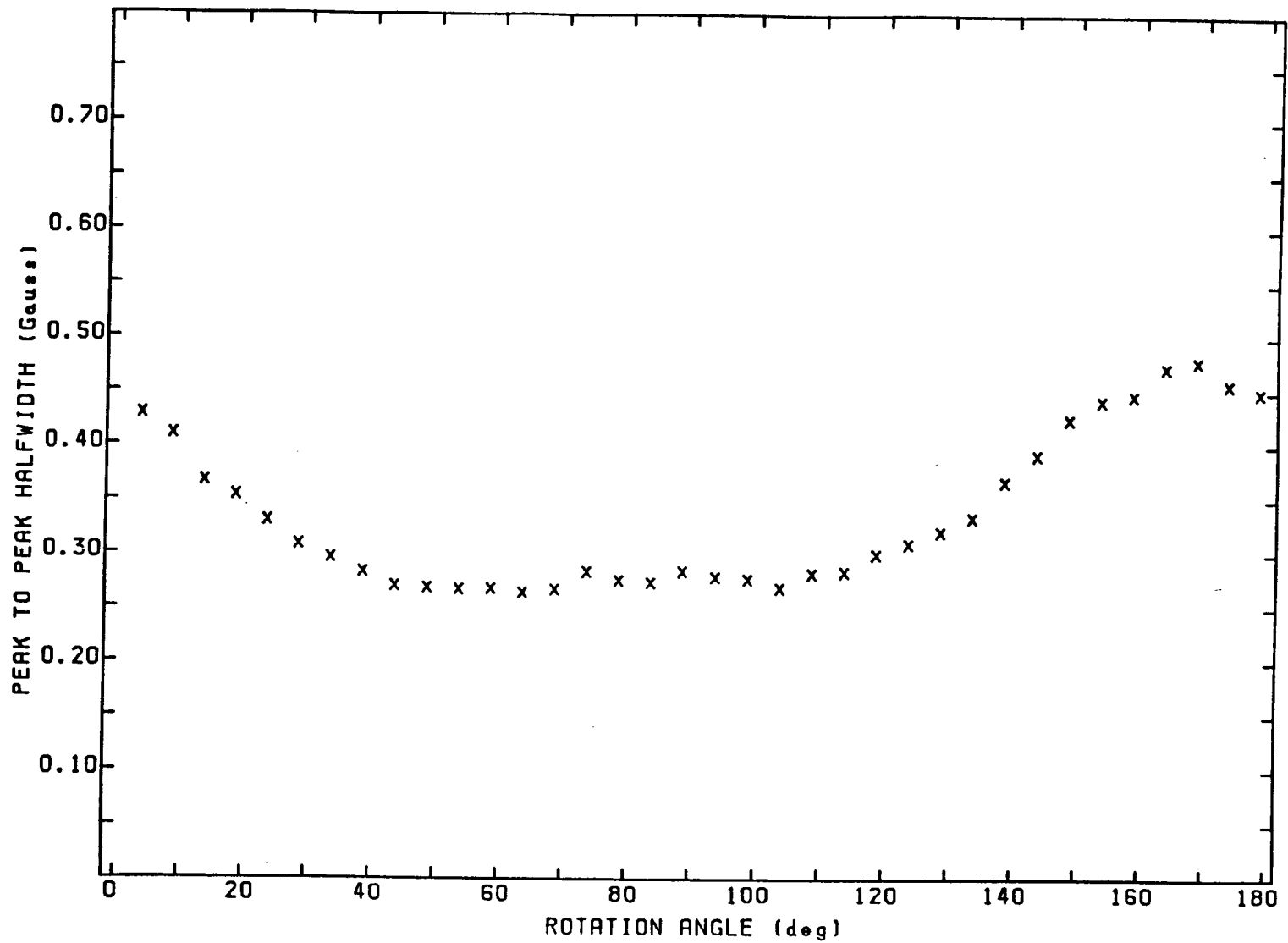


Figure 17: Peak to peak halfwidth of MEM(TCNQ)<sub>2</sub> for a rotation about b at 77 K

Figure 18: Peak to peak halfwidth of MEM(TCNQ)<sub>2</sub> for a rotation about c at 77 K



### 3.3 Discussion of the Results

The  $g$  tensor principal values at 298 K are quite close to the results at 77 K, but there is a significant difference that cannot be accounted for by the experimental errors. The corresponding direction cosines on the other hand are the same for the 298 K and 77 K results. This indicates that there is some variation with temperature of the  $g$  tensor that cannot be attributed to a structural change in the crystal. The  $g$  tensor principal values were found to be close to the average values for  $g_M$ ,  $g_L$ , and  $g_N$ , that are quoted by Oostra[4, p.104]. The difference is however significantly more than our experimental errors. There is an indication from the MEM(TCNQ)<sub>2</sub> results alone that the  $g$  tensors do depend on the environment of the TCNQ molecules; however this matter should be considered together with the DEM(TCNQ)<sub>2</sub> results. The temperature dependence of the linewidth in MEM(TCNQ)<sub>2</sub> has been discussed by Huizinga[3, p. 119]. Our results at 298 K are qualitatively the same as Huizinga's. A quantitative comparison is not feasible because the rotation axes are not the same. There is a significant difference between our results at 298 K and 77 K. This is in qualitative agreement with the behaviour that Huizinga observes.

## Chapter 4

### Theory for Salts with Crossing Energy Levels

#### 4.1 Introduction

Anomalous effects in the susceptibilities of individual stacks for TCNQ salts with more than one kind of stack was first reported in  $\text{DEM}(\text{TCNQ})_2$  by Schwerdtfeger *et al.* [22,13]. A satisfactory explanation of this phenomenon has not yet been presented. Previous experimental results have however placed certain conditions on any theory for this effect. The experimental data of Schwerdtfeger *et al.* [13] requires the coupled modes to exist at high temperatures, have  $g$  values close to the  $g$  values of uncoupled stacks, and have strongly anisotropic sub-chain susceptibilities with a constant total susceptibility. The data of Oostra *et al.* [15] on  $\text{HMM}(\text{TCNQ})_2$  also implies requirement that the effect occur in samples with both equivalent and inequivalent stacks. A further requirement is that the growing line when the level-crossing is approached always is the low field line. We will later see that this is related to the sign of the interaction.

Let us first consider the spin-Hamiltonian in the presence of a constant magnetic field,  $\mathbf{H}_0$ , for a TCNQ compound with stacks  $A$  and  $B$ .

$$\mathcal{H} = \mathcal{H}_{spin,A} + \mathcal{H}_{spin,B} + \mathcal{H}_{Zee.,A} + \mathcal{H}_{Zee.,B} + \mathcal{H}_{int.} \quad (4.1)$$

$\mathcal{H}_{spin,A}$  and  $\mathcal{H}_{spin,B}$  are the zero-field spin-Hamiltonians for each stack and would be

given by equation 1.3 The Zeeman terms for a given orientation of the crystal are of the form

$$\mathcal{H}_{Zeem.} = g\beta H_0 \sum_i S_{zi} \quad (4.2)$$

We are finally left to postulate a form for  $\mathcal{H}_{int.}$ . The experimental result that the  $g$  values of the coupled stacks be close to the  $g$  values of uncoupled stacks indicates that  $\mathcal{H}_{int.}$  is much smaller than the Zeeman terms in equation 4.1. The simplest type of interaction to consider in an isotropic exchange-type interaction of the form

$$\mathcal{H}_{int.} = \sum_{i,j} J_{i,j} \mathbf{S}_{Ai} \cdot \mathbf{S}_{Bj} \quad (4.3)$$

An important consequence of this type of interaction is that no requirements are placed on the symmetry of the crystal. This allows for the resulting theory to be valid in general for TCNQ compounds with inequivalent stacks.

If we substitute equation 4.3 into equation 4.1 we obtain a Hamiltonian that is in general impossible to solve exactly. There are however various useful approximations. We first consider the terms  $\mathcal{H}_{spin,A}$  and  $\mathcal{H}_{spin,B}$ . In the case of non-interacting stacks this type of term is treated in terms of a broadening of the ESR resonances. The energy levels are obtained from the Zeeman terms alone. If we make the same approximation for the case of interacting stacks we must also consider how we wish to treat  $\mathcal{H}_{int.}$ . The basic question is whether the correlation between a spin on stack A with a spin on stack B remains when each of the spins interact with like spins on the same stack. The cases of complete correlation and no correlation allow for the treatment of  $\mathcal{H}_{spin,A}$  and  $\mathcal{H}_{spin,B}$  in the same manner as for non-interacting stacks. These two cases correspond to  $J_{i,j} = J\delta_{i,j}$  and  $J_{i,j} = J/N$  respectively. Where  $N$  is the total number of A or B spins with the assumption that the number of A and B spins in the same. We will now solve equation 4.1 for both cases.

## 4.2 Complete Correlation between the $A$ and $B$ Spins

In this case the sums in equation 4.1 become only sums over one variable. We can consider only the two spin Hamiltonian

$$\mathcal{H} = g_A \beta H_0 S_{Az} + g_B \beta H_0 S_{Bz} + 2J \mathbf{S}_A \cdot \mathbf{S}_B \quad (4.4)$$

The  $\mathcal{H}_{spin,A}$  and  $\mathcal{H}_{spin,B}$  terms are treated in terms of a broadening of the spectra in a similar manner to the case with non-interacting stacks. This involves the assumption that the much stronger terms  $\mathcal{H}_{spin,A}$  and  $\mathcal{H}_{spin,B}$  do not affect the interaction between the stacks. This assumption is dubious at best and we will find that this theory does not explain the experimental data. The theory does however have some features that do agree with the experimental results. The eigenvalues and eigenstates of this Hamiltonian can readily be found. We first consider the eigenvalues and eigenstates of the Zeeman terms in equation 4.4 defined for spin  $A$  by

$$S_{Az} |+\pm\rangle = \frac{1}{2} |+\pm\rangle \quad \text{and} \quad S_{Az} |-\pm\rangle = -\frac{1}{2} |-\pm\rangle$$

and similarly for spin  $B$  by

$$S_{Bz} |\pm+\rangle = \frac{1}{2} |\pm+\rangle \quad \text{and} \quad S_{Bz} |\pm-\rangle = -\frac{1}{2} |\pm-\rangle$$

We define the triplet  $|t\rangle$  and singlet  $|s\rangle$  states by

$$|t\rangle = \frac{1}{\sqrt{2}} (|+\rightarrow\rangle + |-\rightarrow\rangle) \quad \text{and} \quad |s\rangle = \frac{1}{\sqrt{2}} (|+\rightarrow\rangle - |-\rightarrow\rangle)$$

The eigenvalues and eigenvectors of this Hamiltonian are then calculated by diagonalizing the Hamiltonian matrix. We only have to consider a  $2 \times 2$  matrix since  $|++\rangle$  and  $|--\rangle$  are eigenstates of  $\mathbf{S}_A \cdot \mathbf{S}_B$ . The resulting eigenvalues and eigenstates

are as follows

$$\begin{array}{c}
 \frac{J}{2} + \frac{1}{2}\beta H_0 g_+ \\
 -\frac{J}{2} + \sqrt{J^2 + [\frac{1}{2}\beta H_0 g_-]^2} \\
 -\frac{J}{2} - \sqrt{J^2 + [\frac{1}{2}\beta H_0 g_-]^2} \\
 \frac{J}{2} - \frac{1}{2}\beta H_0 g_+
 \end{array}
 \left| \begin{array}{l}
 |++\rangle \\
 \frac{1}{\Delta_+ \sqrt{2}} [(\beta H_0 g_- - J - \sqrt{J^2 + (\beta H_0 g_-)^2})|t\rangle - \\
 (\beta H_0 g_- + J - \sqrt{J^2 + (\beta H_0 g_-)^2})|s\rangle] \\
 \frac{1}{\Delta_- \sqrt{2}} [(\beta H_0 g_- - J + \sqrt{J^2 + (\beta H_0 g_-)^2})|t\rangle - \\
 (\beta H_0 g_- + J + \sqrt{J^2 + (\beta H_0 g_-)^2})|s\rangle] \\
 |--\rangle
 \end{array} \right.$$

where

$$g_+ = g_A + g_B \quad \text{and} \quad g_- = g_A - g_B$$

and

$$\begin{aligned}
 \Delta_+ &= (\beta H_0 g_- - \sqrt{J^2 + (\beta H_0 g_-)^2})^2 + J^2 \\
 \Delta_- &= (\beta H_0 g_- + \sqrt{J^2 + (\beta H_0 g_-)^2})^2 + J^2
 \end{aligned}$$

In order to consider the intensity of the ESR transitions we treat the microwave field Hamiltonian,  $\mathcal{H}_m = (S_{Ax} + S_{Bz})H_1 \cos \omega t$ , in second order perturbation theory. The intensities of the ESR transitions are proportional to the matrix elements of  $\mathcal{H}_m$  between the eigenstates of the unperturbed Hamiltonian. The only non-zero matrix elements are found between the state  $|t\rangle$  and the states  $|++\rangle$  and  $|--\rangle$ . This leads in general to four allowed transitions. The strength of these transitions would vary in proportion to the coefficients of  $|t\rangle$  in the eigenstates of the unperturbed Hamiltonian since the eigenstates  $|++\rangle$  and  $|--\rangle$  do not vary with the crystal orientation. This predicts in general four ESR lines with strongly anisotropic intensities but with a constant total overall intensity.

We consider some special cases. For  $|J| \ll |g_- \beta H_0|$  we are close to the uncoupled system. The spectra will consist of two doublet lines with the positions and total intensities for each doublet very close to the position and intensity of each line found in the uncoupled system. In the other extreme with  $|J| \gg |g_- \beta H_0|$  the spectra will consist of a strong central doublet with nearly all the susceptibility of the system and two small lines, one on each side of the doublet, with a separation in energy close to  $2J$  from the central doublet. When  $g_- = 0$  the eigenstates are pure triplet and singlet and there is only one single line with all the susceptibility of the system.

The predicted ESR spectra from this case have some of the features of the observed spectra. We first consider the orientations of the crystal where the  $g$  values,  $g_A$  and  $g_B$  are equal. For this orientation there is only one ESR line, both predicted by this theory and observed experimentally. The dependence of the strength of the ESR resonances with crystal orientation is also similar to the observed ESR spectra in that the anisotropy of predicted ESR lines is qualitatively similar to the anisotropy in the observed experimental spectra. The most significant difference is the number of lines. The separation of the predicted lines is such that they would be resolved by the Q-band ESR measurements. In particular the presence of weak ESR lines on both sides of the strong central line is not observed experimentally. This leads to the conclusion that the results cannot be entirely explained by this model.

In order to understand the failure of the model we look for the features of the model that lead to the prediction of four ESR resonances for most orientations of the crystal. The basic reason for four lines is that for each resonance of the  $A$  spins for example we have two distinct resonances depending on the state of the  $B$  spins and vice-versa. This is a direct result of the assumption of complete correlation between the  $A$  and  $B$  spins since we remember the state of an  $A$  spin when considering a

$B$  spin and vice-versa. This is encouraging for a consideration of the uncorrelated case where there is no memory of the state of a particular  $B$  spin when considering an  $A$  spin.

### 4.3 No Correlation between the $A$ and $B$ Spins

In this case we are replacing  $J_{i,j}$  in equation 4.3 by the average value  $\langle J_{i,j} \rangle = J/N$  where the average is taken over all the sites on the  $A$  lattice for an  $A$  spin and on the  $B$  lattice for a  $B$  spin. This approximation is justified if we consider that exchange between like spins is much more probable than exchange of  $A$  and  $B$  spins by many orders of magnitude. The typical experimentally measured values of  $J$  for like spin exchange are around  $20 K$  to  $200 K$  [4, p. 53] while we anticipate the effective average  $J$  for the exchange of  $A$  and  $B$  spins to be around  $5 \times 10^{-2} K$  for a Q-band measurement.

If we substitute  $J/N$  for  $J_{i,j}$  in equation 4.1 we have the Hamiltonian

$$\mathcal{H} = g_A \beta H_0 \sum_i S_{Azi} + g_B \beta H_0 \sum_i S_{Bzi} + \frac{J}{N} \sum_i \mathbf{S}_{Ai} \cdot \sum_i \mathbf{S}_{Bi} \quad (4.5)$$

The terms  $\mathcal{H}_{spin,A}$  and  $\mathcal{H}_{spin,B}$  in equation 4.1 are treated in terms of a broadening of the resonances and can be incorporated at a later point. We can perform the sums in equation 4.5 and obtain the following Hamiltonian in terms of the macroscopic spin variables

$$\mathcal{H}_{mac} = g_A \beta H_0 S_{Az} + g_B \beta H_0 S_{Bz} + \frac{J}{N} \mathbf{S}_A \cdot \mathbf{S}_B \quad (4.6)$$

In performing the sums the number of spins on the  $A$  and  $B$  stacks are assumed to be equal but the macroscopic spin variables due to the spins on each stack are not in general equal.

By the correspondence principle the macroscopic spin variables are treated as classical variables. This allows the calculation of a set of classical equations of

motion from the Hamiltonian 4.6 using Hamilton's equations of motion for the spin variables. The resulting equations of motion are as follows

$$\frac{d\mathbf{S}_A}{dt} = \omega_A(\mathbf{S}_A \times \mathbf{h}) + \frac{J}{N}(\mathbf{S}_A \times \mathbf{S}_B) \quad (4.7)$$

$$\frac{d\mathbf{S}_B}{dt} = \omega_B(\mathbf{S}_A \times \mathbf{h}) + \frac{J}{N}(\mathbf{S}_B \times \mathbf{S}_A)$$

where

$$\mathbf{h} = (H_1 \cos \omega t, H_1 \sin \omega t, H_0)/H_0 \quad \text{and} \quad \omega_i = g_i \beta H_0 / \hbar, \quad (i = A, B)$$

We can introduce at this stage the broadening of the resonances in a manner similar to the Bloch equations [23]. The nature of the terms  $\chi_{spin,A}$  and  $\chi_{spin,B}$  in equation 4.1 leads to an exchange-narrowed line for the uncoupled system. The expected lineshape would be a Lorentzian line. A Lorentzian spectrum is in fact observed experimentally in MEM(TCNQ)<sub>2</sub>. If we assume a Lorentzian lineshape then we can introduce a single spin-spin relaxation time  $T_2$  for each of the  $A$  and  $B$  spins. In our model we will neglect initially spin lattice relaxation effects; however we will allow for cross-relaxation effects. We propose to treat cross-relaxation in terms of a single relaxation time  $T_c$  for each kind of spin. It is also simpler to work in a frame rotating with the microwave field related to the lab frame by

$$\left( \frac{d\mathbf{S}}{dt} \right)_{rot} = \left( \frac{d\mathbf{S}}{dt} \right)_{lab} - \boldsymbol{\omega} \times \mathbf{S}$$

The equations of motion are then in the rotating frame

$$\begin{aligned}
\frac{dS_{Ax}}{dt} &= (\omega_A - \omega)S_{Ay} - \frac{S_{Ax}}{T_{2A}} + \frac{S_{Dx}}{T_{D'}} + \frac{J}{N\hbar}(S_{Ay}S_{Bz} - S_{By}S_{Az}) \\
\frac{dS_{Ay}}{dt} &= -(\omega_A - \omega)S_{Ax} - \frac{S_{Ay}}{T_{2A}} + \frac{S_{Dy}}{T_{D'}} - \frac{J}{N\hbar}(S_{Ax}S_{Bz} - S_{Bx}S_{Az}) - \frac{\omega_A H_1 S_{Ax}}{H_0} \\
\frac{dS_{Bx}}{dt} &= (\omega_B - \omega)S_{By} - \frac{S_{Dx}}{T_{2D}} + \frac{S_{Ax}}{T_{A'}} + \frac{J}{N\hbar}(S_{By}S_{Az} - S_{Ay}S_{Bz}) \\
\frac{dS_{By}}{dt} &= -(\omega_B - \omega)S_{Bx} - \frac{S_{Dy}}{T_{2D}} + \frac{S_{Ay}}{T_{A'}} - \frac{J}{N\hbar}(S_{Bx}S_{Az} - S_{Ax}S_{Bz}) - \frac{\omega_B H_1 S_{Dx}}{H_0}
\end{aligned} \tag{4.8}$$

This set of equations can be treated as a linear system by making the approximation that  $S_{Ax}$  and  $S_{Bz}$  are constant. This approximation is valid provided that  $H_1 \ll H_0$  allowing an approximation of the form  $\sin \theta = \theta$  to be valid. We then define  $\Omega_{Ae} = JS_{Ax}/N$ ,  $\Omega_{Be} = JS_{Bz}/N$ , and introduce the complex variables

$$S_{A\pm} = S_{Ax} \pm iS_{Ay} \quad \text{and} \quad S_{B\pm} = S_{Bx} \pm iS_{By}$$

The equations of motion then become

$$\begin{aligned}
\frac{dS_{A+}}{dt} &= -i(\omega_A - \omega + \Omega_{Be})S_{A+} + i\Omega_{Ae}S_{B+} - \frac{S_{A+}}{T_{2A}} + \frac{S_{D+}}{T_{D'}} - \frac{iN\hbar\omega_A H_1}{JH_0}\Omega_{Ae} \\
\frac{dS_{B+}}{dt} &= -i(\omega_B - \omega + \Omega_{Ae})S_{B+} + i\Omega_{Be}S_{A+} - \frac{S_{B+}}{T_{2B}} + \frac{S_{A+}}{T_{A'}} - \frac{iN\hbar\omega_B H_1}{JH_0}\Omega_{Be}
\end{aligned} \tag{4.9}$$

The solution of these equations is

$$\begin{pmatrix} S_{A+} \\ S_{B+} \end{pmatrix} = \frac{-NH_1}{JH_0(\Delta^2 + \delta_A \delta_D)} \begin{bmatrix} (\Omega_{Ae} \delta_A \delta_B \omega_A - \delta_B \Omega_{Ae} \Delta \omega_B) \frac{1}{\lambda_+} + \\ (-\Omega_{Be} \delta_A \Delta \omega_A + \Delta^2 \Omega_{Be} \omega_B) \frac{1}{\lambda_+} + \\ (\Omega_{Ae} \delta_B \Delta \omega_B + \Delta^2 \Omega_{Ae} \omega_A) \frac{1}{\lambda_-} \\ (\Omega_{Be} \delta_A \delta_B \omega_B + \delta_A \Omega_{Be} \Delta \omega_A) \frac{1}{\lambda_-} \end{bmatrix} \tag{4.10}$$

where

$$\begin{aligned}
\lambda_{\pm} &= \frac{1}{2} \left\{ \omega_A + \omega_B + \Omega_{Ae} + \Omega_{Be} - 2\omega - i \left( \frac{1}{T_{2A}} + \frac{1}{T_{2B}} \right) \right. \\
&\quad \pm \left( \left[ \omega_A - \omega_B + \Omega_{Be} - \Omega_{Ae} - i \left( \frac{1}{T_{2A}} - \frac{1}{T_{2B}} \right) \right]^2 \right. \\
&\quad \left. \left. + 4 \left[ \Omega_{Ae} \Omega_{Be} - \frac{1}{T_{Ae} T_{Be}} - i \left( \frac{\Omega_{Ae}}{T_{Ae}} + \frac{\Omega_{Be}}{T_{Be}} \right) \right] \right)^{\frac{1}{2}} \right\} \\
&= \omega_{\pm} - \omega - i/T_{\pm} \\
\Delta &= \frac{1}{2} \left\{ \omega_B - \omega_A + \Omega_{Ae} - \Omega_{Be} - i \left( \frac{1}{T_{2B}} - \frac{1}{T_{2A}} \right) \right. \\
&\quad \left. + \left( \left[ \omega_A - \omega_B + \Omega_{Be} - \Omega_{Ae} - i \left( \frac{1}{T_{2A}} - \frac{1}{T_{2B}} \right) \right]^2 \right. \right. \\
&\quad \left. \left. + 4 \left[ \Omega_{Ae} \Omega_{Be} - \frac{1}{T_{Ae} T_{Be}} - i \left( \frac{\Omega_{Ae}}{T_{Ae}} + \frac{\Omega_{Be}}{T_{Be}} \right) \right] \right)^{\frac{1}{2}} \right\} \\
&= \Delta' + i\Delta''
\end{aligned}$$

with

$$\delta_A = \Omega_{Ae} - \frac{i}{T_{Be}} \quad \text{and} \quad \delta_B = \Omega_{Be} - \frac{i}{T_{Ae}}$$

We have also introduced  $\omega_{\pm}$ ,  $T_{\pm}$ ,  $\Delta'$  and  $\Delta''$  as the real and imaginary parts of  $\lambda_{\pm}$  and  $\Delta$ . These quantities can be calculated explicitly with the following results. We first introduce  $\Omega_{\pm}$  defined by

$$\begin{aligned}
\Omega_{\pm} &= -\frac{1}{2\sqrt{2}} \left\{ \left( \left[ (\omega_A - \omega_B + \Omega_{Be} - \Omega_{Ae})^2 - \left( \frac{1}{T_{2A}} - \frac{1}{T_{2B}} \right)^2 \right. \right. \right. \\
&\quad \left. \left. + 4 \left( \Omega_{Ae} \Omega_{Be} - \frac{1}{T_{Be} T_{Ae}} \right) \right] \right)^2 \\
&\quad \left. + \left[ 2(\omega_A - \omega_B + \Omega_{Be} - \Omega_{Ae}) \left( \frac{1}{T_{2A}} - \frac{1}{T_{2B}} \right) + 4 \left( \frac{\Omega_{Ae}}{T_{Ae}} + \frac{\Omega_{Be}}{T_{Be}} \right) \right]^2 \right)^{\frac{1}{2}} \\
&\quad \pm \left[ (\omega_A - \omega_B + \Omega_{Be} - \Omega_{Ae})^2 - \left( \frac{1}{T_{2A}} - \frac{1}{T_{2B}} \right)^2 \right]
\end{aligned}$$

$$+ 4 \left( \Omega_{Ae} \Omega_{Be} - \frac{1}{T_{Be} T_{Ae}} \right) \left. \right\}^{\frac{1}{2}}$$

The quantities  $\omega_{\pm}$ ,  $T_{\pm}$ ,  $\Delta'$  and  $\Delta''$  are then as follows

$$\begin{aligned} \omega_{\pm} &= \frac{1}{2} [\omega_A + \omega_B + \Omega_{Ae} + \Omega_{Be} \pm 2\Omega_+] \\ T_{\pm} &= 2 \left[ \left( \frac{1}{T_A} + \frac{1}{T_B} \right) \pm 2s\Omega_- \right]^{-1} \\ \Delta' &= \frac{1}{2} [\omega_B - \omega_A - \Omega_{Be} + \Omega_{Ae} + 2\Omega_+] \\ \Delta'' &= \frac{1}{2} \left[ \left( \frac{1}{T_A} - \frac{1}{T_B} \right) + 2s\Omega_- \right] \end{aligned}$$

where

$$s = \text{sgn} \left( -2(\omega_A - \omega_B + \Omega_{Be} - \Omega_{Ae}) \left[ \frac{1}{T_{2A}} - \frac{1}{T_{2B}} \right] - 4 \left[ \frac{\Omega_{Ae}}{T_{Ae}} + \frac{\Omega_{Be}}{T_{Be}} \right] \right)$$

with

$$\text{sgn}(x) = \begin{cases} 1 & x > 0 \\ 0 & x = 0 \\ -1 & x < 0 \end{cases}$$

To calculate the susceptibilities we note from our transformation to the rotating frame that

$$(S_{Ax} + S_{Bx})_{lab} = (S_{Ax} + S_{Bx})_{rot} \cos \omega t + (S_{Ay} + S_{By})_{rot} \sin \omega t \quad (4.11)$$

The susceptibilities are related to  $(S_{Ax} + S_{Bx})_{lab}$  by the equation [24, p. 8]

$$(S_{Ax} + S_{Bx})_{lab} = 2H_1(\chi'(\omega) \cos \omega t - \chi''(\omega) \sin \omega t) \quad (4.12)$$

By comparing equations 4.11 and 4.12 we find that the susceptibilities are given by

$$\chi'(\omega) = \frac{1}{2H_1} (S_{Ax} + S_{Bx})_{rot} \quad \text{and} \quad \chi''(\omega) = -\frac{1}{2H_1} (S_{Ay} + S_{By})_{rot} \quad (4.13)$$

If we substitute the real and imaginary parts of equation 4.10 into equations 4.13 we obtain the following result for the susceptibilities

$$\begin{aligned}
\chi'(\omega) &= \frac{N\hbar\omega_0}{2JH_0(\gamma_0'^2 + \gamma_0''^2)} \left[ \frac{(\gamma_0'\gamma_+' + \gamma_0''\gamma_0'')T_+^2(\omega_+ - \omega) - (\gamma_0'\gamma_0'' - \gamma_0''\gamma_+' )T_+}{(\omega_+ - \omega)^2 T_+^2 + 1} \right. \\
&\quad \left. + \frac{(\gamma_0'\gamma_-' + \gamma_0''\gamma_0'')T_-^2(\omega_- - \omega) - (\gamma_0'\gamma_0'' - \gamma_0''\gamma_-' )T_-}{(\omega_- - \omega)^2 T_-^2 + 1} \right] \\
\chi''(\omega) &= \frac{N\hbar\omega_0}{2JH_0(\gamma_0'^2 + \gamma_0''^2)} \left[ \frac{(\gamma_0'\gamma_+' + \gamma_0''\gamma_0'')T_+ + (\gamma_0'\gamma_0'' - \gamma_0''\gamma_+' )T_+^2(\omega_+ - \omega)}{(\omega_+ - \omega)^2 T_+^2 + 1} \right. \\
&\quad \left. + \frac{(\gamma_0'\gamma_-' + \gamma_0''\gamma_0'')T_- + (\gamma_0'\gamma_0'' - \gamma_0''\gamma_-' )T_-^2(\omega_- - \omega)}{(\omega_- - \omega)^2 T_-^2 + 1} \right]
\end{aligned} \tag{4.14}$$

where

$$\begin{aligned}
\gamma_0' &= \Delta'^2 - \Delta''^2 + \Omega_{Ae}\Omega_{Be} - \frac{1}{T_{Ae}T_{Be}} \\
\gamma_0'' &= 2\Delta'\Delta'' - \left( \frac{\Omega_{Ae}}{T_{Ae}} + \frac{\Omega_{Be}}{T_{Be}} \right) \\
\gamma_+' &= \frac{\omega_A}{\omega_0} \left[ \Omega_{Ae} \left( \Omega_{Ae}\Omega_{Be} - \frac{1}{T_{Ae}T_{Be}} \right) - \Delta'' \frac{\Omega_{Be}}{T_{Be}} \right] \\
&\quad + \frac{\omega_B}{\omega_0} \left[ \Omega_{Be} \left( \Delta'^2 - \Delta''^2 \right) - \frac{\Omega_{Ae}}{T_{Ae}} \right] - 2\Omega_{Ae}\Omega_{Be}\Delta' \\
\gamma_+'' &= \frac{\omega_A}{\omega_0} \left[ -\Omega_{Ae} \left( \frac{\Omega_{Ae}}{T_{Ae}} + \frac{\Omega_{Be}}{T_{Be}} \right) + \Delta' \frac{\Omega_{Be}}{T_{Be}} \right] \\
&\quad + \frac{\omega_B}{\omega_0} \left[ 2\Delta'\Delta''\Omega_{Be} + \Delta' \frac{\Omega_{Ae}}{T_{Ae}} \right] - 2\Delta''\Omega_{Ae}\Omega_{Be} \\
\gamma_-' &= \frac{\omega_B}{\omega_0} \left[ \Omega_{Be} \left( \Omega_{Ae}\Omega_{Be} - \frac{1}{T_{Ae}T_{Be}} \right) + \Delta'' \frac{\Omega_{Ae}}{T_{Ae}} \right] \\
&\quad + \frac{\omega_A}{\omega_0} \left[ \Omega_{Ae} \left( \Delta'^2 - \Delta''^2 \right) + \frac{\Omega_{Be}}{T_{Be}} \right] + 2\Omega_{Ae}\Omega_{Be}\Delta' \\
\gamma_-'' &= \frac{\omega_B}{\omega_0} \left[ -\Omega_{Be} \left( \frac{\Omega_{Ae}}{T_{Ae}} + \frac{\Omega_{Be}}{T_{Be}} \right) - \Delta' \frac{\Omega_{Ae}}{T_{Ae}} \right] \\
&\quad + \frac{\omega_A}{\omega_0} \left[ 2\Delta'\Delta''\Omega_{Ae} - \Delta' \frac{\Omega_{Be}}{T_{Be}} \right] + 2\Delta''\Omega_{Ae}\Omega_{Be}
\end{aligned}$$

and

$$\bar{\omega}_0 = \frac{1}{2}(\omega_A + \omega_B)$$

There are various significant features of the model for uncorrelated spins. The model predicts two ESR lines with an angular dependence of the intensity with sample rotation that is very similar to the observed experimental results for samples with inequivalent stacks. The linewidths of the absorption are not strictly Lorentzian but rather contain a slight asymmetry. The degree of asymmetry is due to the linewidth terms in equations 4.14. This asymmetry of the line is a second order effect in the ratio of the linewidth to the separation of the lines.

We can again consider some special cases. For  $|\hbar(\Omega_{Ae} + \Omega_{Be})| \ll |g_- \beta H_0|$  we are close to the uncoupled system. The spectra will consist of two lines with the intensities, positions and linewidths close to those predicted for the uncoupled system. In the other extreme with  $|\hbar(\Omega_{Ae} + \Omega_{Be})| \gg |g_- \beta H_0|$  we have a strong and a weak line at a separation in energy close to  $|\hbar(\Omega_{Ae} + \Omega_{Be})|$ . When  $g_- = 0$  we again find only one line with all the susceptibility of the system.

The sign of  $J$  determines if the symmetric or antisymmetric mode has higher energy. For  $J > 0$  we have the symmetric mode with higher energy or antiferromagnetic coupling between the spins on different stacks and conversely for  $J < 0$  we have a lower energy symmetric mode or ferromagnetic coupling. In the TCNQ salts the vanishing ESR line is observed at higher magnetic field or lower energy. This means that for these TCNQ salts the coupling between the spins on inequivalent stacks is antiferromagnetic.

There are two significant differences between the uncorrelated and the correlated cases. The first is that the uncorrelated case predicts only two lines that are very similar to the observed ESR spectra. A second difference is a direct dependence of the coupling between the stacks on the overall susceptibility of the system. This manifests itself in the dependence on  $\Omega_{Ae}$  or  $\Omega_{Be}$  rather than on  $J$  throughout the theory. One can conclude that the theory for the uncorrelated case is a reasonable

candidate to fit the experimental ESR data for TCNQ samples with inequivalent stacks. In the next section we will explain the method used to fit to experimental data for the case of  $\text{DEM}(\text{TCNQ})_2$  with this model.

#### 4.4 Fit of the Theory for the case of no Correlation to the Experimental Data

In order to consider the parameters for fitting the data to the theory we first recall the case of non-interacting stacks. For a given non-interacting crystal at a fixed temperature we first parametrize the  $g$  values of each each stack for each of the three rotations about three orthogonal axes using equation 2.1. This provides a total of 18 parameters for a system with two independent stacks. The  $g$  value parameters can then be used to calculate the  $g$  tensor for each stack with respect to a set of fixed coordinate axes by the method explained in chapter 2.

The susceptibilities are constant to about 5 parts in  $10^4$  for each stack. Since the experiment is not sensitive enough to detect such a small change in the susceptibility we can treat the susceptibility of each stack as a constant. In our experiment we only detect the susceptibility of each stack normalized to the total susceptibility of both stacks. This means one measurable parameter. We do not fit the halfwidths to a theory so we do not introduce any parameters from this source. Consequently for a non-interacting system of two TCNQ stacks we have a total of 19 parameters.

We now consider the same measurement on the real crystal with interacting stacks. The  $g$  values of each stack enter the theory through the frequencies  $\omega_A$  and  $\omega_B$ . The normalized susceptibility of the stacks depends only on the ratio  $\Omega_{Ae}/\Omega_{Be}$ .

The linewidths involve two more relaxation times,  $T_{Ae}$  and  $T_{Be}$  in the interacting case than in the non-interacting case. We must consequently postulate a relationship

between these extra relaxation times and the relaxation times  $T_A$  and  $T_B$ , in order to calculate the four relaxation times from the data at each orientation of the crystal from the measured linewidth data. We have used for this relationship a dependence of the form  $T_{Ae} = \frac{1}{k}T_A$  and  $T_{Be} = \frac{1}{k}T_B$  with  $k$  either a constant or a function of the other parameters in the theory. The form of  $k$  is chosen to best fit the halfwidth data in the overlap area where the impact of cross-relaxation between the stacks should be most significant. We will discuss this question further when we consider the linewidth results in the next chapter. It should be noted that the relaxation times do not have a very significant impact on the other parameters because the relaxation times enter into the theory for  $g$  values and susceptibilities only in second order in the ratio of the linewidths to the separation of the lines.

Apart from the linewidths that have only a marginal impact on the fit to the  $g$  values and the susceptibilities, the only parameter introduced by the theory is  $\Omega_{Ae} + \Omega_{Be}$ . This is actually the product of  $J/N$  and the total susceptibility of crystal. We will be treating this parameter as a function of temperature for a given TCNQ compound; however we will not assume any particular temperature dependence of this parameter to be that of the total susceptibility. We are actually allowing  $J$  itself to vary with the temperature and with the type of TCNQ compound.

The experimental ESR spectra were fit to Lorentzian lineshapes as explained in section 2.1. This involves ignoring the asymmetry of the lines predicted by the theory. The error introduced by this approximation can be estimated from the calculated asymmetry after a fit of the theory to the data is made. From this fit to Lorentzian spectra the data was reduced to the parameters of the Lorentzian fit. This reduced data consists of the  $g$  values, the ratio of the susceptibilities of each line to the total susceptibility and the halfwidth of the lines. This reduced data was then fit to equations 4.14 and to the equations for the  $g$  values and halfwidths

in the set of equations 4.10 simultaneously with 20 parameters.

The parameters for this fit were determined as follows. The values of  $g_A$  and  $g_B$  were parametrized by equation 2.1 for each of the rotation axes. This provided a total of 18 parameters to the fit. The last two parameters were  $\Omega_{Ae}$  and  $\Omega_{Be}$ . This is in fact only two independent parameters over the parameters that would be used for the uncoupled system.

The halfwidth data were incorporated by making an approximation since a theory that would fit the uncoupled halfwidths well with a few parameters is not known for this particular case. This approximation consisted of assuming the same relaxation time for both stacks thereby neglecting the difference between the relaxation times when compared to the separation between the lines. This should not be confused with the difference between the measured linewidths which is larger particularly in the crossover region. The advantage of this approximation is that only the sum  $\frac{1}{T_A} + \frac{1}{T_B}$  has to be determined. This sum is in fact equal to an experimentally measurable quantity  $\frac{1}{T_+} + \frac{1}{T_-}$  and is consequently easily determined. The same approximation was made in incorporating the cross relaxation times  $T_{Ae}$  and  $T_{Be}$ .

The result is that the theory to which we propose to fit the ESR data of a TCNQ compound with crossing energy levels involves only one extra parameter,  $J$  to account for the interaction between the inequivalent stacks. The other parameters are determined by the theory for non interacting stacks.

## Chapter 5

### DEM(TCNQ)<sub>2</sub> Results

#### 5.1 The $g$ Value Measurements

The ESR measurements on DEM(TCNQ)<sub>2</sub> were performed at both 77 K and 298 K by the method of chapter 2. The data were fit to the theory of section 4.3 as explained in section 4.4. The  $g$  values for rotations about the three orthogonal axes **a**, **b** and **c** are shown in figures 19 to 21 for the measurements at 298 K and in figures 22 to 24 for the measurements at 77 K. The plots show the actual  $g$  value data of the coupled modes. At the orientations where both modes were observed the measured data has been labeled 'o' or 'x' in the plots to correspond to the stack *A* or *B* which has the greater influence in the particular coupled mode. The *A* and *B* labels correspond to the notation of reference [13] This notation will be followed in the fit to the theory shown by the solid line and the  $g$  values of the individual stacks,  $g_A$  and  $g_B$ , determined from the theory shown by the dotted lines. The last two  $g$  values would be the measured  $g$  values of the individual stacks if there were no interaction between the stacks.

The  $g$  values,  $g_A$  and  $g_B$ , are expressed in terms of the parameters  $\alpha_i$ ,  $\beta_i$ , and  $\gamma_i$  using equation 2.1 within the theory and were used to calculate the  $g$  tensor principal values and direction cosines by the method of section 2.3. This method allows

Principal Values	Direction Cosines		
	a	b	c
2.002318(6)	-0.177(8)	0.201(6)	0.963(2)
2.002989(6)	-0.024(8)	-0.980(2)	0.200(4)
2.003273(6)	0.984(1)	0.013(9)	0.178(5)

Table III: Principal Values and Direction Cosines for the  $g$  Tensor of the  $A$  Stack of DEM(TCNQ)<sub>2</sub> at 298 K

Principal Values	Direction Cosines		
	a	b	c
2.002313(6)	-0.601(3)	-0.604(4)	0.522(4)
2.002769(6)	-0.511(4)	0.794(2)	0.330(4)
2.003438(6)	0.614(1)	0.069(2)	0.786(2)

Table IV: Principal Values and Direction Cosines for the  $g$  Tensor of the  $B$  Stack of DEM(TCNQ)<sub>2</sub> at 298 K

a direct comparison between the  $g$  tensors of TCNQ compounds at different temperatures or between different compounds that is independent of the various values of  $J$  or even of the presence of inequivalent stacks and the interaction discussed in chapter 4. The resulting  $g$  tensors and direction cosines are given in tables III and IV for the results at 298 K and in tables V and VI for the results at 77 K.

The experimental errors in the  $g$  tensors in this case have the same sources as in the case of MEM(TCNQ)<sub>2</sub>; however the relative importance of these sources is different. We first consider those errors that are the same as in the case of

Principal Values	Direction Cosines		
	a	b	c
2.002363(6)	-0.164(6)	0.170(8)	0.972(2)
2.002976(6)	0.041(9)	-0.983(2)	0.179(6)
2.003333(6)	0.986(4)	0.069(9)	0.154(6)

Table V: Principal Values and Direction Cosines for the  $g$  Tensor of the  $A$  Stack of DEM(TCNQ)<sub>2</sub> at 77 K

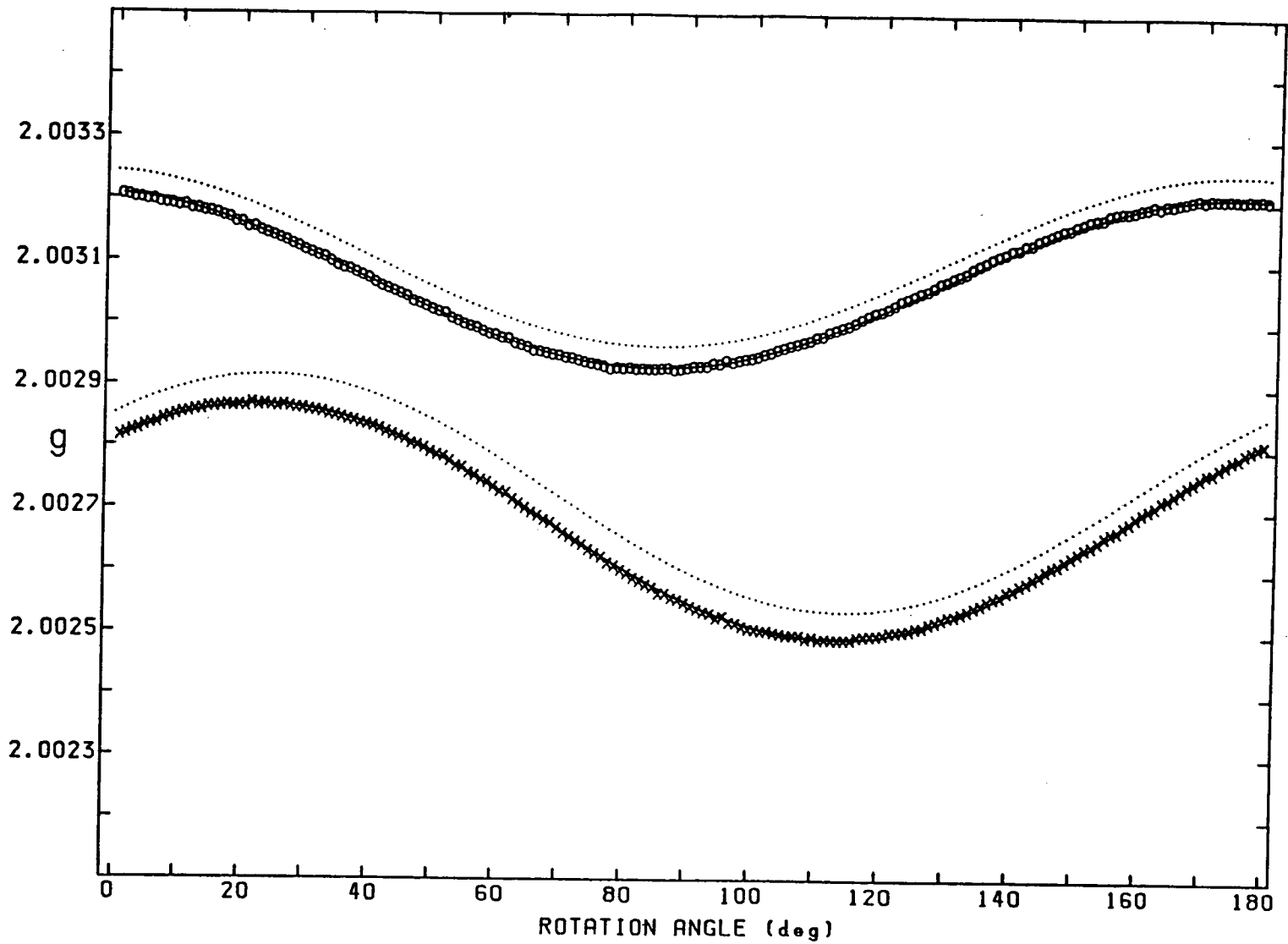


Figure 19:  $g$  Value of  $DEM(TCNQ)_2$  for a Rotation about a at 298 K. The solid line is a fit to the theory. The dotted lines are plots of  $g_A$  and  $g_B$ .

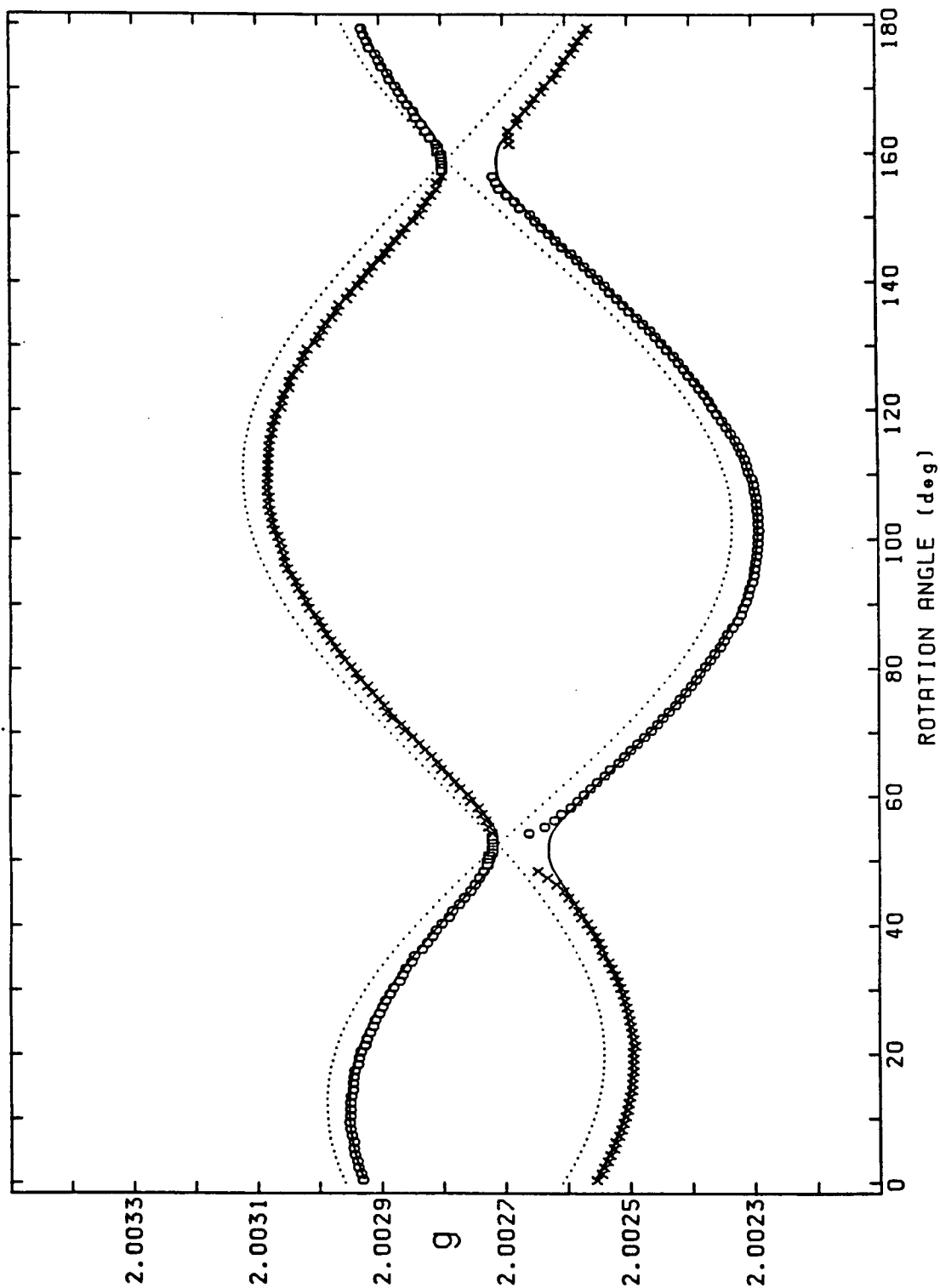


Figure 20:  $g$  Value of  $\text{DEM}(\text{TCNQ})_2$  for a Rotation about  $b$  at 298 K. The solid line is a fit to the theory. The dotted lines are plots of  $g_A$  and  $g_B$ .

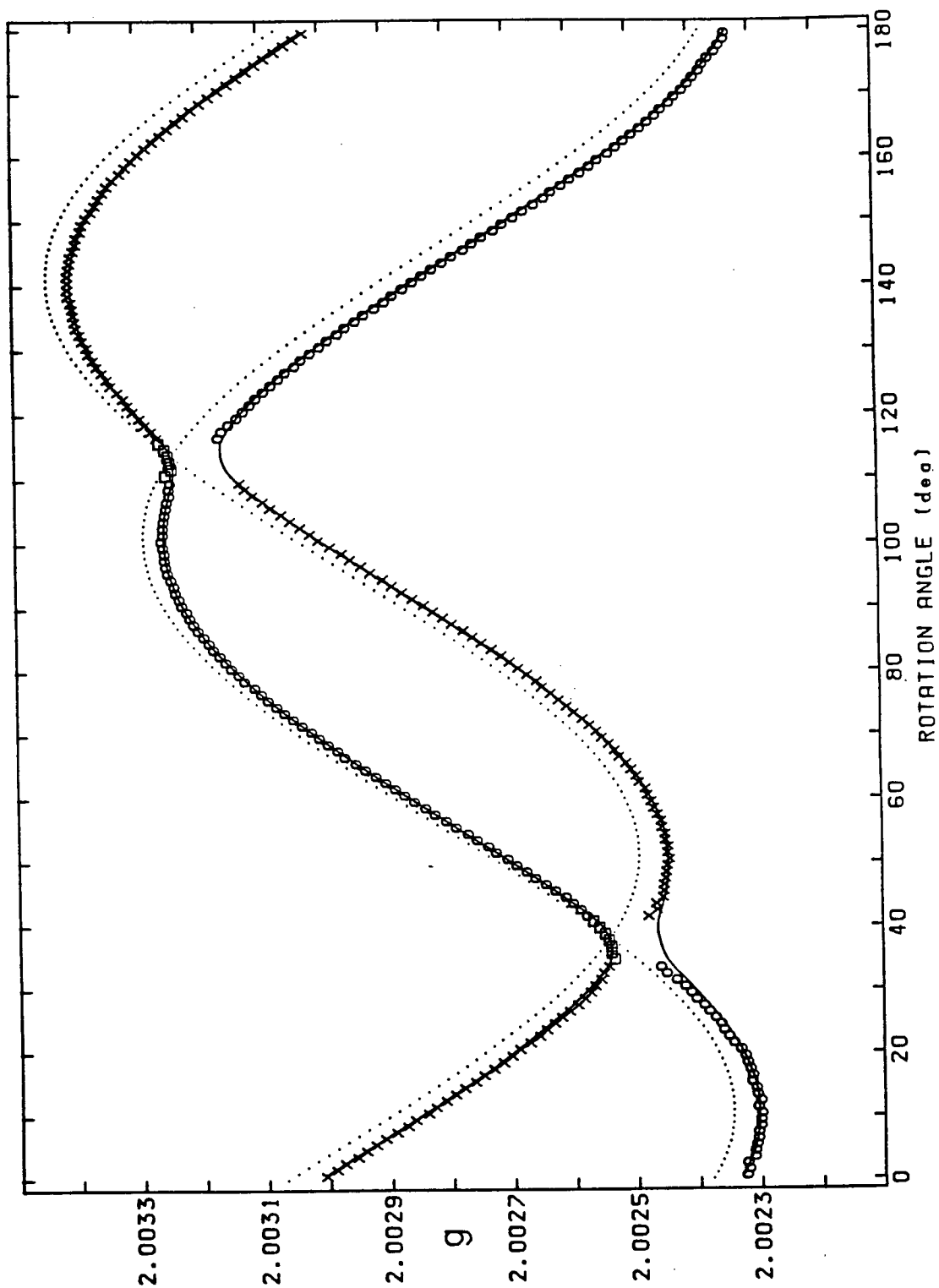


Figure 21:  $g$  Value of  $\text{DEM}(\text{TCNQ})_2$  for a Rotation about  $c$  at 298 K. The solid line is a fit to the theory. The dotted lines are plots of  $g_A$  and  $g_B$ .

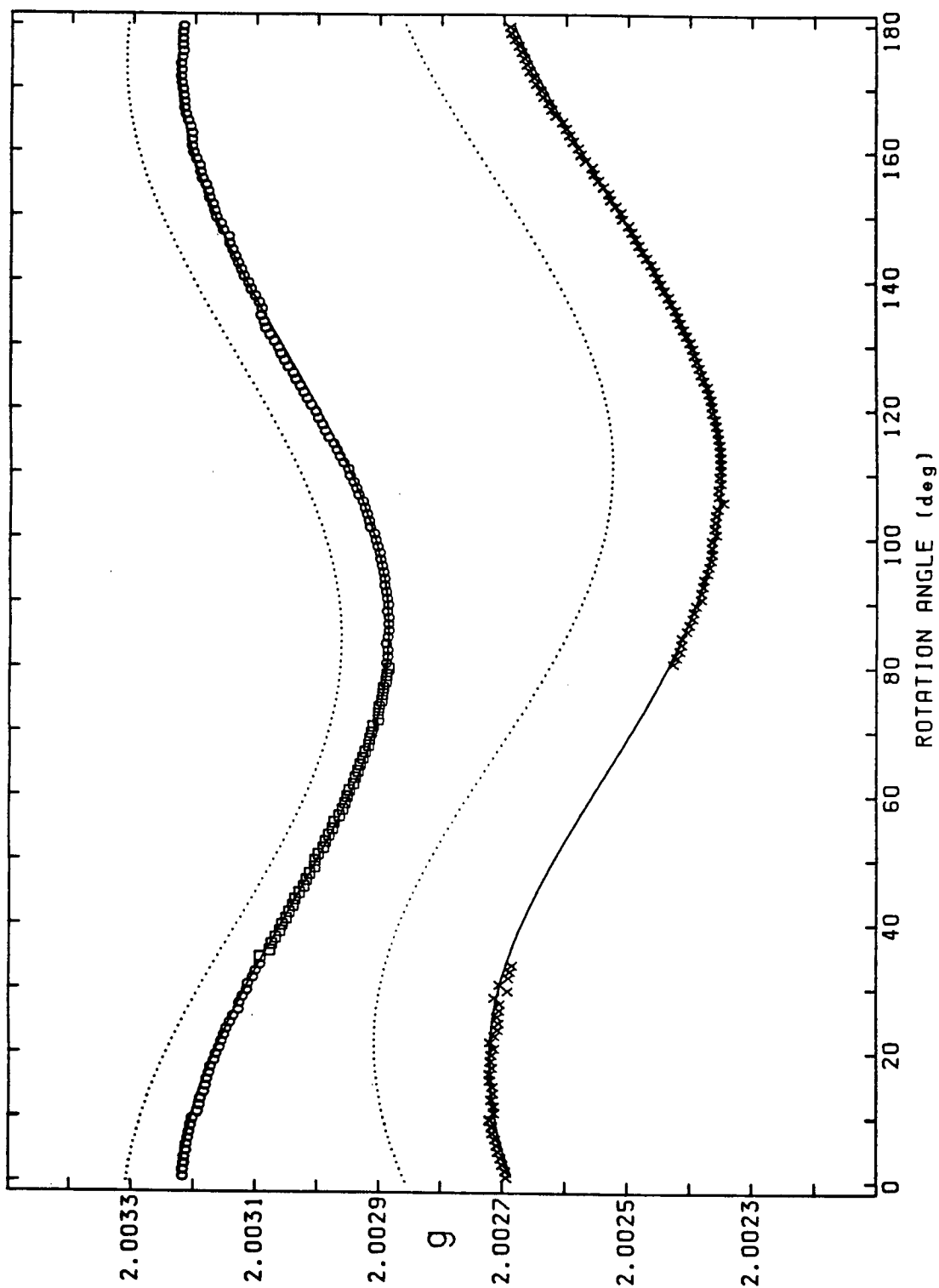


Figure 22:  $g$  Value of  $\text{DEM}(\text{TCNQ})_2$  for a Rotation about  $a$  at 77 K. The solid line is a fit to the theory. The dotted lines are plots of  $g_A$  and  $g_B$ .

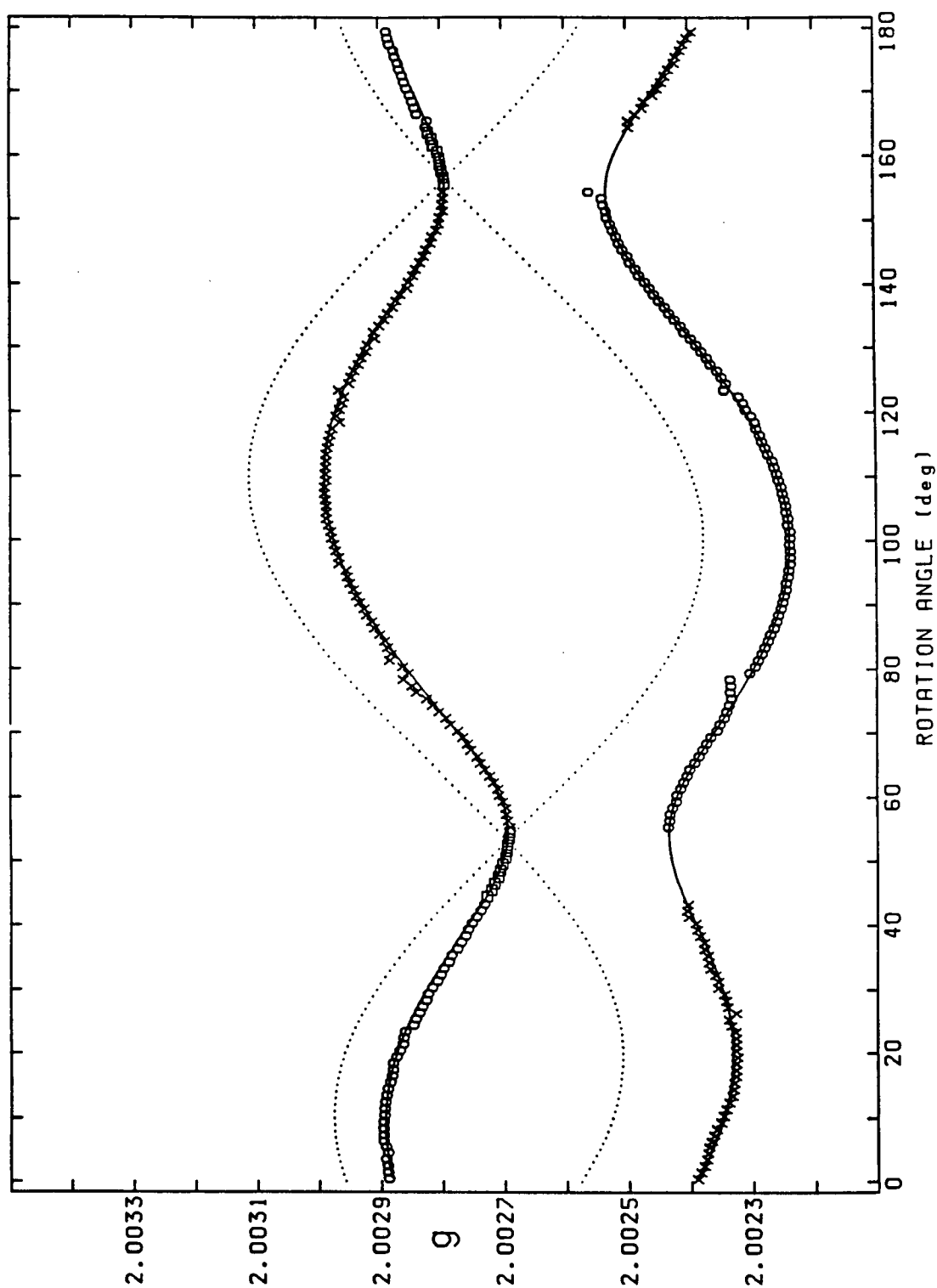


Figure 23:  $g$  Value of  $\text{DEM}(\text{TCNQ})_2$  for a Rotation about  $b$  at 77 K. The solid line is a fit to the theory. The dotted lines are plots of  $g_A$  and  $g_B$ .

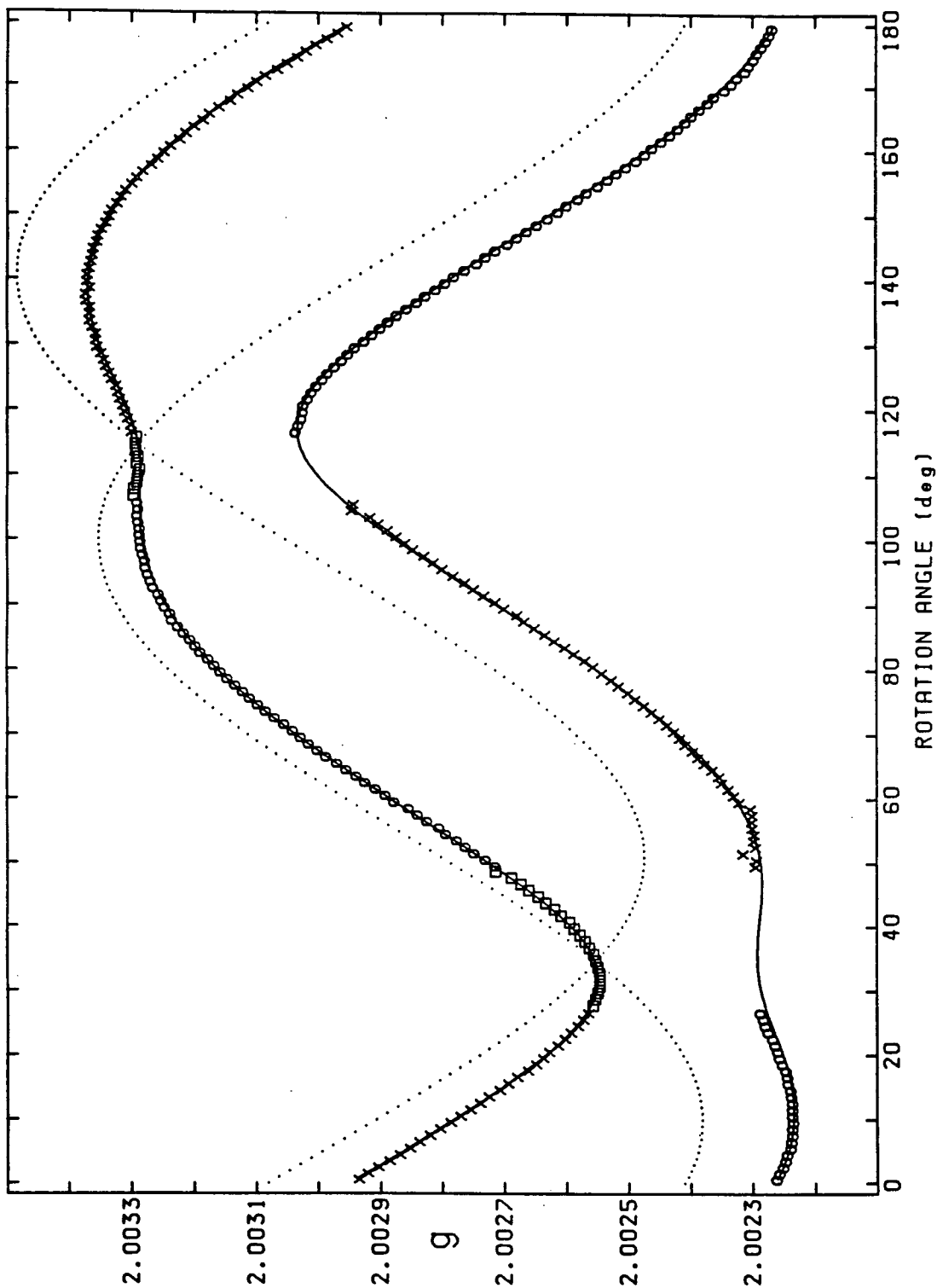


Figure 24:  $g$  Value of  $\text{DEM}(\text{TCNQ})_2$  for a Rotation about  $c$  at 77 K. The solid line is a fit to the theory. The dotted lines are plots of  $g_A$  and  $g_B$ .

Principal Values	Direction Cosines		
	a	b	c
2.002294(7)	-0.593(4)	-0.610(7)	0.525(5)
2.002733(6)	-0.518(4)	0.788(4)	0.332(5)
2.003478(6)	0.617(3)	0.075(3)	0.784(2)

Table VI: Principal Values and Direction Cosines for the  $g$  Tensor of the  $B$  Stack of DEM(TCNQ)<sub>2</sub> at 77 K

MEM(TCNQ)<sub>2</sub>. The quoted experimental error in the calibration sample  $g$  value is still  $2 \times 10^{-6}$ . The error due to the magnetic field inhomogeneity is again less than  $2 \times 10^{-6}$  since the DEM(TCNQ)<sub>2</sub> sample was placed at the same distance from the calibration sample as the MEM(TCNQ)<sub>2</sub> sample. The errors due to the sweep of the magnetic field are again the same with a range between  $1 \times 10^{-7}$  and  $6 \times 10^{-7}$  depending upon the difference in  $g$  value between the calibration and the DEM(TCNQ)<sub>2</sub> samples.

There are two errors that are significantly different. The error in determining the alignment of the cube was estimated to be somewhat lower. This is due to the fact that we now have four sets of  $\delta\theta_i$ , since we have two independent stacks at two different temperatures. We used the average of the  $\delta\theta_i$ , determined from the data of each stack to calculate  $\delta\theta_i$  for the crystal at a given temperature. We then calculate the error by solving for the  $g$  tensor principal values and direction cosines at a given temperature using the  $\delta\theta_i$  from both temperatures using the same method that was used for MEM(TCNQ)<sub>2</sub>. The result is a smaller error in  $g$  from this source since the  $\delta\theta_i$  were determined more accurately using the data from the two inequivalent stacks in DEM(TCNQ)<sub>2</sub> rather than the single type of stack in MEM(TCNQ)<sub>2</sub>. The error from this source was found to be between  $2 \times 10^{-6}$  and  $4 \times 10^{-6}$ .

The other error that is different is the statistical error from the fit of the data to the theory. A typical value for this error is  $6 \times 10^{-7}$ . This is still small when

compared to other sources of error but is significantly larger than the same source of error in the case of MEM(TCNQ)<sub>2</sub> inspite of the fact that five times as many data points were taken for the DEM(TCNQ)<sub>2</sub> measurements. The error arises mostly from the error in the determination of the total coupling frequency,  $\Omega_{Ae} + \Omega_{Be}$ , between the stacks.

There is one source of error that is not present in the MEM(TCNQ)<sub>2</sub> case. This is the error due to the approximation of  $\frac{1}{T_A} - \frac{1}{T_B}$  by 0 in the fit to the theory. This error is about  $5 \times 10^{-7}$  for the 298 K data and  $1 \times 10^{-8}$  for the 77 K data. In calculating the total error in the  $g$  tensor principal values all of these sources of error are treated as statistically independent.

## 5.2 Relationship of the $g$ Tensors to the Crystal Structure

In the case of DEM(TCNQ)<sub>2</sub> we can compare the relative orientations of the  $g$  Tensors to the crystal structure. This comparison can be used to determine whether the principal values of the  $g$  Tensors do in fact correspond to the symmetry directions of the individual TCNQ molecules as determined from the X-ray data of Morssink and von Bodegom [8]. In table VII and we present the angles made between each of the symmetry directions of the  $A$  TCNQ molecule with the corresponding direction on the  $B$  TCNQ molecule together with the angle made between each of the principal vectors of the  $A$   $g$  tensor with the corresponding principal vector of the  $B$   $g$  tensor. This last correspondence is made by identifying the smallest principal value of the  $A$   $g$  tensor with the smallest principal value of the  $B$   $g$  tensor, and similarly for the intermediate and largest  $g$  values. We label the angles between symmetry directions of the TCNQ molecules  $\theta_M$ ,  $\theta_L$  and  $\theta_N$  where  $N$ ,  $L$ , and  $M$  correspond to the directions defined in chapter 2. The angle between the principal vectors of

Temp (K)	$\theta_m$	$\theta_l$	$\theta_n$	$\theta_M$	$\theta_L$	$\theta_N$
298	41.8(4)	60.8(5)	46.6(4)			
294				38.2(1)	57.4(1)	55.4(1)
77	42.7(5)	59.7(6)	46.1(6)			

Table VII: The Relative Orientation of the  $g$  Tensors and the TCNQ molecules in DEM(TCNQ)<sub>2</sub>. The angles  $\theta_m$ ,  $\theta_n$  and  $\theta_l$  are the angles between the principal vectors of the  $A$  and  $B$   $g$  Tensors and the angles  $\theta_M$ ,  $\theta_N$ , and  $\theta_L$  are the angles between the  $N$ ,  $M$ , and  $L$  directions of the  $A$  and  $B$  TCNQ molecules as determined from the data of Morssink and van Bodegom [8].

the  $g$  tensors are labeled  $\theta_m$ ,  $\theta_l$  and  $\theta_n$ , where  $n$ ,  $l$ , and  $m$  are chosen so that  $g_m$  is largest  $g_l$  the intermediate and  $g_n$  the smallest principal value. We choose the all the angles to be in the range  $\theta = 0^\circ$  to  $90^\circ$ . The errors in the angles determined from the  $g$  tensors were determined from the experimental errors in the direction cosines of the  $g$  tensors. The errors in the angles calculated from the X-ray data are the rounding to the first decimal place. The experimental errors that would be calculated from the data of Morssink and van Bodegom [8] are in the second decimal place.

The angles determined from the orientation of the  $g$  tensors at 77 K and 298 K do agree to within the experimental error. This is to be expected since no significant shift in the direction cosines with respect to a fixed set of axis was found between 77 K and 298 K. The most significant result is that the relative angles between the principal vectors of the  $g$  tensor do not agree with the relative angles between the symmetry directions of the TCNQ molecule as determined by the X-ray data. This indicates that the orientation of the the  $g$  tensor is not entirely determined by the orientation of the individual TCNQ molecules, but one must also take into account the environment of these molecules in order to account for the experimental results.

It is interesting to compare the  $g$  values of the individual stacks calculated

using the theory of chapter 4 from the experimentally measured  $g$  values with the experimental data itself. The most significant difference is the repulsion of the coupled modes at the crossover point. This repulsion is proportional to  $\Omega_{Ae} + \Omega_{Be}$ . The difference in  $g$  between the coupled modes and the  $g$  values of the individual stacks is less than  $2 \times 10^{-4}$  at 77 K and in many cases less than  $5 \times 10^{-5}$  at room temperature. This difference is less than the systematic and statistical errors of many of the previous results [4,22]. This has allowed the reasonable fit of the data for coupled stacks to the theory for non interacting stacks that is found in these references.

### 5.3 The Susceptibility Measurements

The results for the normalized susceptibilities are shown in figures 25 to 27 for the 298 K measurements and figures 28 to 30 for the 77 K measurements. The solid line in the figures corresponds to a fit to the theory that was performed at the same time as the fit of the  $g$  value data. The errors in the susceptibilities have a systematic component above the error due to the scatter of the data points. This systematic error arises from the small saturation of the lines which affects the two resonances differently since the linewidths are different. This error was estimated by comparing the results at different power levels within the range that was used for the measurements and was found to produce an error of about 0.04 in normalized susceptibilities.

The measured parameters  $\Omega_{Ae}$  and  $\Omega_{Be}$  are the product of  $J$  and the susceptibilities of each of the TCNQ stacks. In our measurements we do not obtain reliable values of the total susceptibility as a function of angle as explained in chapter 2.

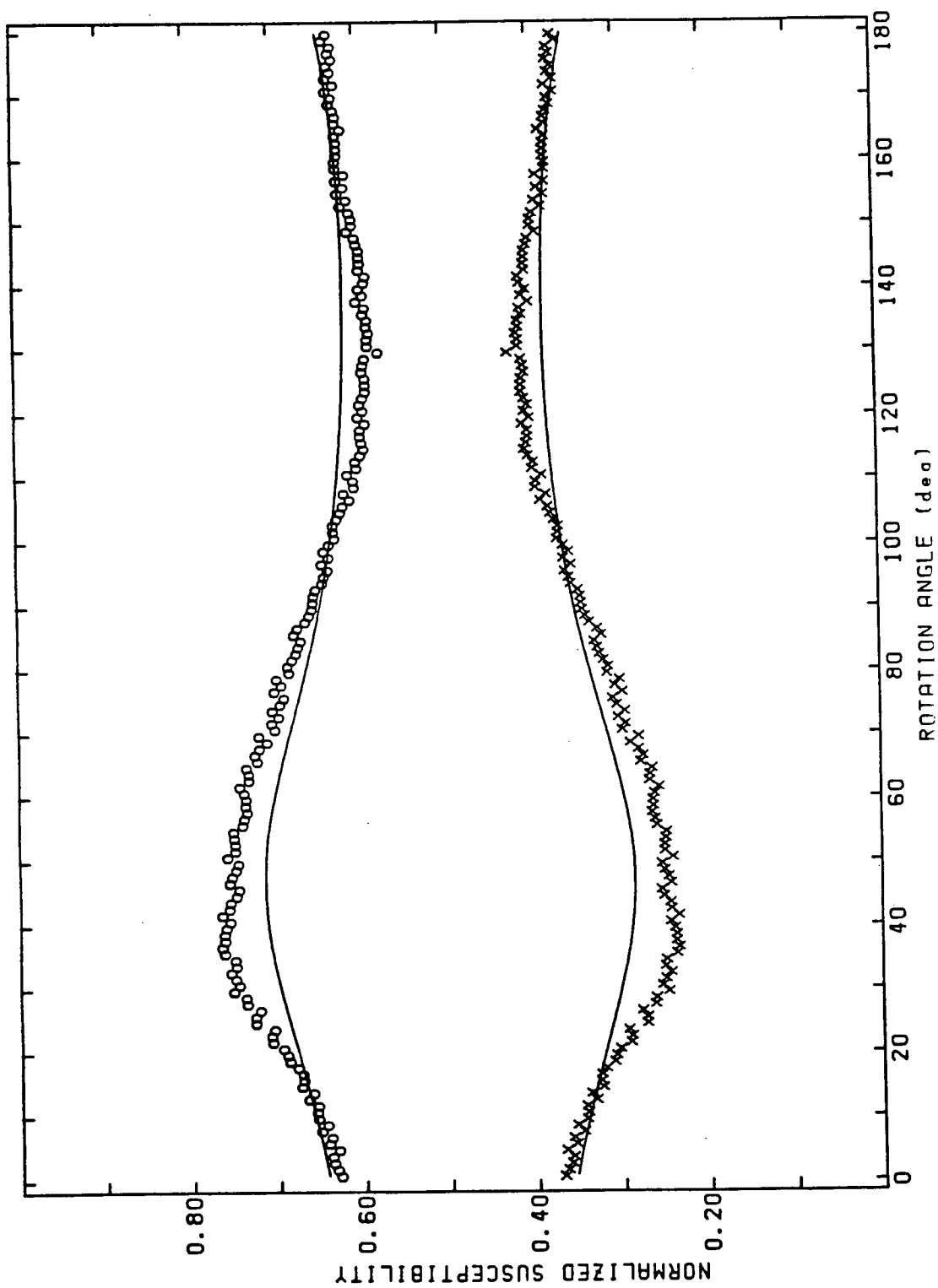


Figure 25: Normalized Susceptibility of  $\text{DEM}(\text{TCNQ})_2$  for a Rotation about  $\mathbf{a}$  at 298 K. The solid line is a fit to the theory.

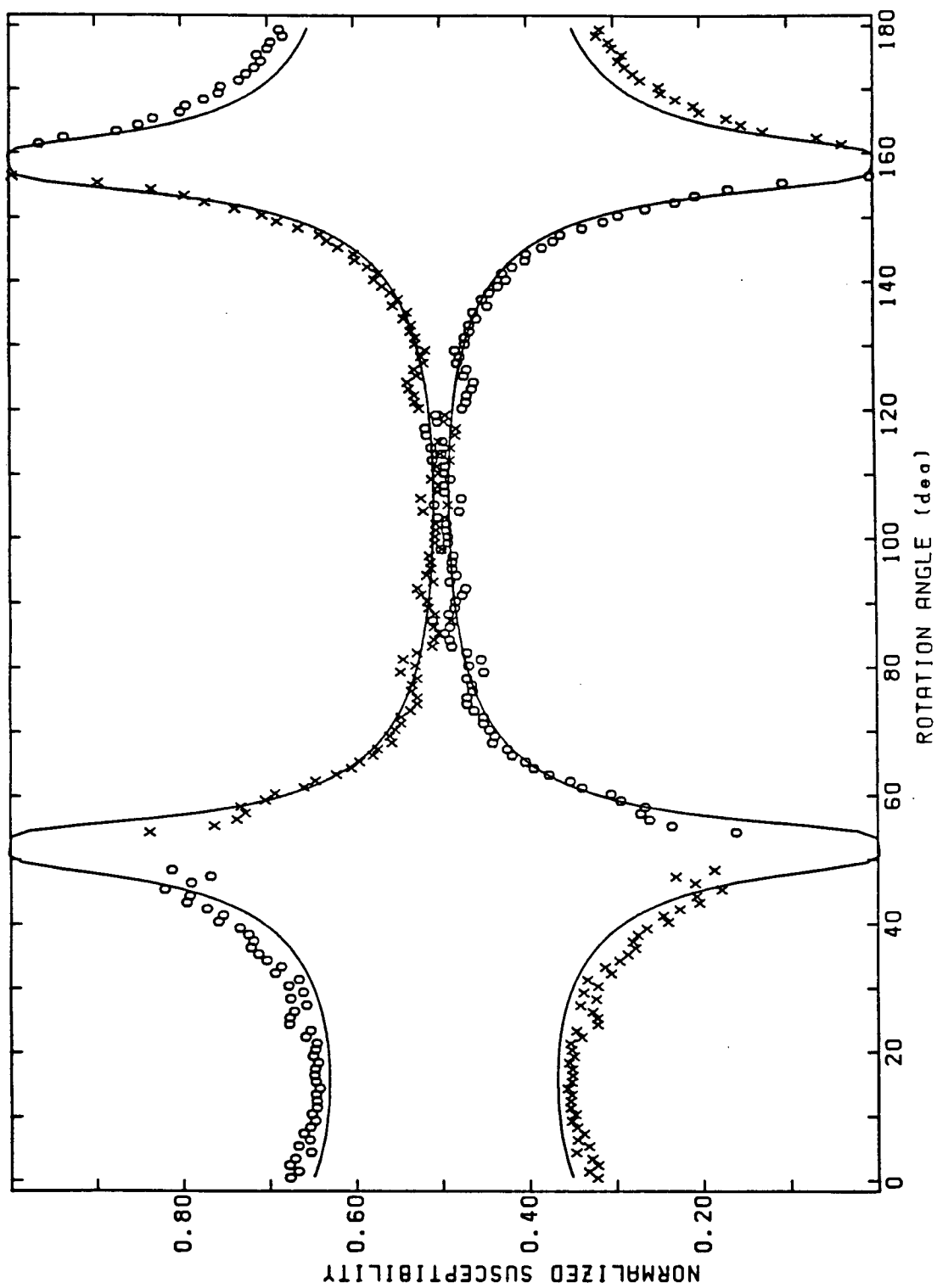


Figure 26: Normalized Susceptibility of  $\text{DEM}(\text{TCNQ})_2$  for a Rotation about  $b$  at 298 K. The solid line is a fit to the theory.

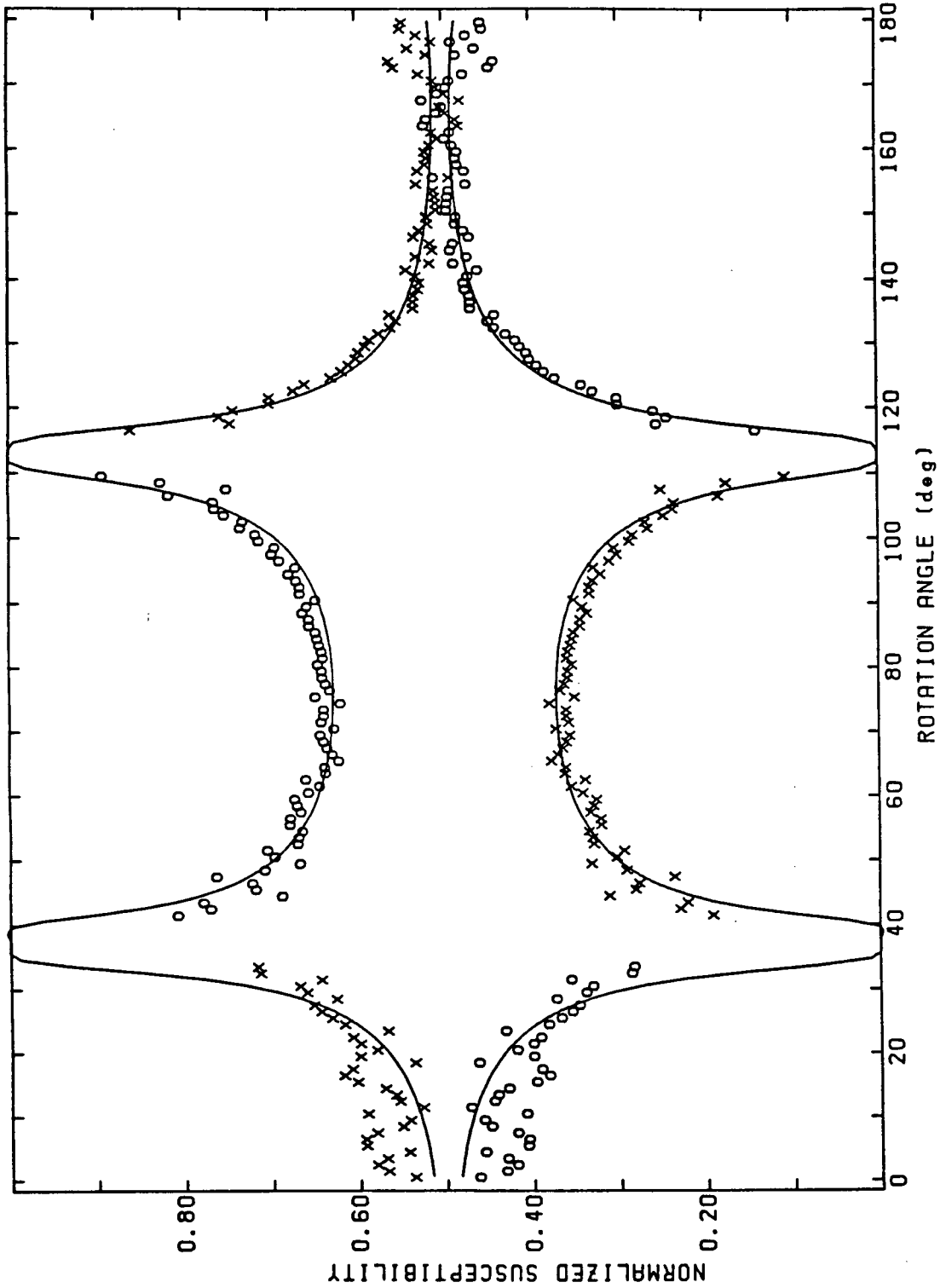


Figure 27: Normalized Susceptibility of DEM(TCNQ)<sub>2</sub> for a Rotation about c at 298 K. The solid line is a fit to the theory.

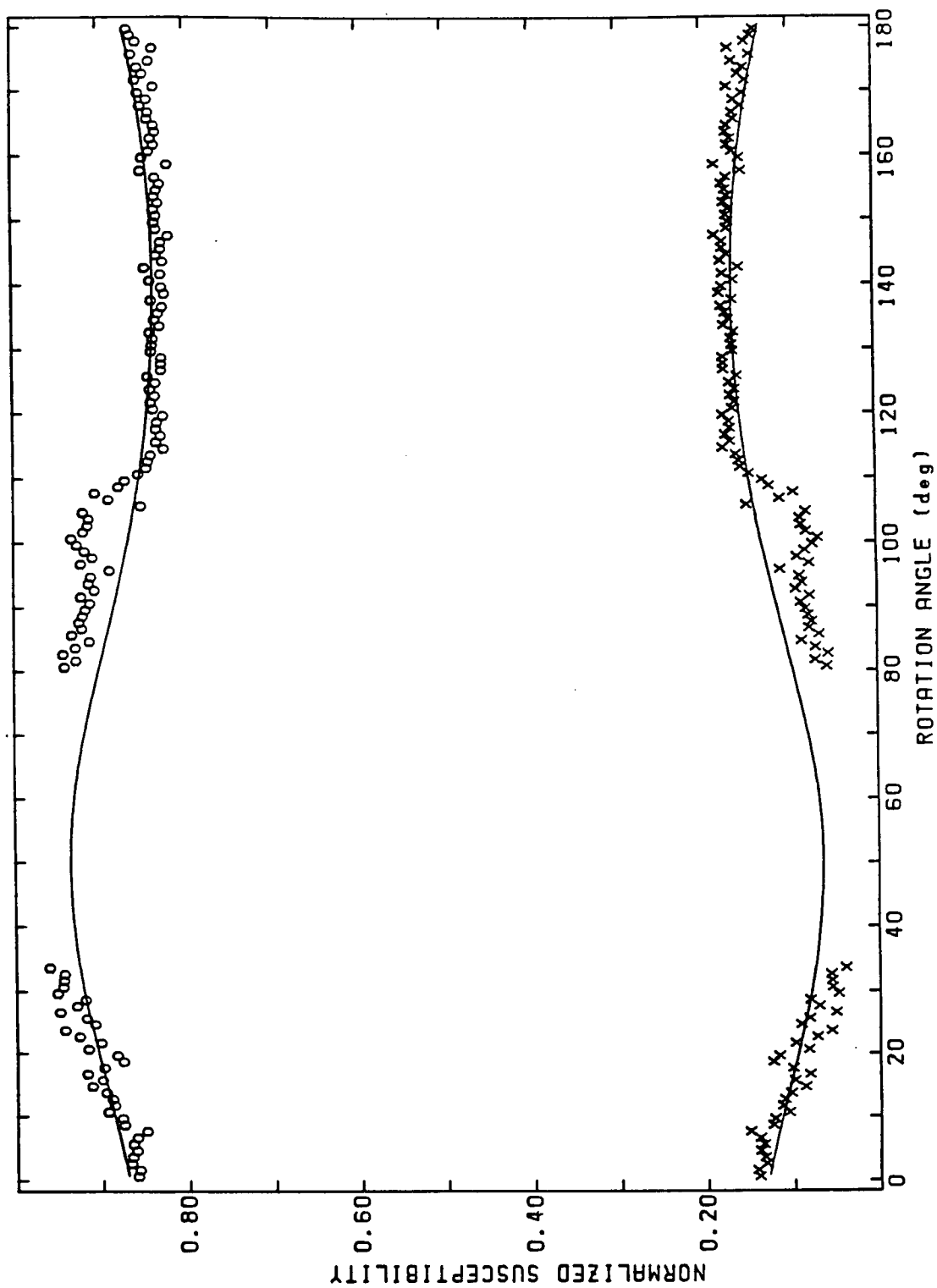


Figure 28: Normalized Susceptibility of  $\text{DEM}(\text{TCNQ})_2$  for a Rotation about a at 77 K. The solid line is a fit to the theory.

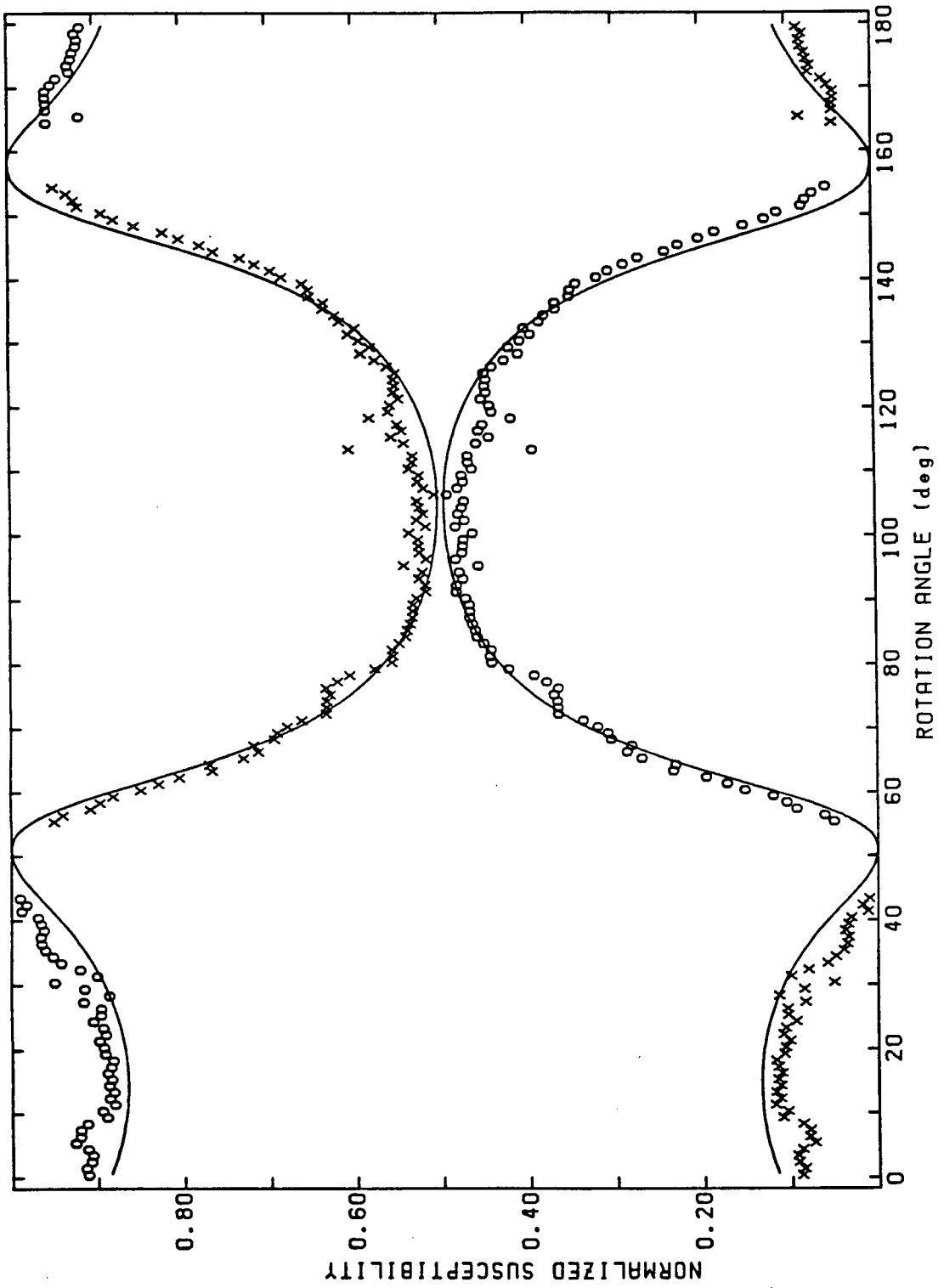


Figure 29: Normalized Susceptibility of DEM(TCNQ)<sub>2</sub> for a Rotation about *b* at 77 K. The solid line is a fit to the theory.

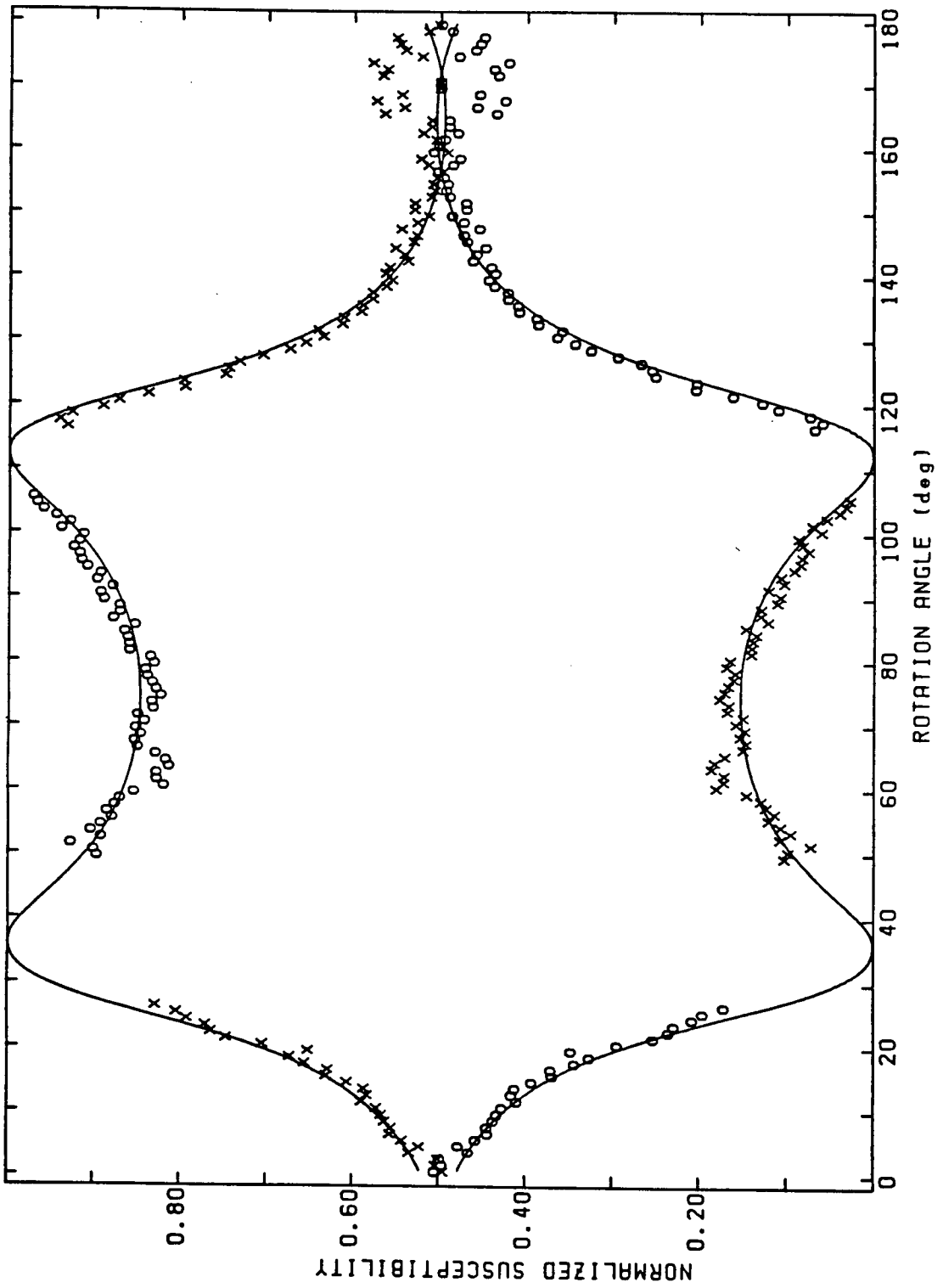


Figure 30: Normalized Susceptibility of DEM(TCNQ)<sub>2</sub> for a Rotation about c at 77 K. The solid line is a fit to the theory.

Band	Temp (K)	$\Delta g$	$J$ ( $\text{K} \times 10^{-2}$ )	$J/\chi$ ( $\text{gauss}^2 \times 10^9$ )	$\chi_A/\chi_B$
Q	298	0.00008078(46)	2.886(28)	2.28(3)	0.944(6)
Q	77	0.00026029(37)	5.194(28)	2.30(2)	0.790(2)
X	77	0.00025(2)	5.0(4)	2.2(2)	—

Table VIII: Inter Stack Exchange Constant and Ratio of Susceptibilities for DEM-(TCNQ)<sub>2</sub>

The value of  $J$  can be calculated by using the published results for the total susceptibility,  $\chi$ , of DEM(TCNQ)<sub>2</sub> [26]. Measurements of the total susceptibility do not need to take into account the coupling between the stacks and consequently should not be affected by the theory of chapter 4. The values of  $\chi$  from reference [26] are 0.00105(1) emu/mol and 0.00188(1) emu/mol at the temperatures 298 K and 77 K respectively. These values were estimated for DEM(TCNQ)<sub>2</sub> from the plot of the susceptibility of DEM(TCNQ)<sub>2</sub> given in reference [26]. The value of  $J$  is then calculated using the equation

$$J = \frac{\beta^2 \Delta g N_0}{\chi} \quad (5.1)$$

where  $\Delta g = \frac{\Omega_A + \Omega_B}{\beta H N}$  and  $N_0$  is Avogadro's number since the susceptibilities are given for a mole in reference [26].

The experimentally measured values for  $\Delta g$ ,  $J$ ,  $J/\chi$  and  $\chi_A/\chi_B$  are given in table VIII. We also include the values calculated from the data of Schwerdtfeger and Wagner [22] at X-band and 77 K for comparison. No result for  $\chi_A/\chi_B$  was estimated from the X-band data, instead the value of  $\chi_A/\chi_B$  from the Q-band data at 77 K was used. The most significant result is that the value of  $J/\chi$  is the same in all the cases to within the experimental error. This indicates that  $J$  depends only on the susceptibility when the results at Q-band at 77 K and 298 K and the results at X-band at 77 K are compared.

The experimental errors in  $\Delta g$  were the errors obtained from the fit and the halfwidth approximation explained in the analysis of the errors in  $g$  since the other systematic errors in  $g$  can be neglected in this case. The errors in the results derived from published data only include the error in estimation from the published plots and do not include any errors in the the actual data since no estimate of these errors were given by the authors.

As a check on how well the theory fits the experiment a  $\chi^2_\nu$  test was performed on the  $g$  value and susceptibility data using the formula from Bevington [25, p. 202]. We found values for  $\chi^2_\nu$  of 0.99 and 1.03 for the 298 K and 77 K data respectively. In this calculation the systematic errors in the experiment were used as the estimated errors in the data points since the systematic errors were the dominant errors in both the susceptibility and the  $g$  value data. The values for  $\chi^2_\nu$  obtained indicate, by being close to 1, that the theory does fit the data well and that the error estimates were accurate.

#### 5.4 The Halfwidth Measurements

The halfwidth data are presented in figures 31 to 33 for the data at 298 K and in figures 34 to 36 for the data at 77 K. The solid lines are calculated from the theory with the assumption that the individual halfwidths  $\frac{1}{T_A}$  and  $\frac{1}{T_B}$  are smooth functions of the rotation angle. We have assumed that the cross relaxation times  $\frac{1}{T_{Ae}}$  and  $\frac{1}{T_{Be}}$  are related to the relaxation times  $\frac{1}{T_A}$  and  $\frac{1}{T_B}$  by a relationship of the form

$$\frac{1}{T_{ie}} = k \frac{1}{T_i}$$

with  $i = A, B$ . The parameter  $k$  is then assumed to be a function of the 20 parameters of the fit to the  $g$  value and susceptibility data. This functional relationship

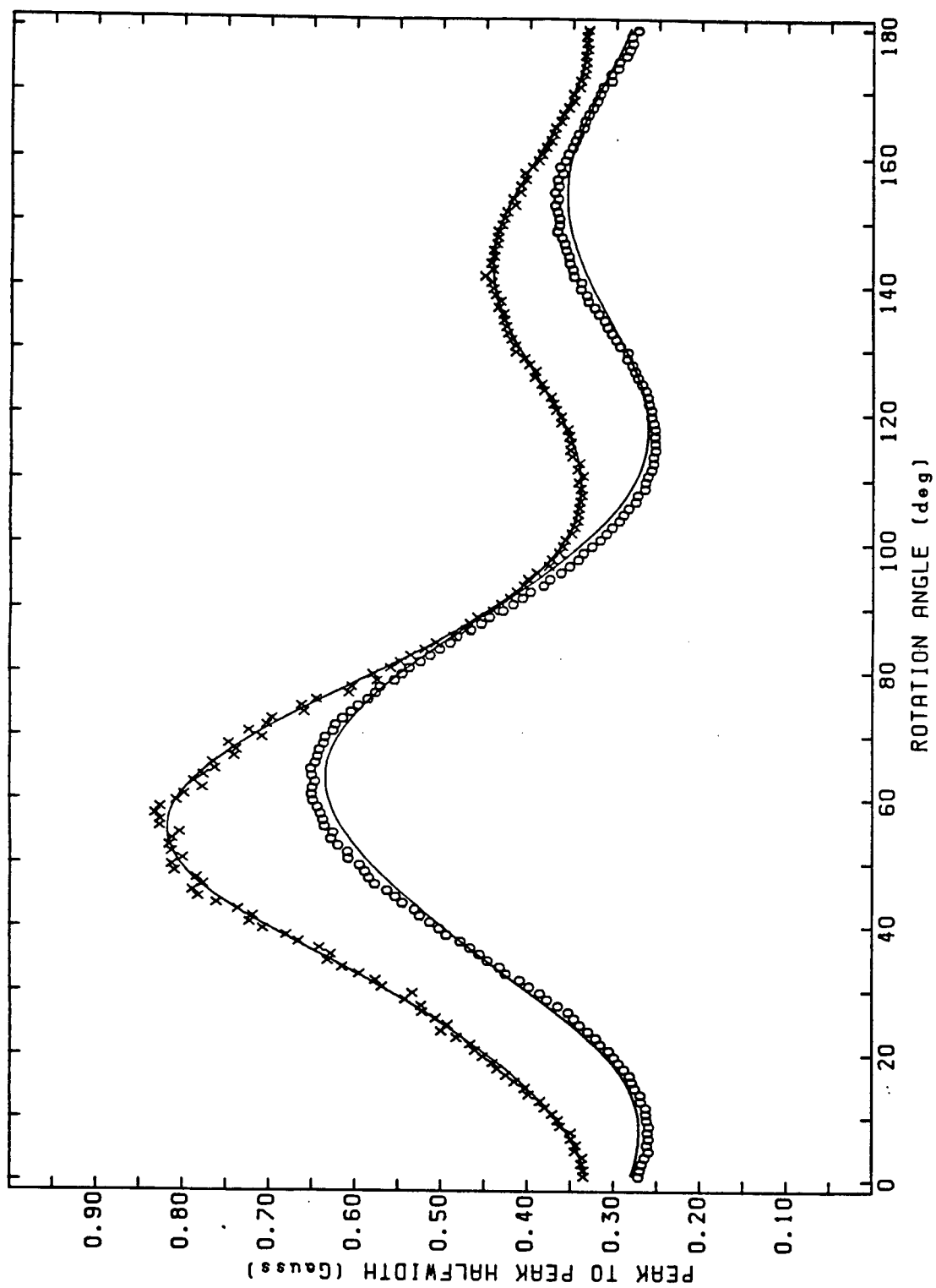


Figure 31: Linewidths of  $\text{DEM}(\text{TCNQ})_2$  for a Rotation about a at 298 K. The solid line is a fit to the theory.

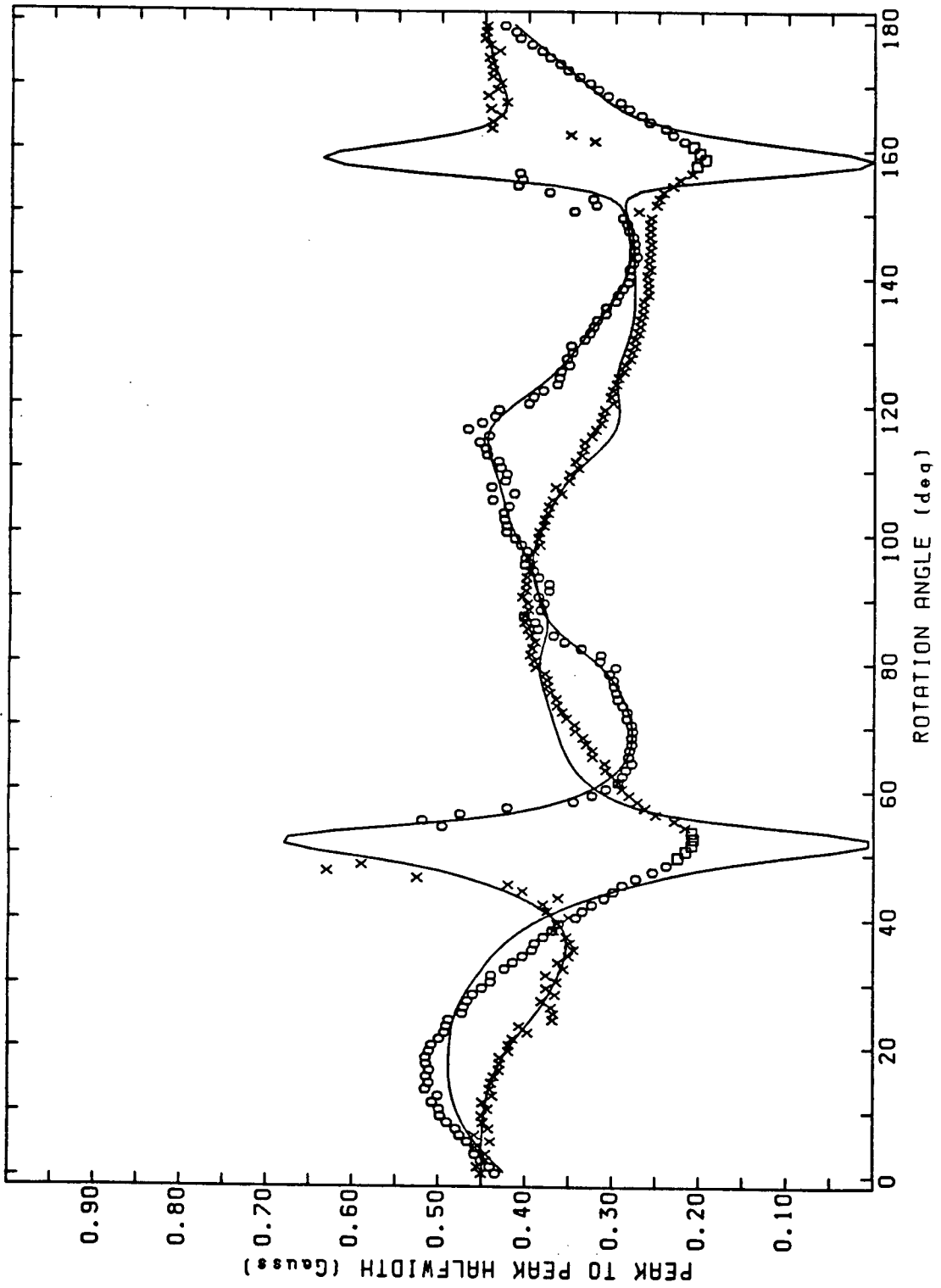


Figure 32: Linewidths of  $\text{DEM}(\text{TCNQ})_2$  for a Rotation about  $b$  at 298 K. The solid line is a fit to the theory.

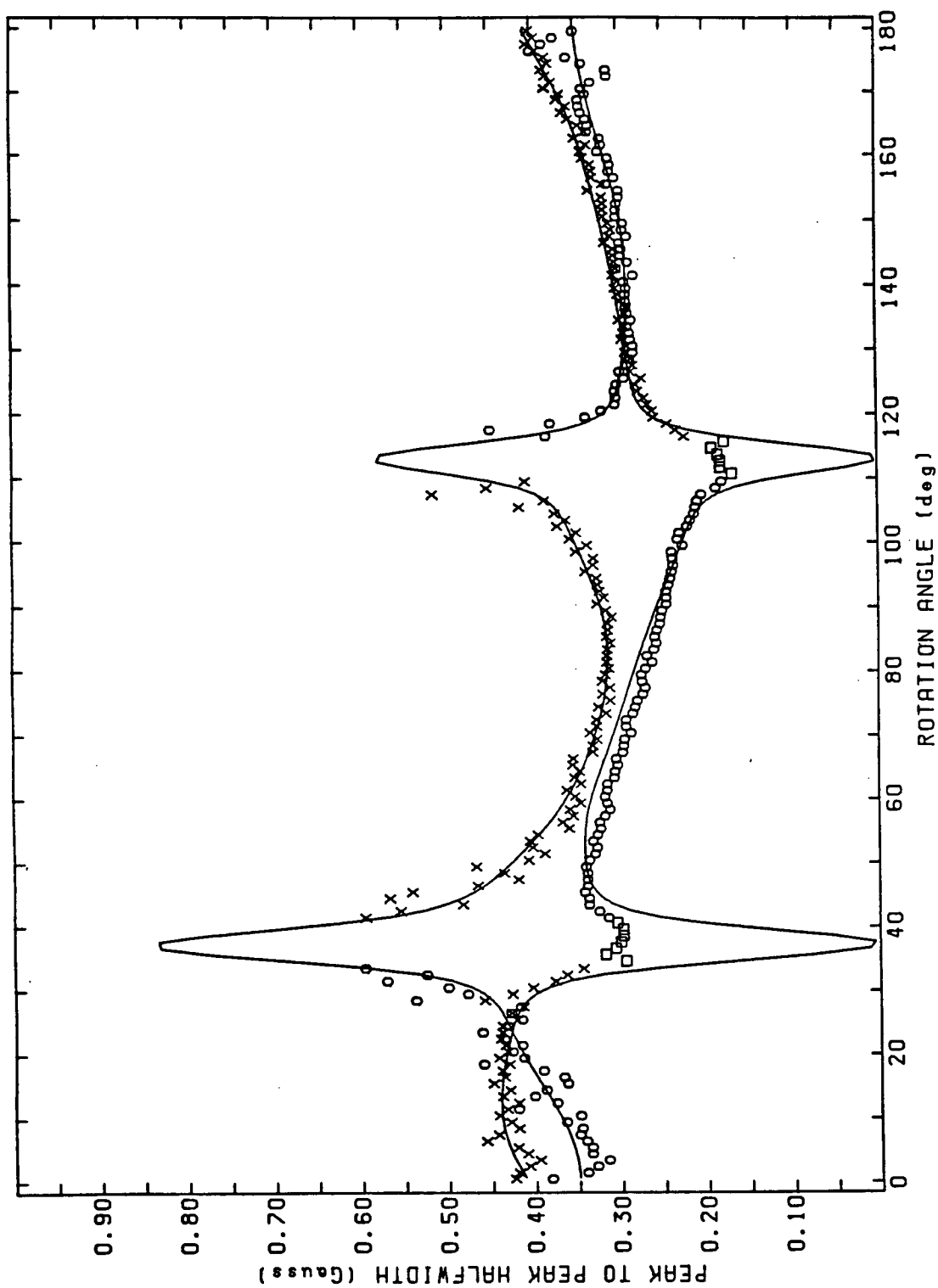


Figure 33: Linewidths of  $\text{DEM}(\text{TCNQ})_2$  for a Rotation about  $c$  at 298 K. The solid line is a fit to the theory.

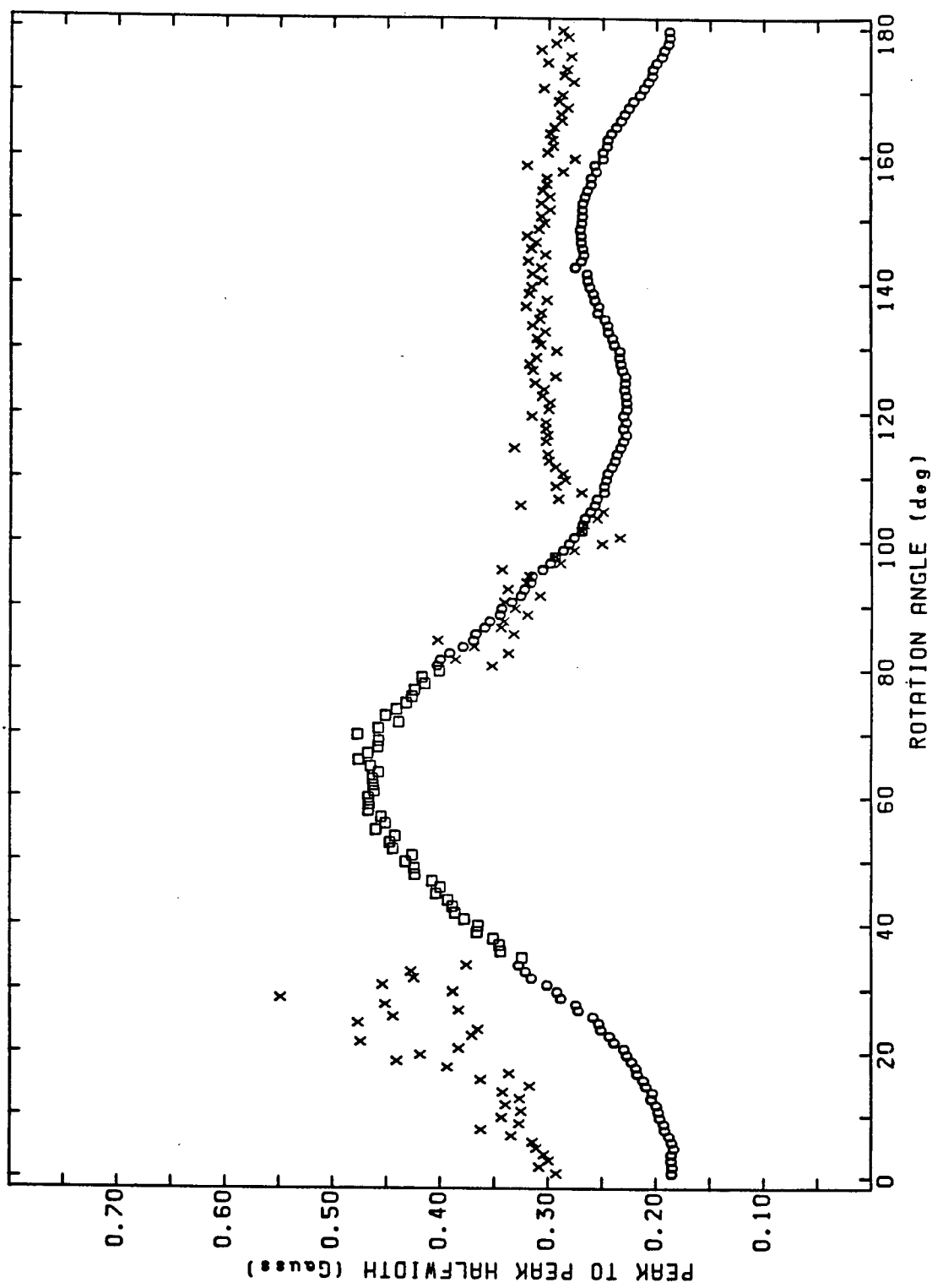


Figure 34: Linewidths of  $\text{DEM}(\text{TCNQ})_2$  for a Rotation about a at 77 K.

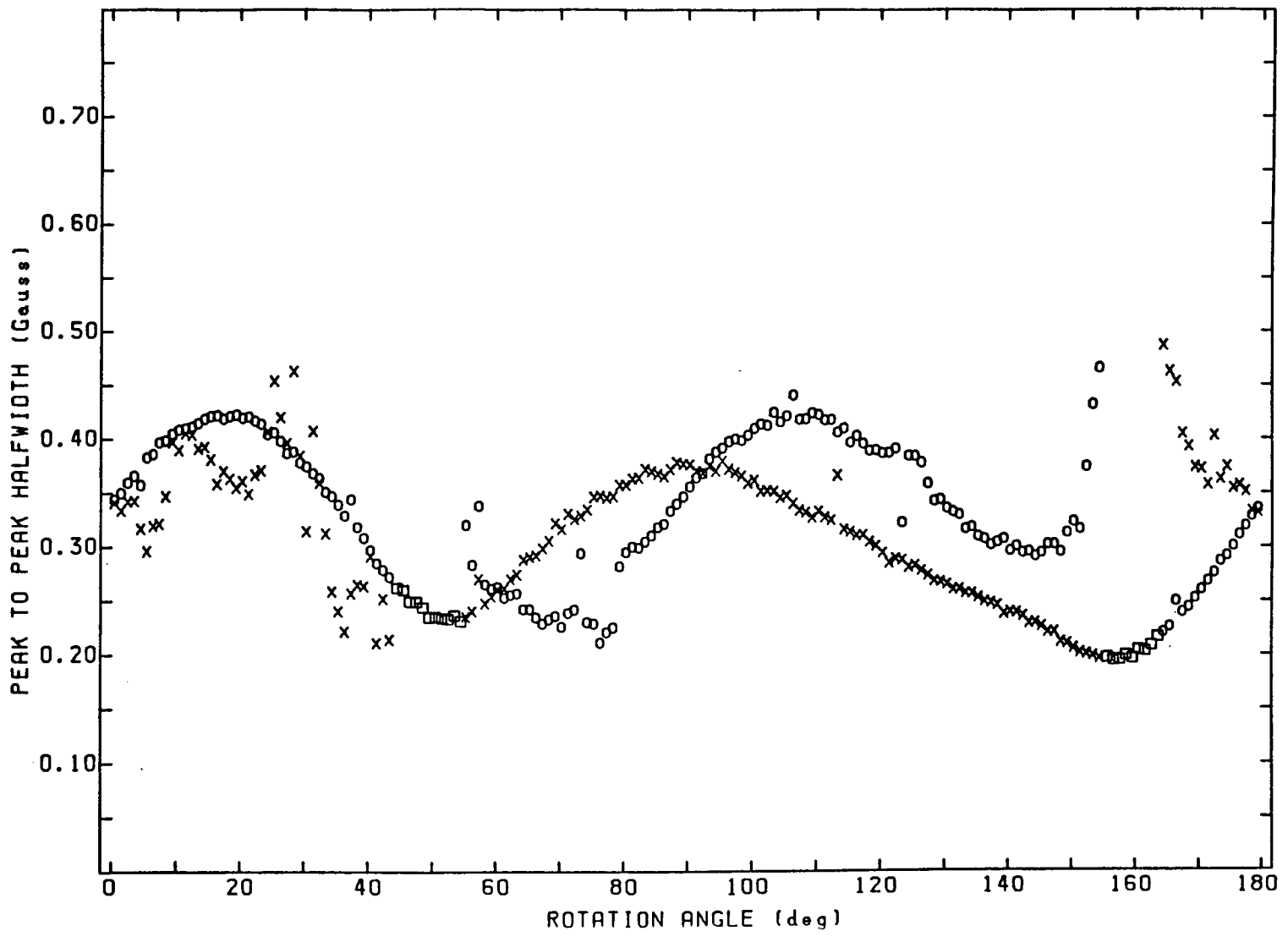


Figure 35: Linewidths of DEM(TCNQ)<sub>2</sub> for a Rotation about b at 77 K.

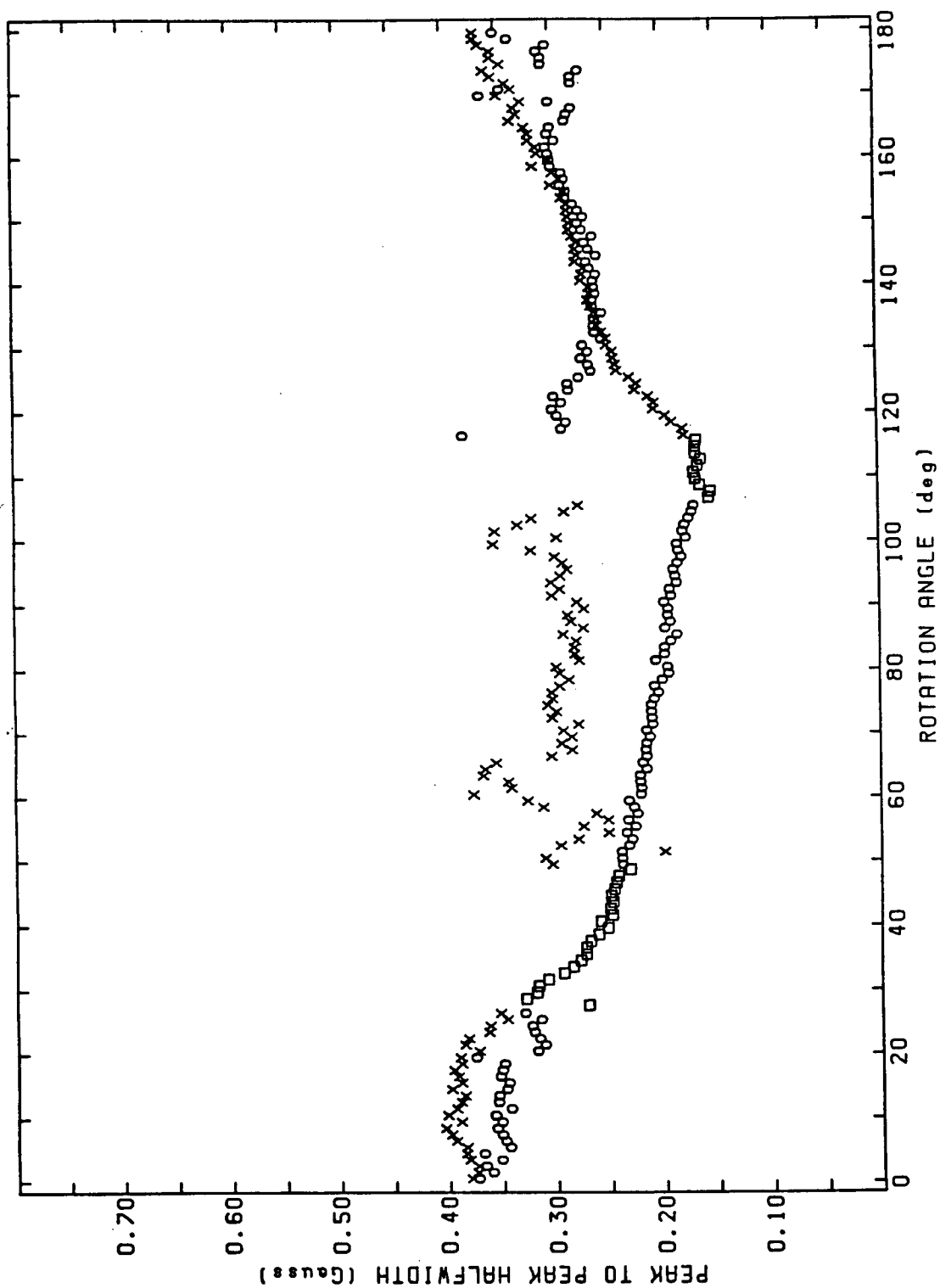


Figure 36: Linewidths of DEM(TCNQ)<sub>2</sub> for a Rotation about c at 77 K.

is chosen to best fit the halfwidth data particularly in the orientations close to the level crossing. A further requirement is that the spin-spin relaxation times  $\frac{1}{T_A}$  and  $\frac{1}{T_B}$  be smooth functions of the orientation in the region of the overlap.

We now consider the form of the linewidths of the experimentally measured lines in the overlap region. We find that the sum of the experimentally measured linewidths has an unexpected increase in the overlap region. This sum is equal to  $\frac{1}{T_A} + \frac{1}{T_B}$  and consequently should not increase in the overlap region. We find that this unexpected increase is close to the inverse relaxation time of the narrower of the two lines with the inverse relaxation time of the broader line being close to what we expect for the sum of the measured relaxation times. This leads us to expect saturation of the narrower line in the crossover region. According to our theory for  $k = 1$  at the crossover point the relaxation time of the narrower line should become infinite when compared to that of the broader line at the point where the levels cross, consequently saturation and overmodulation of this line would be expected. We will see in the next chapter that this is indeed the case.

If we consider a region far from the level crossing we expect the cross relaxation times become infinite. This means that  $k = 0$  in this region. With this in mind we have postulated a plausible functional form for  $k$  given by

$$k = \frac{\Delta_g \Omega_{Ae} \Omega_{Be}}{\Delta_g^2 + \Omega_{Ae} \Omega_{Be}} \quad (5.2)$$

with

$$\Delta_g = \frac{1}{2} \left[ \omega_B - \omega_A + \Omega_{Ae} - \Omega_{Be} - \sqrt{(\omega_B - \omega_A + \Omega_{Ae} - \Omega_{Be})^2 + 4\Omega_{Ae} \Omega_{Be}} \right]$$

This functional form for  $k$  was used to calculate the spin-spin relaxation times  $T_A$  and  $T_B$ , at each data point, of each individual stack using the values for the  $g$  values and susceptibilities obtained from the fit of the theory to the  $g$  value

and susceptibility data. The calculated relaxation times of each stack were then smoothed using cubic splines with the further constraint of no variation of the individual relaxation times in the crossover region. These smoothed relaxation times together with the assumed functional form of  $k$  were used to calculate again the linewidths of the experimentally measured lines. These calculations show that if we have no variation in  $T_A$  and  $T_B$  over the crossover region and a functional form for  $k$  as given by equation 5.2 we can predict the experimental form of the linewidths in the crossover region. The predicted linewidths are shown as the solid lines that are drawn through the linewidth data at 298 K. This calculation was not performed at 77 K because reliable estimates of the spin-spin relaxation times of each individual stack could not be obtained in the overlap position due to the scatter in the data.

The results of this calculation agree with the measured linewidth in the crossover region for the broad line. This calculation also predicts that the narrow line should have a vanishing linewidth which is not observed experimentally. We will see in the next chapter that this narrow line is saturated and overmodulated in the crossover region, and this prevents the experimental observation of the linewidth. If the line is so narrow in the overlap region then this can only be tested by a pulsed ESR experiment where this long spin-spin relaxation time could be measured.

## 5.5 Discussion of the Results

The most significant conclusion from the experimental results of this chapter is that the experimental data can be fit to the theory for the case of no correlation between the stacks. In introducing this theory only one extra parameter  $J$  is introduced. We have found  $J$  to have a temperature dependence that is the same as that found

for the total susceptibility to within the experimental error. This in fact means that only one parameter is introduced by the theory for measurements at 77 K and 298 K.

The  $g$  tensor data show some significant results. The first is that there is a small but measurable temperature dependence in the  $g$  value data even after accounting for the effect of the coupling between the stacks. A similar effect was also found in the results for MEM(TCNQ)<sub>2</sub>. As was the case for the MEM(TCNQ)<sub>2</sub> results there was no change in the direction cosines of the  $g$  tensor. This indicates that there were no measurable structural changes between the 77 K and 298 K data that could account for the difference in  $g$  value between the results at 77 K and 298 K.

Another significant result is that the  $g$  tensor principal values of the  $A$  and  $B$  stacks are different. These values are also different from those found for MEM(TCNQ)<sub>2</sub>. It was also found that the relative orientation of the principal values does not correspond exactly to the relative direction of the TCNQ stacks as found from X-ray data of Morssink and van Bodegom [8]. The basic conclusion is that the  $g$  tensors do in fact depend on the environment of the TCNQ molecules and not just on the TCNQ molecules themselves as proposed by Tomkiewicz *et al.* [16]. We will discuss this matter further and compare to other published results in chapter 7.

## Chapter 6

### Power Saturation Measurements of DEM(TCNQ)<sub>2</sub>

#### 6.1 The ESR Experiment

In this chapter we propose to address the question of possible overmodulation or saturation of the resonance lines particularly in the region where there is an crossover of the resonances. We can detect the presence of saturation and overmodulation by comparing the susceptibility and halfwidth as a function of power with the results that would be expected for a saturated or an overmodulated line.

In chapter 2 we described the ESR spectrometer and experimental method. We found that as a function of angle it was impossible to obtain reliable data for the total susceptibility. This was due to the fact that the power level at the sample could not be determined absolutely since the TCNQ and calibration samples were at different parts of the microwave mode in the cavity. We can however obtain reliable relative values of the absolute susceptibility as a function of power provided that the sample is not rotated in the cavity. This alone is not sufficient to determine if there is saturation as a function of angle since we do not have even an approximate estimate of the power as a function of angle.

In order to determine if there is saturation as a function of angle we need an estimate of the possible variation in the microwave power at the TCNQ sample as

the sample is rotated in the cavity. We can obtain such an estimate by comparing the measured values of the total susceptibility of  $\text{DEM}(\text{TCNQ})_2$  at points where the energy levels of the two kinds of TCNQ stacks are far apart so that any possible saturation would be the same in both cases. If we make such a comparison we find that the power variation is at most 50% as a function of angle. We can then make comparisons between runs at different angles if we keep in mind that the power at the TCNQ sample can vary by not more than 50% over a  $180^\circ$  rotation of the crystal in the magnetic field. This allows a the detection of saturation of the resonances at certain angles.

The measurement of the linewidth as a function of power provides an independent determination of saturation or overmodulation of the resonances. This allows us to detect an overmodulated line, since we can check for any saturation of the lines with the susceptibility measurements alone, by comparing the measured linewidth as a function of power with the results that would be expected for a resonance that is saturated but not overmodulated.

## 6.2 Saturation and Overmodulation of the Coupled Spin System

In treating the saturation and overmodulation of the coupled system we are assuming two uncoupled resonances at the positions of the actual resonances. We now consider the assumptions that have been made implicitly in this approximation. We first consider the saturation of the coupled system. To the equations 4.8 we must add two equations of motion for  $\frac{dS_{A_z}}{dt}$  and  $\frac{dS_{B_z}}{dt}$  to obtain the following equations of

motion

$$\begin{aligned}
\frac{dS_{Ax}}{dt} &= (\omega_A - \omega)S_{Ay} - \frac{S_{Ax}}{T_{2A}} + \frac{S_{Dx}}{T_{Dc}} + \frac{J}{N\hbar}(S_{Ay}S_{Bz} - S_{By}S_{Az}) \\
\frac{dS_{Ay}}{dt} &= -(\omega_A - \omega)S_{Ax} - \frac{S_{Ay}}{T_{2A}} + \frac{S_{Dy}}{T_{Dc}} - \frac{J}{N\hbar}(S_{Ax}S_{Bz} - S_{Bx}S_{Az}) - \frac{\omega_A H_1 S_{Az}}{H_0} \\
\frac{dS_{Az}}{dt} &= -\frac{S_{Az} - S_{Az0}}{T_1} - \frac{\omega_A H_1 S_{Ay}}{H_0} \\
\frac{dS_{Bx}}{dt} &= (\omega_B - \omega)S_{By} - \frac{S_{Bx}}{T_{2B}} + \frac{S_{Ax}}{T_{Ac}} + \frac{J}{N\hbar}(S_{By}S_{Az} - S_{Ay}S_{Bz}) \\
\frac{dS_{By}}{dt} &= -(\omega_B - \omega)S_{Bx} - \frac{S_{By}}{T_{2B}} + \frac{S_{Ay}}{T_{Ac}} - \frac{J}{N\hbar}(S_{Bx}S_{Az} - S_{Ax}S_{Bz}) - \frac{\omega_B H_1 S_{Bz}}{H_0} \\
\frac{dS_{Bz}}{dt} &= -\frac{S_{Bz} - S_{Bz0}}{T_1} - \frac{\omega_B H_1 S_{By}}{H_0}
\end{aligned} \tag{6.1}$$

We have assumed a single spin-lattice relaxation time for both stacks of the crystal. The second assumption is that the spin lattice relaxation does not depend on the interaction of the stacks. This approximation involves neglecting terms of the form  $\frac{J}{N\hbar}(S_{Ay}S_{Bz} - S_{By}S_{Az})$  in the equations for  $\frac{dS_{Az}}{dt}$  and  $\frac{dS_{Bz}}{dt}$  and neglecting the effects of cross relaxation between the stacks on the measured spin-lattice relaxation time.

We treat the  $S_{iz}$  as constants when solving for the  $S_{ix}$  and  $S_{iy}$ . This involves the  $\sin \theta = \theta$  approximation discussed in chapter 4. The solution for  $S_{ix}$  and  $S_{iy}$  is then the same as in chapter 4. We then approximate the results of chapter 4 by assuming a lorentzian lineshape when there is no saturation. This involves neglecting the asymmetry in the lineshape introduced by the spin-spin relaxation times in the theory of chapter 4. With all of these approximations we find that the saturation behavior of the coupled resonances can be treated as the saturation of two uncoupled resonances. The treatment for a single resonance is given in many standard texts for example Poole [27, p. 563]. We can then have a standard that

can be used to compare our experimental data.

### 6.3 Experimental Results

The experimental results for the susceptibilities and halfwidths are shown in figs 37 and 38. The random experimental errors in these results are manifested in the scatter of the data points. A more significant experimental error is the relative error in the power between the various angles and the absolute error in the power. The power measurements correspond to the power entering the cavity. The measurements do not indicate the power at the sample. The latter power is not known in absolute terms. This is not critical since the values of the susceptibility are given in arbitrary units. The critical error is the variation in power between the various angles. In the previous section we estimated this variation to be about 50% over the full 180° rotation. For the range in angles the variation in power is about 20%. This variation occurs because of a change in the position of the TCNQ sample in the mode of the cavity that is not the same as the change in the position of the LiF:Li calibration when the sample is rotated. This error would be significant if we seek a quantitative measurement of  $T_1$  from the power measurements; however it is not significant if we seek only qualitative results as to the presence of saturation or overmodulation.

### 6.4 Conclusions from the Power Data

When we consider the power data we find that there is a profound difference in the susceptibility and halfwidth as a function of power between those angles close to the crossover and those angles that are far away from the crossover. A crossover angle from the data of chapter 5 is  $\theta = 113.0^\circ$  for this orientation. The angle  $112.5^\circ$

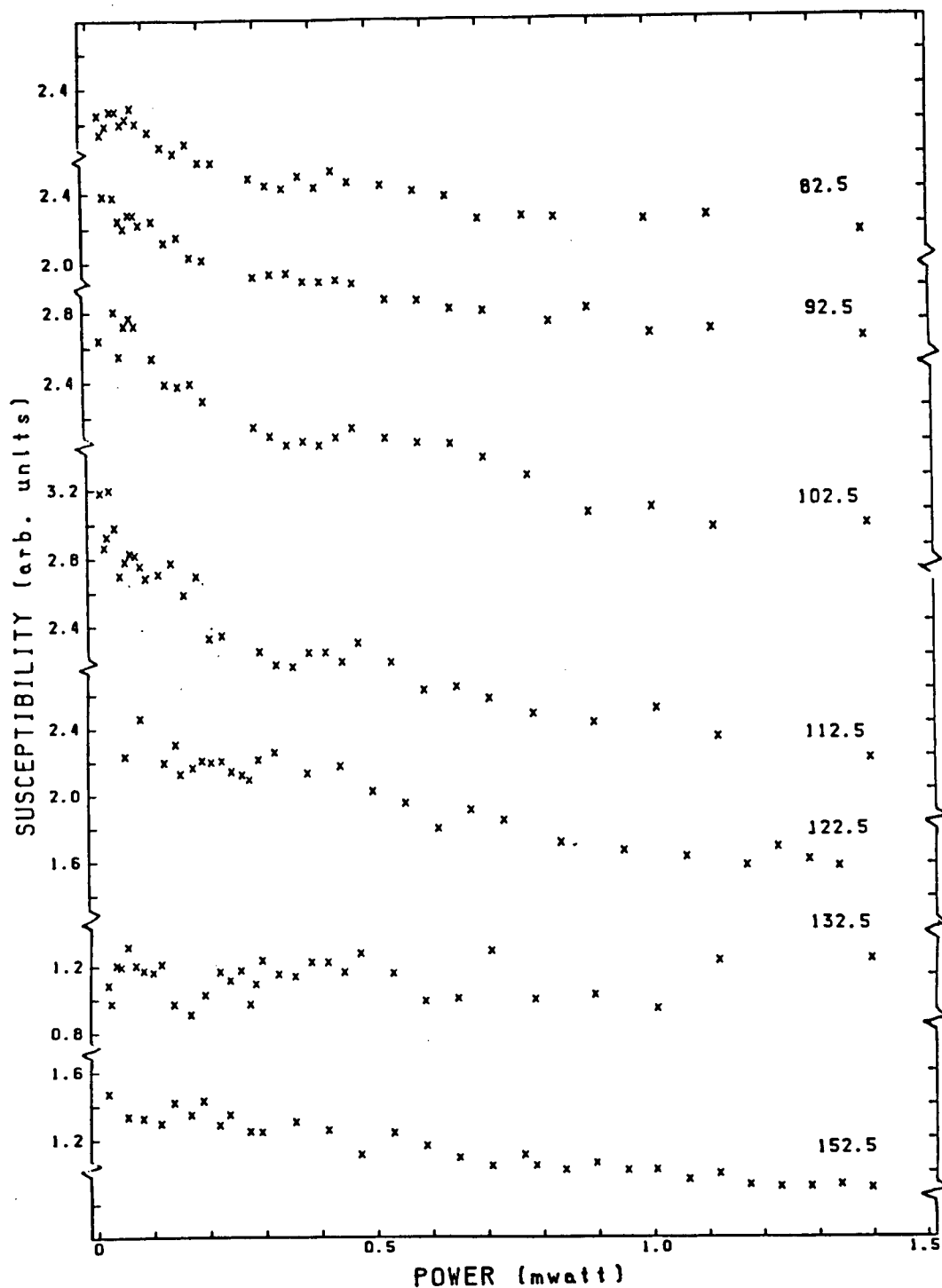


Figure 37: Susceptibility of the High  $g$  value Mode of  $\text{DEM}(\text{TCNQ})_2$  as a Function of Power for Angles between 82.5 and 152.5° of a Rotation about  $c$ .

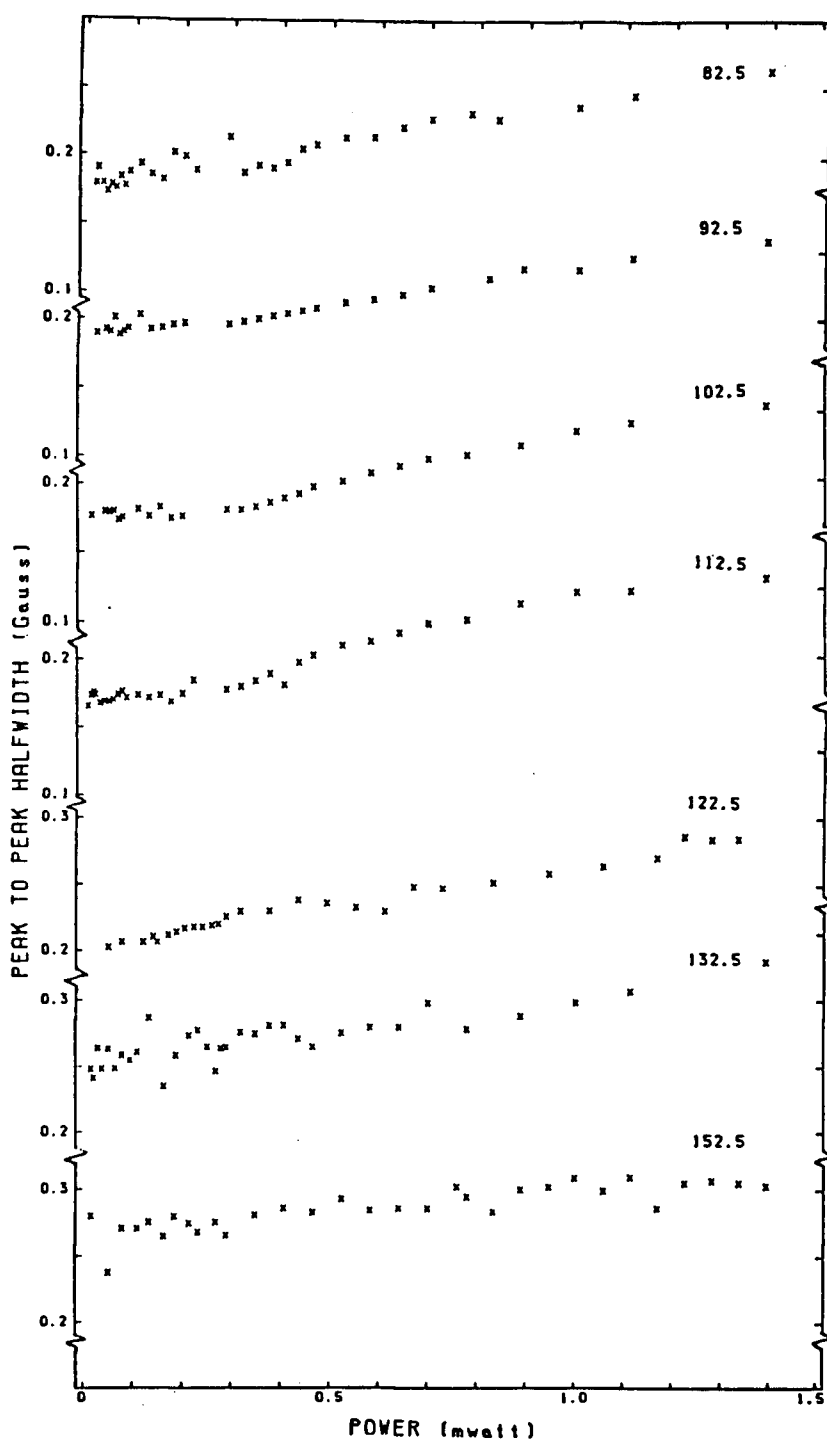


Figure 38: Peak to Peak Halfwidth of the High  $g$  value Mode of  $\text{DEM}(\text{TCNQ})_2$  as a Function of Power for Angles between  $82.5$  and  $152.5^\circ$  of a Rotation about  $c$ .

shows the most profound effect. The line is overmodulated. This can be seen from the change in the measured susceptibility with a constant halfwidth at low power. The increase in the susceptibility with higher power shows the effect of saturation. If we move away from the crossover region we find a less pronounced effect; however some overmodulation and saturation are still present.

The qualitative picture is consistent with a very narrow line at the crossover point. It is not possible from these measurements to determine the actual linewidth of this line; however the measurements do show that the line is both overmodulated and saturated in the crossover region. Away from the crossover region there is still some overmodulation and saturation of this line, however the effect is much less significant particularly for orientations where the linewidth due to the spin-spin relaxation times is significantly broader than the minimum linewidth measured.

In reaching these conclusions we first considered the case of saturation and no overmodulation. In such a case Poole [27, p. 593] predicts a constant measured susceptibility in the region where the halfwidth is constant. This was not measured experimentally particularly in the runs close to the crossover. It is this last result that leads to the prediction of overmodulation as well as saturation in the lines at angles close to the crossover region.

An important experimental question is the source of the overmodulation. We found that reducing the applied modulation of the magnetic field did not affect the linewidth of these resonances. The source of this overmodulation is due to modulation of the microwave frequency by the A.F.C. This has the same effect on the linewidth as an equivalent modulation in the magnetic field. When the effective magnetic field modulation from this source is calculated it is indeed found that the variation in the microwave frequency at a given point in a magnetic field scan is comparable to the linewidth of the high  $g$  value line in the crossover region. As a

further check of this effect the A.F.C modulation was varied and a profound effect on the lineshape was found when this modulation was increased. Schwerdtfeger [28] had found a similar distortion of the resonances at X-band for the ESR lines of DEM(TCNQ)<sub>2</sub> at 40 K, the temperature where the narrowst lines occurred.

We must now relate the measurements of this chapter to the results of chapter 5. The power levels were typically 0.05 mwatt to 0.10 mwatt for the input power to the cavity. This would indicate some saturation of the resonances but the most significant distortion would be the overmodulation of the high  $g$  value line in the crossover region. The basic conclusion is that the linewidth of the high  $g$  value line in the crossover region is likely much narrower than values given in chapter 5. The measurements as a function of power have shown that the results of chapter 5 do not contradict the prediction of a vanishing linewidth given in of chapter 4; however the power measurements do not confirm this prediction either.

## Chapter 7

### Conclusion and Comparison with Other Results

#### 7.1 Preliminary Results on $\text{HMM}(\text{TCNQ})_2$

As mentioned in the introduction  $\text{HMM}(\text{TCNQ})_2$  shows a similar behavior to  $\text{DEM}(\text{TCNQ})_2$ . When considering the case of  $\text{HMM}(\text{TCNQ})_2$  we must first consider the crystal structure. This crystal structure has been given by Oostra *et al.* [15] and by Visser [5, p. 49]. This salt contains four TCNQ stacks in the unit cell that are connected by a four-fold screw axis. A significant difference in  $\text{HMM}(\text{TCNQ})_2$  is that unlike the case of  $\text{DEM}(\text{TCNQ})_2$  the stacks are related to each other by a symmetry operation. This means that the  $g$  tensors of each of the four TCNQ stacks should also be related by the same symmetry operation. In particular the principal values of the  $g$  tensor should be the same for the four stacks in  $\text{HMM}(\text{TCNQ})_2$ . This difference is significant because, unlike the case of  $\text{DEM}(\text{TCNQ})_2$ , it would not be possible to determine if the  $g$  tensor depends on the crystalline environment from measurements on  $\text{HMM}(\text{TCNQ})_2$  alone. In most orientations the four stacks in  $\text{HMM}(\text{TCNQ})_2$  will lead to four ESR resonances. A maximum of twelve possible crossovers in the  $g$  values are possible for an rotation through  $180^\circ$  since each pair of stacks can produce two crossovers.

We first consider the results of Oostra [4, p. 107] at 40 K shown in fig. 39.

The data show the experimental results for a rotation about the  $a$  crystal axis, the latter being determined to an accuracy of  $15^\circ$ , together with the theory for no interaction between the stacks. Although the data are close to the theory, the differences cannot be explained entirely by the quoted experimental error. The most important of these is the repulsion of the levels that is indicated in figure 40 by the solid line. This repulsion is very similar in magnitude to the effects observed in the data of chapter 5 for  $\text{DEM}(\text{TCNQ})_2$ .

The behaviour of the susceptibilities is again similar to the results for  $\text{DEM}(\text{TCNQ})_2$  in that the low  $g$  value line vanishes as the crossover is approached. In this case however the lower  $g$  value pair of lines vanishes with respect to the high  $g$  value pair as the crossover is approached. This behavior is in qualitative agreement with the theory given in chapter 4.,

There are also very recent preliminary measurements by Radzikowski and Chernin [29] and by Ma [30] at 77 K that show the same kind of repulsion of the levels at some of the crossovers. The results for the susceptibilities in these two sets of measurements are again in qualitative agreement with the results of Oostra.

One can conclude that the theory of chapter 4 if expanded to allow for the multiple interactions in  $\text{HMM}(\text{TCNQ})_2$  can be used as a starting point to explain the  $g$  values and susceptibilities of  $\text{HMM}(\text{TCNQ})_2$ . A quantitative comparison would require the full solution of the theory for this case together with more accurate experimental data.

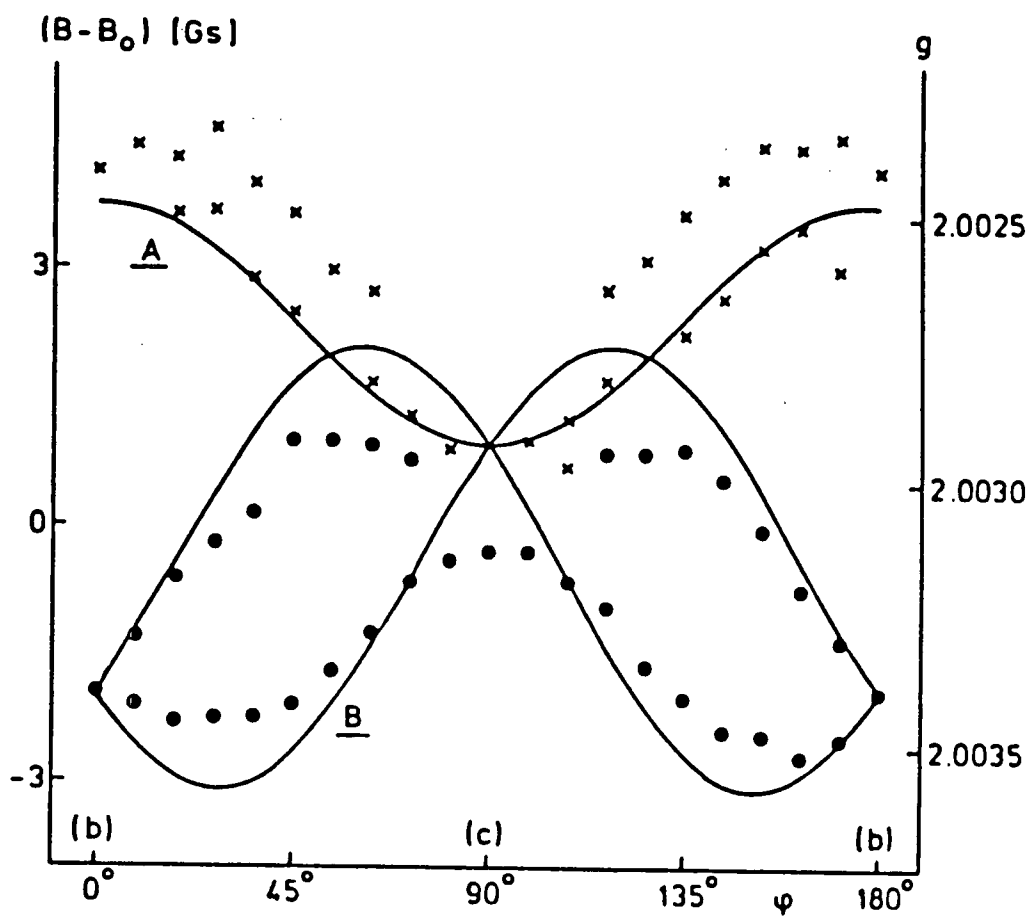


Figure 39:  $g$  value of  $\text{HMM}(\text{TCNQ})_2$  for a rotation about  $a$  from ref. [4, p. 107]. Dots represent the most intense lines. Drawn lines: theory (for no interaction between the stacks).

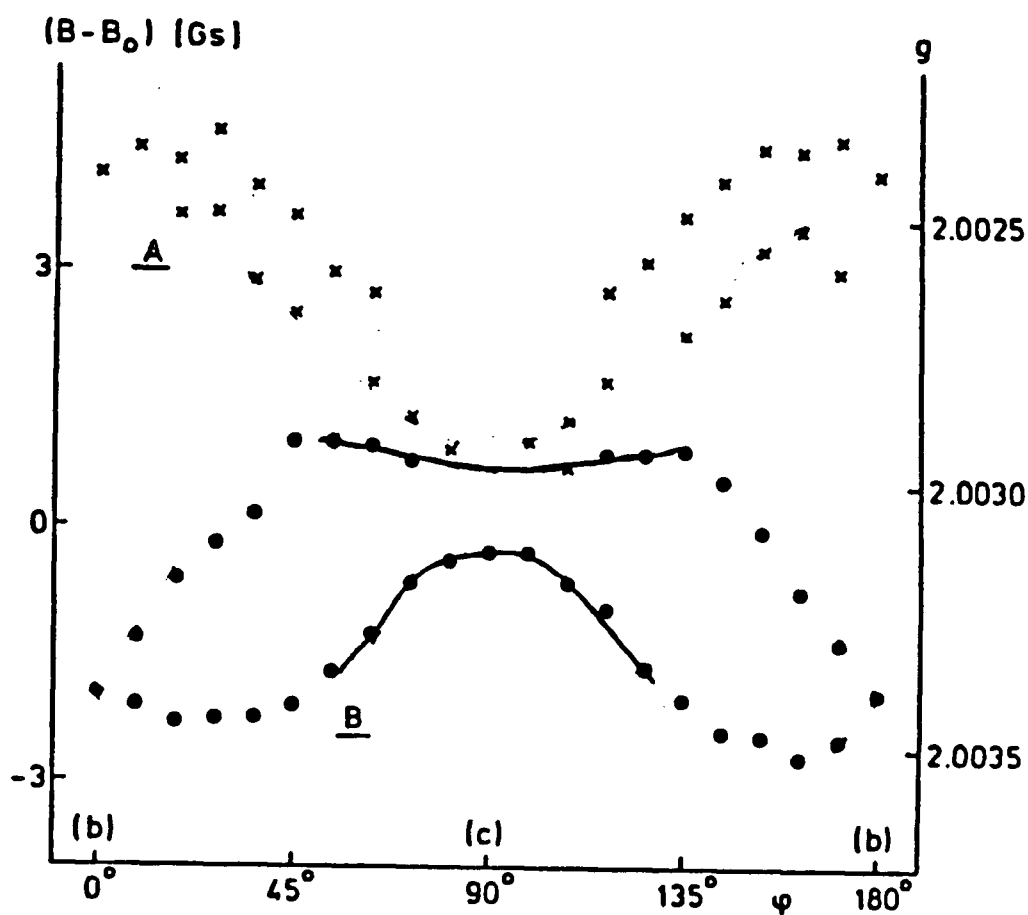


Figure 40:  $g$  value of  $\text{HMM}(\text{TCNQ})_2$  for a rotation about  $a$  from ref. [4, p. 107]. Dots represent the most intense lines. Drawn lines: An Estimate of the repulsion that would be expected for a similar interaction between the TCNQ stacks to the interaction found in  $\text{DEM}(\text{TCNQ})_2$ .

## 7.2 The Dependence of the $g$ Tensor on the Environment of the TCNQ Molecules and on the Temperature

Previous authors have found the angular dependence of the  $g$  value to have a small anisotropy for the TCNQ salts [4, p. 104], typical results would be  $g_L = 2.0028$ ,  $g_M = 2.0036$ , and  $g_N = 2.0024$ , where **L**, **M**, and **N** correspond to, the long axis in the plane of the TCNQ molecule, a direction perpendicular to **L** in the plane of the TCNQ, and the normal to the plane. Tomkiewicz *et al.* [16] and Walsh *et al.* [17] have proposed that the  $g$  values only depend on the direction of the magnetic field with respect to the TCNQ molecule [17,16], and do not depend on the temperature or on the environment of the TCNQ molecules; however as noted in the introduction Tomkiewicz *et al.* allow for an error of up to  $\pm 0.0004$  in the  $g$  value. The results of Kürti and Menczel place a limit of  $\pm 0.00005$  for the differences in the  $g$  tensors of three TCNQ salts. These results are shown in table IX. A fundamental question is whether the results of Kürti and Menczel can be extrapolated to other TCNQ salts as proposed by Oostra [4, p. 104]. The question as to the significance of the slightly different results reported by various authors [4, p. 104] for different compounds is by no means clear.

We present a collection in table IX of previous results and compare these results with our results for  $\text{MEM}(\text{TCNQ})_2$  and  $\text{DEM}(\text{TCNQ})_2$ , in an attempt to elucidate this question. These results show that based on the previous experimental errors the assumption that the  $g$  tensor only depends on the orientation of the TCNQ molecules in the magnetic field was a plausible assumption. The results for  $\text{DEM}(\text{TCNQ})_2$  and  $\text{MEM}(\text{TCNQ})_2$  show however that there are small but measurable differences in the  $g$  tensor when the temperature or the crystalline environment is changed. A very significant difference is found between both kinds of TCNQ

Compound	Temp. (K)	$g_M$	$g_L$	$g_N$	Ref.
NPQn(TCNQ) <sub>2</sub>	295	2.00356(5)	2.00279(5)	2.00236(5)	[31]
TEA(TCNQ) <sub>2</sub>	295	2.00355(5)	2.00276(5)	2.00236(5)	[31]
Qn(TCNQ) <sub>2</sub>	295	2.00360(5)	2.00273(5)	2.00242(5)	[31]
HEM(TCNQ) <sub>2</sub>		2.00363	2.00277	2.00242	[4, p. 104]
MEM(TCNQ) <sub>2</sub>	298	2.003332(8)	2.002770(7)	2.002318(7)	Chapt. 3
MEM(TCNQ) <sub>2</sub>	77	2.003413(8)	2.002776(6)	2.002333(7)	Chapt. 3
DEM(TCNQ) <sub>2</sub> (A)	298	2.003273(6)	2.002989(6)	2.002318(6)	Chapt. 5
DEM(TCNQ) <sub>2</sub> (A)	77	2.003333(6)	2.002976(6)	2.002363(6)	Chapt. 5
DEM(TCNQ) <sub>2</sub> (B)	298	2.003438(6)	2.002769(6)	2.002313(6)	Chapt. 5
DEM(TCNQ) <sub>2</sub> (B)	77	2.003478(6)	2.002733(6)	2.002294(6)	Chapt. 5

Table IX:  $g$  Tensor of Various TCNQ Compounds. The errors for ref [31] are relative errors. The absolute error in this data is  $3 \times 10^{-4}$ . The data of ref. [4] contain no error or temperature since none were given.

stacks in DEM(TCNQ)<sub>2</sub>. This difference is larger than even the previously quoted experimental errors.

The results at different temperatures show that the systematic trend proposed by Conwell [18] in the data of Clark *et al.* [19] for Qn(TCNQ)<sub>2</sub> is significant. Conwell's assertion is that there is an increase in the largest principal value of the  $g$  tensor of 0.00011 between 298 K and 1.4 K is in good agreement with the increase in the analogous principal values of both stacks of DEM(TCNQ)<sub>2</sub> and of the single stack of MEM(TCNQ)<sub>2</sub> when the temperature is lowered from 298 K to 77 K. This indicates that the trend in the data of Clark *et al.* is indeed real since the errors in the DEM(TCNQ)<sub>2</sub> and MEM(TCNQ)<sub>2</sub> results are much less than the error of  $\pm 0.00010$  estimated for the Qn(TCNQ)<sub>2</sub> data.

### 7.3 Conclusions and Further Experiments

We have shown that the behavior of the ESR resonances when there is a level crossing in TCNQ compounds can be explained in terms of an interaction of the form  $J \sum_{i,j} \mathbf{S}_i \mathbf{S}_j$  between the different type of TCNQ stacks. The incorporation of this interaction can account for the significant variation in the susceptibilities of each mode without a comparable change in the  $g$  value. We can also explain the repulsion of the levels that is observed at the crossovers. The theory predicts a vanishing linewidth for the high  $g$  value mode at the crossovers. This linewidth was not observed due to the experimental limitations.

The experimental results also have shown to what extent the  $g$  tensors depend on both the temperature and the crystalline environment of the TCNQ molecules. This dependence could be as high as  $8 \times 10^{-5}$  for the temperature and  $2 \times 10^{-4}$  for the crystalline environment of the molecules for  $\text{DEM}(\text{TCNQ})_2$  and  $\text{MEM}(\text{TCNQ})_2$ . An example of this conclusion is that the data of Kürti and Menczel cannot be extrapolated to other TCNQ salts with the same differences in the  $g$  tensor between compounds. We have also obtained an estimate of the minimum error introduced by making the assumption that the  $g$  tensors of TCNQ salts are given by the molecular  $g$  tensors as proposed by Tomkiewicz *et al.* [16] and Walsh *et al.* [17].

An interesting question for further research is the linewidth of the high  $g$  value line at the crossover points. This would require a fundamentally different approach to the experiment. One could consider a pulsed type of experiment or an continuous wave experiment where there was no magnetic field modulation and no AFC with a very low  $Q$  cavity. The latter experiment would pose considerable detection problems if it were at all feasible.

## Bibliography

- [1] I. F. Shchegolev, *Phys. Stat. Sol.* **A12**, 9 (1972).
- [2] L. van Bodegom, "Crystal Chemistry of TCNQ Complexes: Role of Cations, Composition and Temperature", Ph.D. dissertation, University of Groningen, 1979.
- [3] S. Huizinga, " $2k_F$  and  $4k_F$ , A Study of Spin and Electronic Peierls Transitions in One-Dimensional TCNQ Salts", Ph.D. dissertation, University of Groningen, 1980.
- [4] S. Oostra, "Electric and Magnetic Properties of the Morpholinium (TCNQ)<sub>2</sub> Family", Ph.D. dissertation, University of Groningen, 1984.
- [5] R. J. J. Visser, "TCNQ Complexes with Morpholinium Type Cations" Ph.D. dissertation, University of Groningen, 1985.
- [6] J. B. Torrance, in *Synthesis and Properties of Low Dimensional Materials*, *Annals of the New York Academy of Sciences*, vol. 313, edited by J. S. Miller and A. J Epstein (The New York Academy of Sciences, New York, 1978), p. 210.
- [7] J. Hubbard, *Phys. Rev.* **17**, 494 (1977).
- [8] H. Morssink and B. van Bodegom, *Acta Cryst.* **B37**, 107 (1981).

- [9] A. Bosch and B. van Bodegom, *Acta Cryst.* **B33**, 119 (1977).
- [10] M. Morrow, W. N. Hardy, J. F. Carolan, A. J. Berlinsky, L. Weiler, V. K. Gujral, A. Janossy, K. Holczer, G. Mihlay, G. Grüner, S Huizinga, A. Verwey and G. A. Sawatzky, *Can. J. of Phys.* **58**, 334 (1980)
- [11] J. C. Bonner and M. E. Fisher, *Phys. Rev.* **135**, A640 (1964).
- [12] S. Huizinga, J Kommandeur, G. A. Sawatzky, B. T. Thole, K. Kopinga, W. J. M. de Jonge and J. Roos, *Phys. Rev.* **B19**, 4723 (1979).
- [13] C. F. Schwerdtfeger, S Oostra and G. A. Sawatzky, *Phys. Rev.* **B25**, 1786 (1982).
- [14] F. X. Cabañas and C. F. Schwedtfeger, *Phys. Rev.* **B26**, 3534 (1982).
- [15] S. Oostra, R. J. J. Visser, G. A. Sawatzky and C. F. Schwerdtfeger, *J. de Physique* **C3**, 1381 (1983).
- [16] Y. Tomkiewicz, A. R. Taranko and J. B .Torrance, *Phys. Rev.* **B22**, 3113 (1980).
- [17] W. M. Walsh, Jr., L. W. Rupp, Jr., D. E. Schaefer, G. A. Thomas and R. Genner, *Solid State Commun.* **33**, 415 (1980).
- [18] E. Conwell, *Phys. Rev.* **B22**, 3107 (1980).
- [19] W. G. Clark, J. Hammann, J. Sanny, and L. C. Tippie, in *Proceedings of the Dubrovnik Conference on Quasi-one-dimensional Conductors, 1978*, ed. by S. Barisic *et al.* (Springer, Berlin, 1980), pp. 255-264.
- [20] R. J. Pressley and H. L. Berk, *Bull. American Phys. Soc.* **8**, 345 (1963).

- [21] W. G. Waller and M. T. Rogers, *J. of Mag. Res.* **9**, 92 (1973).
- [22] C. F. Schwerdtfeger, H. J. Wagner and G. A. Sawatzky, *Solid State Commun.* **35**, 7 (1980).
- [23] F. Bloch, *Phys. Rev.* **70**, 460 (1946).
- [24] C. P. Poole Jr. and H. A. Farach, *Relaxation in Magnetic Resonance* (Academic Press, New York, 1971).
- [25] P. R. Bevington, *Data Reduction and Error Analysis for the Physical Sciences* (McGraw-Hill, New York, 1969).
- [26] P. I. Kuindersma, G. A. Sawatzky and J. Kommandeur, *J. Phys. C* **8** 3005 (1975).
- [27] C. P. Poole Jr., *Electron Spin Resonance, A Comprehensive Treatise on Experimental Techniques* (John Wiley and Sons, New York, 1983).
- [28] C. F. Schwerdtfeger, *private communication*.
- [29] M. Radzikowski and L. Chernin, "An Electron Spin Resonance Study of  $\text{HMM}(\text{TCNQ})_2$ ", Undergraduate Report, University of British Columbia 1987.
- [30] C. Ma, *private communication*.
- [31] J. Kürti and G. Mencil, *Phys. Stat. Sol.* **B102**, 639 (1980).